HARVARD UNIVERSITY
Graduate School of Arts and Sciences

DISSERTATION ACCEPTANCE CERTIFICATE

The undersigned, appointed by the

Committee on Higher Degrees in Biophysics

have examined a dissertation entitled

Molecular mechanisms of the formation and maintenance of the tubular endoplasmic reticulum network

presented by **Robert Edward Powers**

candidate for the degree of Doctor of Philosophy and hereby certify that it is worthy of acceptance.

Signature _____

Typed name: Prof. Rachelle Gaudet

Signature _____

Typed name: Prof. Andrew C. Kruse

Signature _____

Typed name: Prof. Maofu Liao

Signature _____

Typed name: Prof. James M. Hogle

Date: April 30, 2018

Molecular mechanisms of the formation and maintenance of the tubular endoplasmic reticulum network

A dissertation presented

by

Robert Edward Powers

to

The Committee on Higher Degrees in Biophysics

in partial fulfillment of the requirements

for the degree of

Doctor of Philosophy

in the subject of

Biophysics

Harvard University

Cambridge, Massachusetts

April 2018

Dissertation Advisor:
Professor Tom A. Rapoport

Author:
Robert Edward Powers

Molecular mechanisms of the formation and maintenance of the tubular endoplasmic reticulum network

Abstract

Membrane-bound organelles, a defining feature of eukaryotic cells, display a diverse set of characteristic shapes that range from highly spherical, to flattened sheets, and even thin tubules. Therefore, how the characteristic shape of an organelle is generated, maintained, and modified is a fundamental question in eukaryotic cell biology. A powerful model system for studying organelle morphology is the endoplasmic reticulum (ER), which consists of a network of membrane sheets and tubules that extend throughout a cell. Previous studies have shown that the high membrane curvature of the tubules is generated and stabilized by integral membrane proteins of the reticulon and Yop1/REEP families and that individual tubules are fused together by the dynamin-like GTPases Atlastin (in metazoans) and Sey1p/RHD3 (yeast/plants). Although an *in vitro* assay for ER network formation has been developed using *Xenopus* egg extracts, the minimal set of components needed to form a tubular ER network has not been identified, and whether these minimal components allow for the ER dynamics observed *in vivo* is not known.

In this thesis, I will focus on the molecular mechanisms responsible for shaping the endoplasmic reticulum and offer insight into how these mechanisms give rise to the distinct tubular architecture observed for particular subdomains of the endoplasmic reticulum. I demonstrate that the minimal set of proteins needed to form the tubular ER network consists solely of a curvature-stabilizing protein and a membrane-fusing protein. Co-reconstitution of *Saccharomyces cerevisiae* Sey1p with a number of different curvature-stabilizing proteins of the reticulon and Yop1/REEP families yield proteoliposomes that, when incubated with GTP, form

tubular networks that are nearly indistinguishable from those observed in the extracts of *Xenopus laevis* eggs. Furthermore, these reconstituted networks have the same dynamic behaviors as ER networks in cells, including junction sliding and ring closure. Finally, the integrity of the synthetic network is dependent upon the GTPase activity of the membrane-fusing protein, as incubation of pre-formed reconstituted networks with GTPγS leads to rapid network disassembly. Taken together, these results demonstrate that the tubular ER can be generated by a surprisingly small set of proteins and represents an energy-dependent steady state between formation and disassembly.

I also describe my initial steps toward obtaining a structure of a curvature-stabilizing protein of the Yop1/REEP family using x-ray crystallography. The lack of an atomic-resolution structure of any of these proteins has left their exact mechanism of curvature generation and stabilization unknown. Unfortunately, given their small size and lack of hydrophilic surfaces, the Yop1/REEP proteins represent a difficult target for structural studies. To this end, I sought to use new tools that have been adapted for membrane protein crystallization to attempt to obtain a structure of the protein REEP5. These tools included lipidic cubic phase crystallization (LCP) techniques, as well as nanobody-aided crystallization. While initial LCP crystallization experiments failed to yield any crystals, I successfully isolated a number of nanobodies that bind to REEP5 with high affinity using an *in vitro* yeast display system. These nanobodies will be useful in future crystallization as well as *in vitro* biochemical experiments aimed at understanding REEP5 function, and more broadly, at how the reticulon and Yop1/REEP proteins generate and stabilize membrane curvature.

Contents

Acknowledgements

As is often the case, it is only near the end of a journey do you begin to realize how many people there are to thank for the help they so willingly gave you along the way.

First and foremost I would like to thank Tom. Not only did he let me, a headstrong 23 year old, join his lab (some may argue his first mistake), but he also entrusted me with a remarkably exciting and challenging project—to reconstitute the tubular ER. Over the past few years I have had the privilege of learning from one of the true leaders in the field of cell biology. His passion for science, particularly that of the *in vitro* flavor, has been simply infectious, and his keen insights and suggestions helped lead my project to success. By far, I will miss Tom's stories the most—he has collected so many over the course of his storied career. Thank you Tom, for all that you have taught me, and for all of the doors that you have opened for me. I am sure I will continue to read your papers in *Cell*, *Nature*, and/or *Science* for years to come.

I would also like to thank my undergraduate research advisor, my dissertation advisory committee member, and my thesis committee member Rachelle Gaudet. As that long preamble

may suggest, Rachelle has been a mentor to me in so many ways. From training me in the gritty details of biochemistry and crystallography, to teaching me how to write in a technical, scientific manner. Most importantly, she has been a constant example of how to conduct oneself professionally and with the upmost dignity. Thank you Rachelle, for the multitudes you have done for me.

And thank you to all of the members of the Gaudet lab, past and present, with whom I have shared so many laughs over the course of the past eight years. Especially Marcos Sotomayor, my first mentor in the laboratory, who taught me not only how to conduct a meticulous experiment, but how to have an incredible amount of fun while doing so.

I would also like to thank the other members of my dissertation advisory and thesis committees—Andrew Kruse, Stephen Liberles, and Maofu Liao. Their keen insights, questions, and positive encouragement helped to keep my PhD flowing smoothly. I would like to particularly thank Andrew, and the members of his lab, for providing me with and helping me use the fantastic nanobody yeast display library. Andrew and his lab were incredibly generous with their time and their materials, and for that I am extremely grateful.

I would also like to thank Jim Hogle, the chair of the Biophysics program, and Michele Jakoulov, our program administrator. It would be the greatest understatement in history to say that Jim and Michele pour their entire hearts into providing the very best for their Biophysics students. Their tireless advocacy and enthusiasm for the program was a much-needed rock on which I was able to craft a memorable PhD experience. Also, in case you did not know, Michele throws the best retreat parties in the history of parties.

I would like to thank all of the members of the Rapoport lab, both past and present, including Long, Thomas, Julie, Nick, Ryan, Songyu, Neil, Marco, Fabian, Hanna, Stefan, Arati,

Peiqiang, Ning, Navdar, Zhejian, Yuan, Lorna, and Carol. Thank you for all of the help, guidance, and laughs over the past years. Special thanks to Xudong for all his technical help in the lab—in the world of protein purification and biochemistry he is second to none. Special thanks also to my fellow Bay One Bro, Nick. Thanks for all the laughs, good luck in Medical School, and may you always get just one ping.

A very special thanks to my collaborator, friend, and mentor in the Rapoport lab, Songyu. In the lab, we formed an amazing team to tackle some of the most difficult problems in endoplasmic reticulum morphology. Alone I would not have been able to accomplish as much as we did working together. Thank you for all that you taught me and congratulations on your exciting new job on the golden coast.

A special thanks to Macro, my fellow biophysics student and Rapoport lab member. Marco was most generous in sharing his witty insults (directed towards me) and his interesting (although I have to admit good) taste in music. In all seriousness, thanks Marco for being a terrific colleague and an even better friend. You really should get a haircut though.

A special thank you to all of my fellow biophysics (and honorary biophysics) classmates, including Hugo, Christina, Cara, Meng-Xaio, Gleb, Shu, Eran, and Ben. Your camaraderie and friendship helped to truly enrich my PhD experience. Even as we are all scattered our separate ways, I hope that we will always stay in touch.

Finally, I would like to thank the people to whom I owe everything—my family.

My mother, Christine. Mom, I feel as though I will never be able to fully grasp all of the sacrifices you have made so that I can be where I am today. Your devotion will always be an inspiration to me, although I fear there is no way I will ever be able to repay you for all that you have done for me. Thank you Mom, from the bottom of my heart.

My father, Ronald. Dad, you always taught me that things were only worth doing if I did them right. Your unwavering support has shaped me into the person, the scholar, and the man that I am today. I hope I can make you proud. Thank you Dad.

My sister, Rebecca. Becca, your uncanny wit and ability to keep me honest never ceases to amaze me. Your tenacity in all you do will always be an inspiration to me. Thank you little sis.

My late dog, Lucky. Thanks Lucky-bucky, for the joy and comfort you brought my family.

And finally to my best friend, my love, and my partner in this crazy game of life, Alison. Alison, your constant support, love, and encouragement is one of the greatest gifts I have been blessed with in my life. I am looking forward with great anticipation to all of our future adventures together. Thank you Dear.

This thesis is dedicated to my family:

my mother Christine,

my father Ronald,

my sister Rebecca,

and my love Alison.

1

Introduction to endoplasmic reticulum morphology

Membrane-bound organelles, a defining feature of eukaryotic cells, display a diverse set of characteristic shapes that range from highly spherical, to flattened sheets, and even thin tubules. The conservation of these shapes across species suggests a strong link between the three-dimensional structure of an organelle and its cellular function. Therefore, how the characteristic shape of an organelle is generated, maintained, and modified is a fundamental question in eukaryotic cell biology. In this thesis, I will focus on the molecular mechanisms responsible for shaping the endoplasmic reticulum and offer insight into how these mechanisms give rise to the distinct tubular architecture observed for particular subdomains of the endoplasmic reticulum.

1.1 Endoplasmic reticulum morphology: tubules and sheets

In 1902, Emilio Veratti made the first observations of the organelle that scientists now call the endoplasmic reticulum while investigating the structure of muscle fibers (Veratti, 1961). Using a light microscope, Veratti described in detail "a reticular apparatus of the sarcoplasm" that was distributed along the muscle striation. Despite his thorough account, it took another 50 years, and the invention of the electron microscope, for biologists to "rediscover" the endoplasmic reticulum. The pioneering electron microscopy (EM) studies of George Palade, aided by Keith Porter, in the early 1950s, revealed a net-like structure of tubules within the cytoplasm of cells (Palade and Porter, 1954; Porter, 1953), later called the endoplasmic reticulum (ER). Shortly thereafter, Palade published a method to isolate ER microsomes—sealed vesicles derived from the ER (Palade and Siekevitz, 1956). For the first time, these microsomes allowed researchers to perform *in vitro* biochemical assays, ushering in decade's worth of research into ER function (Schuldiner and Schwappach, 2013).

Fast-forward to the present, and we now appreciate that the ER is a highly dynamic organelle that is the site of a variety of essential cellular processes including protein synthesis, lipid synthesis, glycosylation, and calcium storage and handling (reviewed in Baumann and Walz, 2001; Schwarz and Blower, 2016). New imaging technologies, including three-dimensional electron tomography, ultrathin sectioning electron microscopy, confocal fluorescence microscopy, and super-resolution light microscopy, have also given us a better understanding of the three-dimensional shape of the ER (reviewed in Westrate et al., 2015). These techniques have revealed that the ER is a single continuous membrane system composed of two subdomains, the nuclear envelope (NE) and the peripheral ER (pER), that are morphologically distinct. The NE contains the flat, cisternal membranes of the inner and outer

nuclear membranes. The pER is comprised of a polygonal networks of tubules fused at three-way junctions with interspersed sheets (Figure 1.1). The pER extends throughout the cytoplasm of a cell, with the sheets typically located proximal to the NE and the tubules positioned further away from the NE, near the edges of the cell.

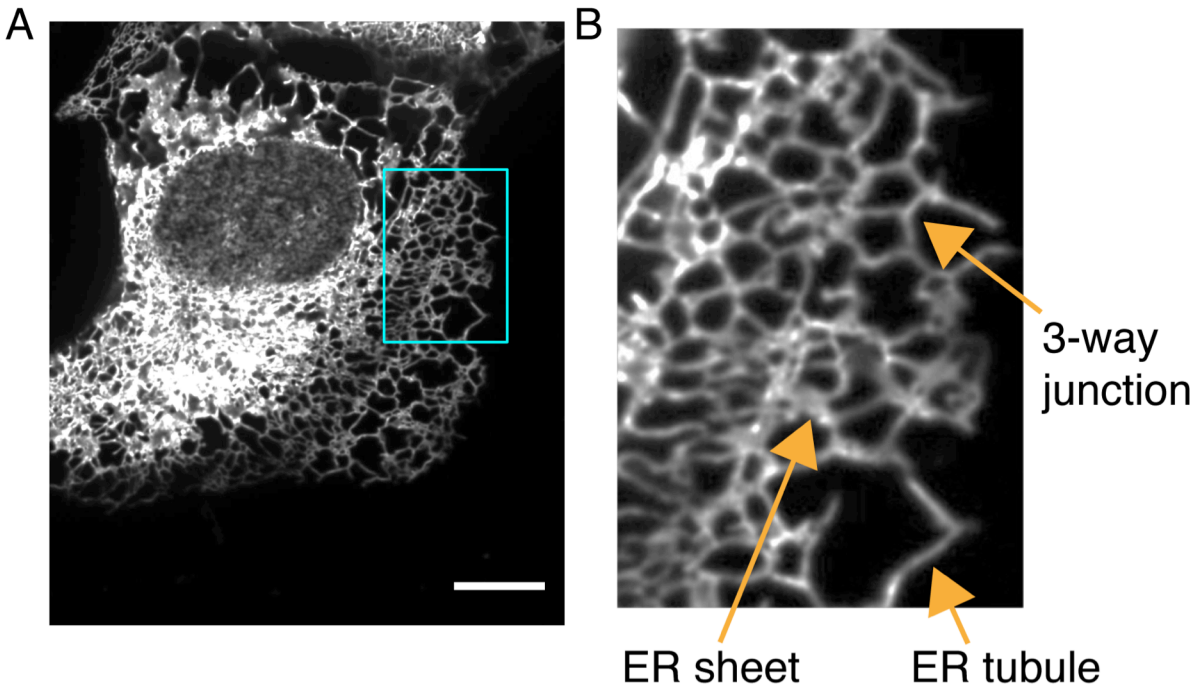

Figure 1.1 The tubular ER network extends throughout the cytoplasm
A) A U2OS cell expressing the luminal ER marker GFP-calreticulon reveals the extent of the ER network in cells. Particularly note the tubular ER network present towards the edge of the cell, away from the nucleus. Image courtesy of H. Tukachinsky. Scale bar = 10 μm. **B)** Enlarged image of the tubular ER network from the cell in panel A (area enlarged is highlighted with a cyan box). Arrows indicate the specific structures located within the tubular ER including individual tubules, three-way junctions, and peripheral sheets.

As one may expect, the shape of the ER seems to be intimately linked with its function. Accordingly, different cell types, particularly cells with specialized roles within a tissue, exhibit specific pER morphologies that allow the cells to perform their dedicated tasks (Fawcett, 1981; PALADE, 1956). ER sheets have historically been referred to as the "rough ER", a name given to describe the rough appearance imparted by the high concentration of bound ribosomes found on the surface of most ER sheets (Shibata et al., 2006; Voeltz et al., 2002). Given their high

volume-to-surface ratio, ER sheets are hypothesized to be the primary location for protein translocation, subsequent protein folding, and certain initial posttranslational modifications. Supporting this hypothesis are experiments that demonstrate that the protein translocation machinery is located primarily within ER sheets as opposed to ER tubules (Shibata et al., 2010; Westrate et al., 2015). Accordingly, the pER of "professional" secretory cells, including plasma B cells and pancreatic cells, is primarily composed of stacked sheets studded by bound ribosomes, allowing these cells to handle the increased secretory load (Baumann and Walz, 2001).

ER tubules are often referred to as "smooth ER", given their lack of bound ribosomes. Given their high surface-to-volume ratio, tubules are well suited to perform surface-dependent functions such as lipid synthesis, hormone synthesis, and signaling processes (Friedman and Voeltz, 2011; Westrate et al., 2015). Appropriately, cells tasked with producing steroid hormones in the adrenal cortex, testis, and ovaries, exhibit a pER that is primarily composed of tubules (Baumann and Walz, 2001; Fawcett, 1981). The highly specialized tubular ER of muscle cells, also known as the sarcoplasmic reticulum, is responsible for regulating the intracellular calcium signals that are necessary for muscle contraction (Voeltz et al., 2002). Their high surface to volume ratio also allows tubules to efficiently extend the ER over a large distance. This is important in larger cells types, most notably in neurons, which exhibit elongated neuronal processes. The pER found in axons and dendrites is primarily tubular in shape, with tubules that may be even thinner than ER tubules found in other cells types (Gonzalez and Couve, 2014; Ramirez et al., 2011; Terasaki, 2018). Furthermore, mutations in proteins that generate and maintain the tubular pER network in neurons cause the neurodegenerative disease Hereditary Spastic Paraplegia (HSP) (Hubner and Kurth, 2014; Salinas et al., 2008; Westrate et al., 2015).

1.2 Formation, maintenance, and dynamics of the tubular ER network

In 1984, Terasaki et al. published a groundbreaking study in which they used a fluorescent dye, $DiOC_6$, to visualize the ER in a living cell for the first time. Although $DiOC_6$ had previously been used to stain mitochondria, Terasaki et al. discovered that using higher concentrations of the dye led to the staining of a "lace-like reticular structure remarkable for its elaborate continuity throughout the cell" (Terasaki et al., 1984). They correctly identified this "continuous net-like structure" as the ER. Since these initial observations, fluorescence microscopy has revealed that the ER, in particular the tubular ER network, is highly dynamic and displays certain characteristic behaviors (Westrate et al., 2015). These behaviors include junction sliding, in which a three-way junction will slide along the length of a tubule (Lee and Chen, 1988; Lee et al., 1989). Eventually this sliding junction encounters another three-way junction, resulting in the fusion of the two junctions. Junction sliding and subsequent junction fusion results in ring-closure, in which polygons formed by the tubular ER network disappear, and the ER network is simplified. Other ER dynamics include tubule branching, in which new tubules are formed, seemingly by being pulled out from existing tubules or sheets, and tubule fusing, in which two tubules fuse together at a particular point to create a new three-way junction (Lee and Chen, 1988; Lee et al., 1989; Terasaki et al., 1984).

It has been observed that particular associations between the ER and the cytoskeleton underlie many observed ER dynamics (Friedman and Voeltz, 2011; Westrate et al., 2015). Early observations in mammalian cells noted that ER tubules were aligned with microtubules, and that the growth of tubules seemed to primarily occur along existing microtubules (Lee and Chen, 1988; Lee et al., 1989; Terasaki et al., 1984, 1986). One particular ER tubule-cytoskeleton association occurs through a protein complex called the tip attachment complex (TAC), which

has been shown to connect the unfused tips of ER tubules to the plus end of microtubules (Waterman-Storer and Salmon, 1998; Waterman-Storer et al., 1995). The TAC includes EB1, a microtubule plus end-binding protein. EB1 interacts with stroma-interacting molecule 1 (STIM1), which is an integral ER membrane protein that acts as a calcium sensor (Bola and Allan, 2009; Grigoriev et al., 2008; Waterman-Storer and Salmon, 1998; Waterman-Storer et al., 1995). The connection between the plus end of microtubules and ER tubules means that the ER tubules grow and shrink jointly with the microtubules. One of the more commonly observed behaviors of the tubular ER is the sliding of an ER tubule along a microtubule (Friedman et al., 2010; Grigoriev et al., 2008; Waterman-Storer and Salmon, 1998). This sliding is driven by kinesin-1 and cytoplasmic dynein, and perturbation of these motor proteins results in changes to the architecture of the tubular ER network (Bannai et al., 2004; Bola and Allan, 2009; Feiguin et al., 1994; Waterman-Storer and Salmon, 1998; Wozniak et al., 2009). Interestingly, this motor-driven sliding seems to occur primarily along microtubules that are acetylated (Friedman et al., 2010). It should be noted that while in metazoans, it appears that connections with microtubules play the most important role in tubular ER dynamics, observations in plant and yeast cells have demonstrated that actin filaments play the primary role in modulating ER dynamics in these organisms (Boevink et al., 1998; Bola and Allan, 2009; Fehrenbacher et al., 2002; Ueda et al., 2010).

An interesting observation in early studies of the tubular ER network in mammalian cells noted that when the microtubules were depolymerized by treating the cells with nocodazole, the majority of the tubular ER network eventually retracted towards the nucleus (Terasaki et al., 1984, 1986). This observation, combined with the extensive connections between the tubular ER network and the cytoskeleton, led to the hypothesis that the tubular ER network was primarily

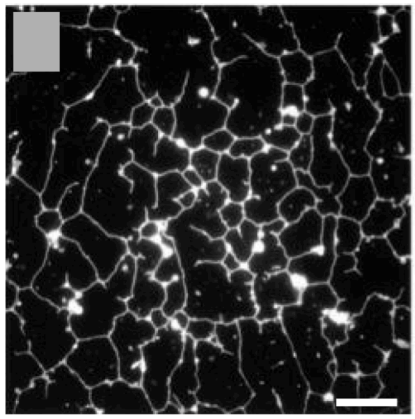

Figure 1.2 *In vitro* ER networks can be generated from *Xenopus laevis* egg extracts
Washed, light membranes from *X. laevis* egg extracts were incubated with cytosol for 60 minutes, stained with a hydrophobic dye, and imaged to reveal a tubular ER network. Scale bar = 10 μm. Image originally from Lars Drier and Tom Rapoport. Journal of Cell Biology 2000;148(5):883-898. Reproduced under a Creative Commons license.

shaped by and completely dependent upon the cytoskeleton. However, the tubule retraction after nocodazole treatment occurred on a much slower time scale than the microtubule depolymerization. Furthermore, there were a number of tubules that remained despite the disassembly of the microtubule network. In pioneering work, Dreier and Rapoport demonstrated that light membrane vesicles and cytosol derived from the extracts of *Xenopus laevis* eggs could be combined to form a tubular ER network *in vitro* (Dreier and Rapoport, 2000; Figure 1.2). Most importantly, the formation and maintenance of this network was unaffected by microtubule-depolymerizing agents or by the depletion of tubulin (Dreier and Rapoport, 2000). This was subsequently followed by work showing that light membrane vesicle fractions, which lack tubulin, could form tubular ER networks upon treatment with a physiological buffer containing GTP (Voeltz et al., 2006). These results unequivocally indicated that other factors, namely those that are associated with the ER membrane, must be primarily responsible for the formation and maintenance of the tubular ER network.

1.3 Proteins that shape the tubular ER network

Given their relatively small diameters, ~30 nm in yeast and ~50 nm in mammalian cells, ER tubules exhibit a high level of positive curvature that must be stabilized. In 2006, a study by Voeltz et al. used *Xenopus laevis* egg extracts to identify two classes of conserved membrane

proteins, the reticulons and the DP1/Yop1/REEP proteins, that are required for the formation and maintenance of ER tubules.

1.3.1 Reticulon proteins

Reticulon proteins are a class of highly abundant, integral membrane proteins that have been shown to generate and maintain the high curvature of ER tubules (Oertle et al., 2003a; Di Sano et al., 2012; Westrate et al., 2015). Reticulon proteins are highly conserved. Mammals have four reticulon genes (*RTN1*, *RTN2*, *RTN3*, and *RTN4*) that are expressed as a variety of different isoforms (GrandPre et al., 2000; Moreira et al., 1999; Oertle et al., 2003a, 2003b; Roebroek et al., 1993, 1996, 1998). The genome of *Saccharomyces cerevisiae* encodes two reticulon genes, *RTN1* and *RTN2* (Voeltz et al., 2006), while the genome of *Caenorhabditis elegans* encodes one reticulon gene, *ret-1*, that is expressed as three different isoforms (Iwahashi et al., 2002). *In vivo*, the overexpression of reticulon proteins increases the number and length of ER tubules and causes a decrease in tubule branching (Shibata et al., 2008; Voeltz et al., 2006; Wang et al., 2016). These tubules are more resistant to retraction after the depolymerization of the microtubule network, indicating that the reticulon proteins are important to the structural integrity of the tubular ER network (Shibata et al., 2008). At very high levels of overexpression, reticulon proteins actually generate so much curvature that a constriction of tubules and eventual fragmentation of the ER is observed (Wang et al., 2016). Consistent with the overexpression data, the depletion of reticulon from tissue culture cells results in a decrease in the number of tubules and an accompanying increase in the number of ER sheets (Anderson and Hetzer, 2008; Shibata et al., 2008, 2010; Voeltz et al., 2006). Furthermore, reticulons have been shown to localize preferentially to the site of high membrane curvature. This includes the ER tubules, as

well as the edges of ER sheets, which are highly curved (Shibata et al., 2008, 2010; Voeltz et al., 2006).

Complementing the *in vivo* data, *in vitro* experiments have also demonstrated the ER-shaping activity of reticulon proteins. Inactivation of reticulon proteins in *Xenopus laevis* egg extracts using sulfhydryl-modifying reagents and reticulon-specific antibodies inhibit network formation and leads to disassembly of the network (Voeltz et al., 2006). Furthermore, purified Rtn1p from *Saccharomyces cerevisiae* converts vesicles into tubules upon detergent-mediated reconstitution (Hu et al., 2008; Figure 1.3B).

Thus, the combination of *in vivo* and *in vitro* results indicate that reticulon proteins are both necessary and sufficient to form, maintain, and regulate the tubular ER network. Exactly how reticulon proteins shape membranes at a molecular level, however, is not completely understood. All reticulon proteins share a common core reticulon homology domain (RHD) that is located at the C-termini of the proteins (Figure 1.3A). The RHD is characterized by two transmembrane hairpin domains that are approximately 30-35 residues long (Hu et al., 2008, 2011; Voeltz et al., 2006). The two hairpin domains are separated by a hydrophilic, cytosolic loop. There is debate as to whether these hairpin domains actually span the entire bilayer, with preliminary NMR evidence showing that the domains do indeed traverse the membrane completely (Brady et al., 2015). The N-termini of reticulon proteins are highly variable, suggesting that particular reticulon proteins may be involved in other specialized cellular tasks, most notably intracellular signaling (Yang and Strittmatter, 2007). Recent studies have also identified a conserved amphipathic helix located at the C-termini of reticulon proteins (Brady et al., 2015; Breeze et al., 2016). This amphipathic helix is protected from trypsin-digestion by

lipids, suggesting that it is primarily associated with the membrane and may even partially insert into the bilayer.

There are several mechanisms by which reticulon proteins, and their distinctive structure, are thought to induce and stabilize positive curvature. First, the RHD is postulated to form a "hydrophobic wedge" (Hu et al., 2008, 2011; Shibata et al., 2010). The unique architecture of the two transmembrane hairpins is hypothesized to result in the formation of a wedge-like shape that occupies more space in the cytoplasmic leaflet of the ER membrane than in the luminal leaflet.

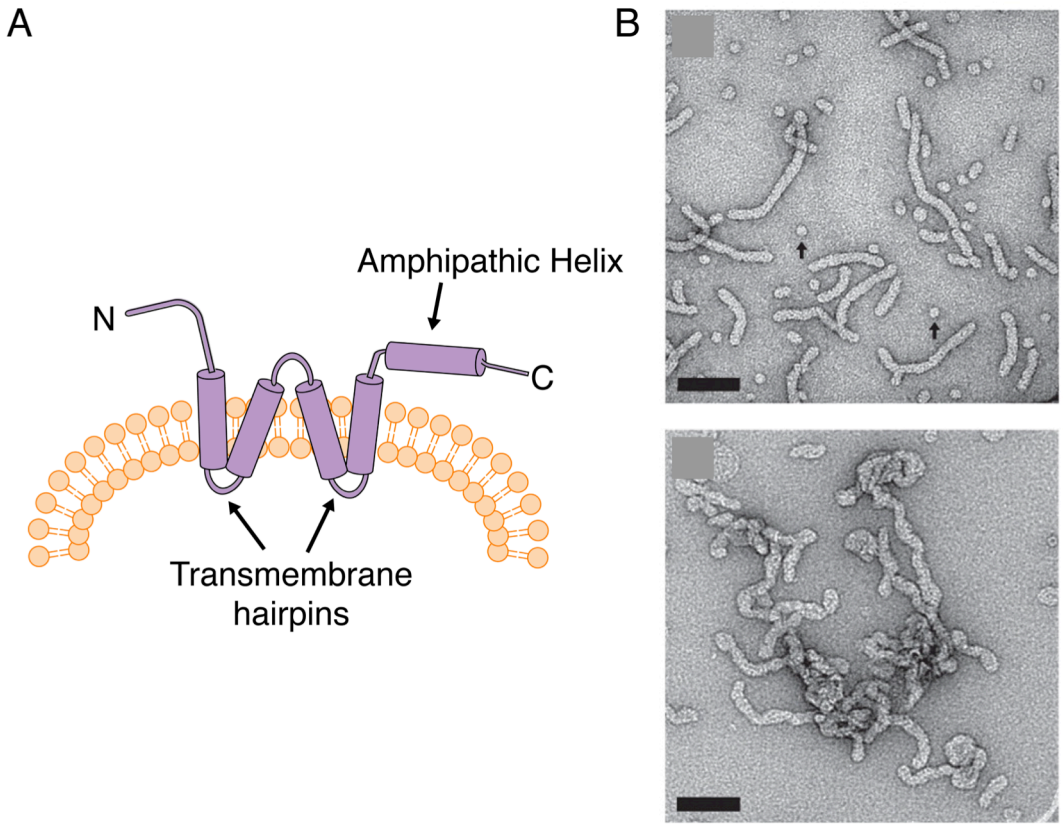

Figure 1.3 The reticulon and Yop1/REEP proteins generate and stabilize high positive curvature
A) Schematic of the structure and domain topology of reticulon and Yop1/REEP proteins. The proteins contain two transmembrane hairpin domains and a C-terminal amphipathic helix. **B)** Negative-stain electron microscopy analysis reveals that detergent-mediated reconstitution of *S. cerevisiae* Yop1p (top) or Rtn1p (bottom) into liposomes converts the liposomes into tubules after detergent removal. Scale bars = 100 nm. Image originally from Junjie Hu et al. Science 2008;319:1247-1250. Reprinted with permission from AAAS.

This causes expansion of the cytoplasmic leaflet, generating and stabilizing positive curvature within the membrane. Consistent with this hypothesis, increasing the length of the hairpin

segments, thereby disrupting the wedge-shape, abrogates the membrane curving activity of reticulon proteins (Tolley et al., 2010; Zurek et al., 2011). Another hypothesis is that reticulon proteins form large, arc-like oligomers that act as scaffolds to generate and stabilize positive curvature (Hu et al., 2008, 2011; Shibata et al., 2008). Reticulon proteins have been shown to form higher-order oligomers both *in vivo* and *in vitro*. The RHD appears to be sufficient for oligomerization. Mutations that disrupt oligomerization diminish the curvature-generating activity of reticulons. Finally, the conserved C-terminal amphipathic helix has been implicated in generating curvature, as deletion or the mutation of the hydrophobic face of this helix have been shown to disrupt reticulons' ability to generate curvature (Brady et al., 2015; Breeze et al., 2016). Amphipathic helices are often found in membrane-modifying proteins, as these helices have been shown to generate and sense membrane curvature, potentially by partial insertion into the membrane (Drin and Antonny, 2010).

1.3.2 Yop1/REEP proteins

Voeltz et al. also identified DP1 (defective in polyposis) as a reticulon interacting protein (Voeltz et al., 2006). DP1 is also known as receptor expression enhancing protein 5 (REEP5), as the expression of REEP proteins in animal cells was linked with the increased expression of certain receptors, most notably GPCRs (Behrens et al., 2006; Bjork et al., 2013; Dunham and Hall, 2009). There are 6 REEP proteins in mammalian cells, while *Saccharomyces cerevisiae* has one REEP protein called Yop1p, which is highly expressed (Hu et al., 2008; Voeltz et al., 2006). While not related in sequence, the Yop1/REEP proteins have a similar membrane topology as the reticulons. The Yop1/REEP proteins contain the same dual, short hairpin structures found in the RHD of reticulon proteins (Hu et al., 2008). The Yop1/REEP proteins also contain a conserved, amphipathic helix located at their C-termini (Brady et al., 2015).

The ER of yeast cells lacking either Yop1p or Rtn1p have a normally shaped ER, indicating that the two proteins could have overlapping functions in tubule formation and maintenance (Voeltz et al., 2006). Indeed, in yeast cells lacking both Yop1p and Rtn1p, the ER was converted mainly into sheets (Voeltz et al., 2006). Like Rtn1p, reconstitution of Yop1p into liposomes yields tubules (Hu et al., 2008; 1.3B), and the Yop1/REEP proteins have been shown to form immobile homo-oligomers (Brady et al., 2015; Hu et al., 2008; Shibata et al., 2008). Furthermore, Yop1p lacking the conserved C-terminal amphipathic helix is unable to tubulate liposomes *in vitro* (Brady et al., 2015). All of these observations indicate that like the reticulons, the Yop1/REEP proteins are responsible for forming and maintaining positive curvature within the tubular ER network. In mammals, particular REEP proteins may also take on other specialized cellular roles. For example, REEP3 and REEP4 contain a putative microtubule-binding domain, and preliminary evidence indicates the two proteins are important in helping to clear the ER away from metaphase chromosomes (Schlaitz et al., 2013).

1.3.3 Sey1/Atlastin proteins

While the reticulon and Yop1/REEP proteins are responsible for generating the membrane curvature needed to form and maintain tubules, individual tubules must be fused together to give rise to the continuous ER network. This homotypic fusion of ER membranes is primarily mediated by a family of ER-localized, dynamin-like GTPases known as the atlastins in metazoans (Hu et al., 2009; Orso et al., 2009). The proteins synthetic enhancer of yop1p (Sey1p) and root hair defective 3 (RHD3) are functional orthologues of atlastin that mediate homotypic ER fusion in yeast and plant cells respectively (Anwar et al., 2012; Hu et al., 2009; Zhang et al., 2013).

While the atlastin and Sey1/RHD3 proteins do not share sequence similarity, they exhibit a similar overall architecture (Figure 1.4A). Located at the N-terminus is a cytosolic GTPase (G) domain, which is immediately followed by a helical bundle (HB) domain. The HB domain of Sey1/RHD3 proteins is much larger than the HB domain of atlastin proteins. Following the HB domain is a transmembrane hairpin (TM) and finally a cytosolic C-terminal (C) domain that contains a conserved amphipathic helix (Bian et al., 2011; Hu and Rapoport, 2016; Liu et al., 2012; Yan et al., 2015).

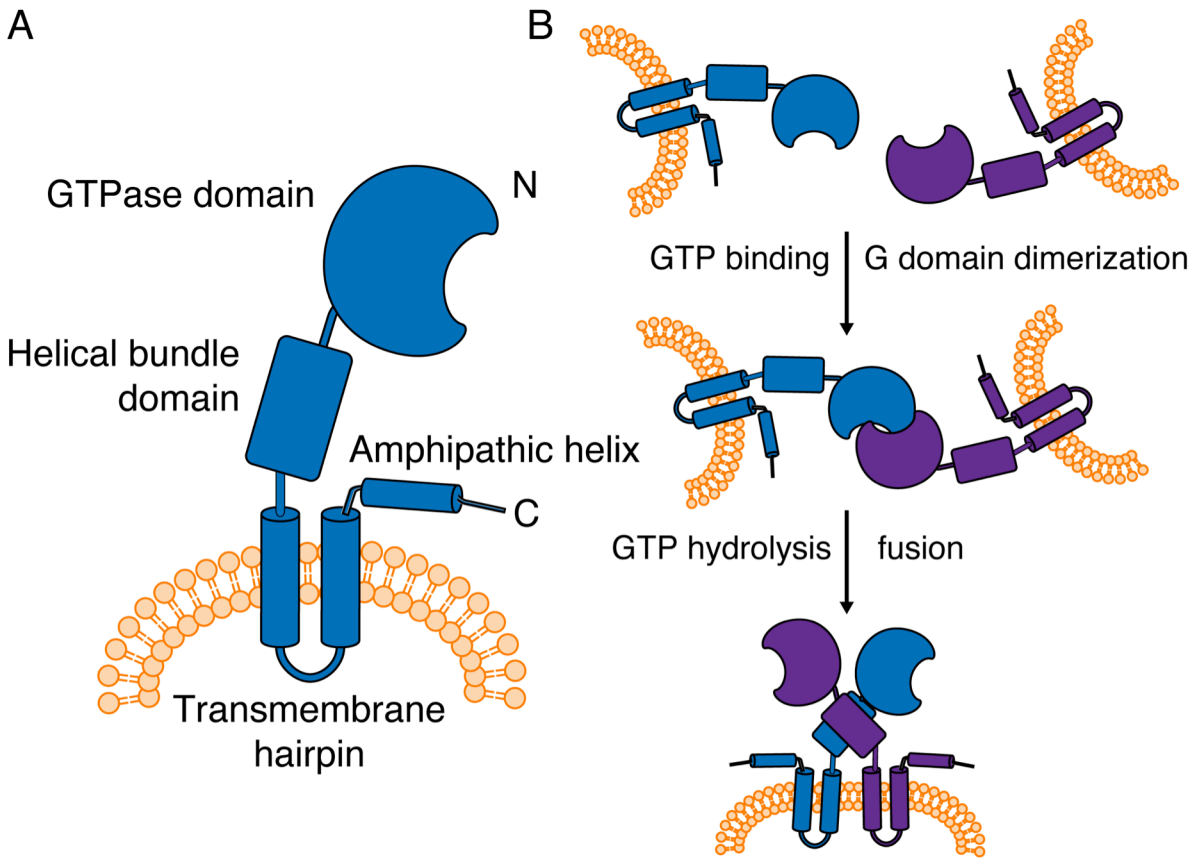

Figure 1.4 Homotypic fusion of ER membranes is mediated by atlastin and Sey1 proteins
A) Schematic of the structure and domain topology of atlastin and sey1 proteins. The proteins contain a N-terminal GTPase (G) domain, followed by a helical bundle (HB) domain, followed by a transmembrane hairpin (TM), and finally a cytosolic C-terminal (C) domain that contains a conserved amphipathic helix. **B)** Model of atlastin/Sey1p-mediated fusion. GTP binding causes dimerization via the G domain of molecules in opposing membranes. GTP hydrolysis causes a conformational change that pulls the two membranes together, causing fusion.

Experiments in both *Drosophila melanogaster* and tissue culture cells have demonstrated the role of atlastin in homotypic ER fusion. Perturbation of atlastin function, whether through depletion, deletion, mutational inactivation, or expression of dominant negative mutants, severely alters the morphology of the tubular ER network (Hu et al., 2009; Orso et al., 2009; Rismanchi et al., 2008; Wang et al., 2016). Low-levels of atlastin inactivation result in the appearance of long, non-branched ER tubules, indicating a lack of fusion between newly formed tubules (Hu et al., 2009; Orso et al., 2009). Higher levels of atlastin inactivation actually cause a fragmentation of the ER, demonstrating that atlastin activity is required for the integrity of the ER tubular network (Wang et al., 2016).

In vitro, ER network formation in *Xenopus laevis* egg extracts can be blocked by either the addition of an atlastin antibody or the soluble form of the atlastin G domain (Wang et al., 2013, 2016). The soluble G domain can only block fusion if it is able to interact with the endogenous atlastin molecules in the *Xenopus laevis* membranes, as a dimerization defective mutant of the soluble G domain does not block ER network formation (Wang et al., 2013). Furthermore, the addition of the soluble G domain can dissemble a preformed tubular ER network (Wang et al., 2016). These results demonstrate that the integrity of the ER network is dependent upon atlastin activity.

Most convincingly, detergent purified *Drosophila melanogaster* atlastin can be reconstituted into liposomes and upon the addition of GTP, catalyzes the fusion of the proteoliposomes (Bian et al., 2011; Faust et al., 2015; Liu et al., 2012, 2015; Orso et al., 2009). Atlastin also mediates the tethering of proteoliposomes (Liu et al., 2015; Saini et al., 2014). This tethering is GTP hydrolysis dependent, and indicates that there may be several futile cycles of GTP hydrolysis that result only in membrane tethering, rather than in membrane fusion. Based

on these results, along with several structures of the G domain solved by x-ray crystallography (Bian et al., 2011; Byrnes and Sondermann, 2011; Byrnes et al., 2013; Wu et al., 2015), a model of atlastin-mediated fusion has emerged in which atlastin molecules on opposing membranes dimerize upon GTP binding via the G domain (Figure 1.4B). GTP hydrolysis results in a conformational change that pulls the two opposing membranes together so that the bilayers can undergo fusion (Hu and Rapoport, 2016).

Further *in vitro* experiments in which different atlastin mutants were reconstituted into liposomes and tested for their ability to catalyze fusion has also demonstrated that the TM and C domains are vital for atlastin function. Both point mutations within the TM domain and the deletion of the conserved amphipathic in the C domain severely decreased the fusion activity of atlastin. Interestingly, the activity of atlastin mutants lacking the amphipathic helix could be rescued by the addition of a soluble, synthetic peptide corresponding to the amphipathic helix. This indicates that the helix most likely binds to and perturbs the membrane in a manner that aids in fusion.

A role for Sey1p in *Saccharomyces cerevisiae* homotypic ER fusion has also been established by a combination of *in vivo* and *in vitro* experiments. Sey1p has been shown to interact with Rtn1p and Yop1p, and the double deletion of Sey1p and Rtn1p in *Saccharomyces cerevisiae* severely perturbs ER morphology (Hu et al., 2009). Furthermore, the deletion of Sey1p delays ER fusion during *Saccharomyces cerevisiae* mating (Anwar et al., 2012). Sey1p and atlastin can also replace each other in yeast and mammalian cells (Anwar et al., 2012; Yan et al., 2015), while RHD3 can replace Sey1p in yeast (Zhang et al., 2013). Finally, like atlastin, Sey1p can be reconstituted into liposomes and catalyzes a GTP-dependent fusion of the proteoliposomes (Yan et al., 2015).

1.4 Proteins implicated in ER sheet formation and maintenance

While not the specific focus of this thesis, the mechanisms underlying the formation of ER sheets have also been investigated. ER sheets consist of two flat membranes that are stacked together, separated by a small luminal space. The edges of these sheets necessarily display a high level of positive curvature. This curvature is hypothesized to be stabilized by the reticulon and Yop1/REEP proteins (Shibata et al., 2010; Voeltz et al., 2006). ER sheets are often found stacked, particularly in professional secretory cells (Baumann and Walz, 2001; Fawcett, 1981). Serial EM methods have revealed that these stacked sheets are connected together by a twisted membrane surface reminiscent of the ramps that typically connect different levels within a parking garage (Terasaki et al., 2013). The thickness of ER sheets seems to be constant, suggesting the presence of a protein that acts as a luminal spacer (Bernales et al., 2006; Shibata et al., 2010). Climp-63 is a type II integral membrane protein that localizes to ER sheets and has been implicated in both sheet formation and maintenance of luminal spacing (Shibata et al., 2006, 2010). Climp-63 contains a luminal coiled coil domain that is thought to homo-oligomerize across the lumen of ER sheets to maintain a constant spacing of 45-50 nm (Klopfenstein et al., 2001). Consistent with this hypothesis, the depletion of CLIMP63 deceases the luminal spacing in ER sheets to 25-30 nm (Shibata et al., 2010). Furthermore, overexpression of CLIMP63 increases the number of ER sheets while decreasing the number of ER tubules (Shibata et al., 2010). The association of ribosomes, particularly polyribosomes, with ER sheets has also been hypothesized to help stabilize the flat surfaces of the membrane (Shibata et al., 2006, 2010). Indeed, the release of ribosomes and polyribosomes from the ER has been correlated with the disruption of ER sheet architecture (Puhka et al., 2007).

1.5 Outstanding questions and summary of thesis

While the curvature stabilizing activity of the reticulon and Yop1/REEP proteins, as well as the fusion activity of the atlastin/Sey1 proteins, have both been extensively studied and characterized *in vivo* and *in vitro*, how these two sets of proteins cooperate to form the tubular ER network is unclear. Moreover, although a powerful *in vitro* assay for ER network formation has been developed using extracts from *Xenopus laevis* eggs, the minimal set of components needed to form and maintain a tubular ER network has not been identified. Furthermore, whether these minimal components allow for the ER dynamics observed *in vivo* is not known. I address these questions directly in the Chapter 2 of this thesis, where I show that the minimal set of proteins needed to form the tubular ER network consists solely of a curvature-stabilizing protein and a membrane-fusing protein. Co-reconstitution of *Saccharomyces cerevisiae* Sey1p with a number of different curvature-stabilizing proteins of the reticulon and Yop1/REEP families yield proteoliposomes that, when incubated with GTP, form tubular networks that are nearly indistinguishable from those observed in the extracts of *Xenopus laevis* eggs. Furthermore, these synthetic networks have the same dynamic behaviors as ER networks in cells, including junction sliding and ring closure. This demonstrates that the minimal set of proteins needed to form the network also allows for network dynamics. Furthermore, the integrity of the synthetic network is dependent upon the GTPase activity of the membrane-fusing protein, as incubation of pre-formed reconstituted networks with GTPγS leads to rapid network disassembly. Taken together, these results demonstrate that the tubular ER can be generated by a surprisingly small set of proteins and represents an energy-dependent steady state between formation and disassembly.

In Chapter 3, I begin to tackle the difficult problem of determining the molecular mechanism by which the reticulon and Yop1/REEP proteins stabilize positive curvature. The

lack of high-resolution structural information about these proteins precludes a complete understanding of how they are able to generate membrane curvature. The size of these proteins demands a crystallographic approach. However, the nature of these membrane proteins, particularly the lack of a large cytosolic domain, means that obtaining crystals is very difficult. In this chapter, I detail the first steps towards obtaining a crystal and eventual structure using new tools available for the crystallization of membrane proteins. These tools include lipidic cubic phase crystallization and nanobody-aided crystallization. I describe initial crystallization trials using REEP5 proteins derived from *Xenopus laevis* as well as different thermophilic yeast species. I also demonstrate the *in vitro* identification of several nanobodies that bind to these REEP5 proteins using a new yeast display library in combination with standard cell sorting techniques. I show that that these nanobodies can bind to the REEP5 proteins with high affinity and in some cases, can co-bind with other nanobodies. These nanobodies will undoubtedly be useful tools not only in future crystallographic trails, but also in other *in vitro* network assays.

2

Reconstitution of the tubular endoplasmic reticulum with purified components

This chapter has been previously published as:

Powers, R.E.*, Wang, S.*, Liu, T.Y., and Rapoport, T.A. (2017). Reconstitution of the tubular endoplasmic reticulum network with purified components. *Nature* 543, 257–260.

* denotes equal contribution

2.1 Abstract

Organelles display characteristic morphologies that are intimately tied to their cellular function, but how organelles are shaped is poorly understood. The endoplasmic reticulum (ER) is particularly intriguing, as it is comprised of morphologically distinct domains, including a dynamic network of interconnected membrane tubules. Several membrane proteins have been implicated in network formation (Chen et al., 2013; English and Voeltz, 2013; Goyal and

Blackstone, 2013; Shibata et al., 2009; Zhang and Hu, 2016), but how exactly they mediate network formation and whether they are all required is unclear. Here, we have reconstituted a dynamic tubular membrane network with purified ER proteins. Proteoliposomes containing the membrane-fusing GTPase Sey1p (Anwar et al., 2012; Hu et al., 2009) and the curvature-stabilizing protein Yop1p (Hu et al., 2008; Voeltz et al., 2006) from *Saccharomyces cerevisiae* form a tubular network upon GTP addition. The tubules rapidly fragment when GTP hydrolysis of Sey1p is inhibited, indicating that network maintenance requires continuous membrane fusion and that Yop1p favors the generation of highly curved membrane structures. Sey1p also forms networks with other curvature-stabilizing proteins, including reticulon (Voeltz et al., 2006) and REEP (Park et al., 2010) proteins from different species. Atlastin, the vertebrate ortholog of Sey1p (Hu et al., 2009; Orso et al., 2009), forms a GTP-hydrolysis dependent network on its own, serving as both a fusion and curvature-stabilizing protein. Our results show that organelle shape can be generated by a surprisingly small set of proteins and represents an energy-dependent steady state between formation and disassembly.

2.2 Introduction

ER tubules have high membrane curvature in cross-section, which is generated by two families of conserved integral membrane proteins, the reticulons (Rtn) and REEPs (Yop1p in yeast) (Voeltz et al., 2006). These proteins are required to maintain a tubular network in cells (Hu et al., 2008; Voeltz et al., 2006) and, upon reconstitution into liposomes, convert vesicles into tubules (Hu et al., 2008). These proteins contain two sets of closely spaced transmembrane domains and a C-terminal amphipathic helix that may be required to induce membrane curvature (Brady et al., 2015; Voeltz et al., 2006). Members of the Rtn and REEP/Yop1p families exist in all eukaryotic cells and have redundant functions in curvature-stabilization. Connecting tubules

into a polygonal network depends on membrane fusion, a process mediated by membrane-bound GTPases, the atlastins (ATL) in metazoans and Sey1p in yeast (Hu et al., 2009; Orso et al., 2009). Proteoliposomes containing purified ATL or Sey1p undergo GTP hydrolysis- dependent fusion *in vitro* (Anwar et al., 2012; Bian et al., 2011; Byrnes and Sondermann, 2011; Orso et al., 2009; Yan et al., 2015). These dynamin-like proteins initially tether opposing membranes and then use GTP hydrolysis to cause their fusion (Liu et al., 2015). In addition to curvature-stabilizing and fusion proteins, other factors have been implicated in ER network formation, including the lunapark protein (Chen et al., 2015; Shemesh et al., 2014; Wang et al., 2016), the Tts1/TMEM33 protein (Zhang et al., 2010), the cytoskeleton, and molecular motors (Wang et al., 2013). Here, we identify a minimal set of components needed for the formation of a tubular ER network.

2.3 Results

We first tested whether a membrane network can be generated with the GTPase Sey1p and a single curvature-stabilizing protein, Yop1p, both derived from *S. cerevisiae*. Purified Sey1p and Yop1p (Figure A.1, Appendix A) were incorporated into liposomes by "directed insertion" (Bian et al., 2011; Orso et al., 2009). The proteins were oriented with their cytosolic domains on the outside (Figure A.2, Appendix A) and used at a molar ratio that approximates their relative abundance in cells (Sey1p:Yop1p~1:10–1:20) (Kulak et al., 2014). A fraction of the vesicles floated in a Nycodenz gradient (Figure A.3, Appendix A). For visualization by fluorescence microscopy, the liposomes also contained rhodamine-labeled phosphatidyl ethanolamine (rhodamine-PE). The reconstituted proteoliposomes were fusion competent, as demonstrated with a lipid- mixing assay (Figure A.4, Appendix A)(Bian et al., 2011; Orso et al.,

2009). In fact, fusion was more efficient with proteoliposomes containing both Sey1p and Yop1p than with those containing only Sey1p.

Next we visualized the proteoliposomes by confocal fluorescence microscopy. In the absence of GTP, the sample consisted of small vesicles, appearing as bright dots (Figure 2.1A). However, when the proteoliposomes were incubated with GTP, an extensive network of interconnected tubules was observed (Figure 2.1A). Although the network displayed variable density (Figure A.5, Appendix A), in most areas it looked strikingly similar to ER networks generated with extracts from *Xenopus laevis* eggs (Figure 2.1B). In addition, like in extracts or intact cells (Lee and Chen, 1988; Wang et al., 2013), the reconstituted ER network exhibited dynamics, including the sliding of junctions along tubules and ring closure, i.e. the merging of two junctions into one (Figure 2.1C; Supplementary Video 1). The network did not form with GTPγS, indicating that GTP hydrolysis by Sey1p is required (Figure A.6A, Appendix A). Network formation was also dependent on both Sey1p and Yop1p. With Sey1p alone, the addition of GTP resulted in larger vesicles, but not tubules (Figure 2.1D and Figure A.6B, Appendix A). With Yop1p alone, only small vesicles or perhaps short tubules were observed in the absence or presence of GTP (Figure 2.1E and Figure A.6C, Appendix A), in agreement with previous results where tubules were observed by EM (Hu et al., 2008). Network formation was seen with different ratios of Sey1p to Yop1p, as well as of protein to lipid (Figure A.7, Appendix A). The lipid composition of the proteoliposomes did not seem to be of major importance, as networks could be generated with *Escherichia coli* or *S. cerevisiae* polar lipid extracts (Figure A.8, Appendix A).

To test whether the reconstituted network contains both Sey1p and Yop1p, we generated fluorescently labeled versions of these proteins. Sey1p was tagged at the N-terminus with GFP,

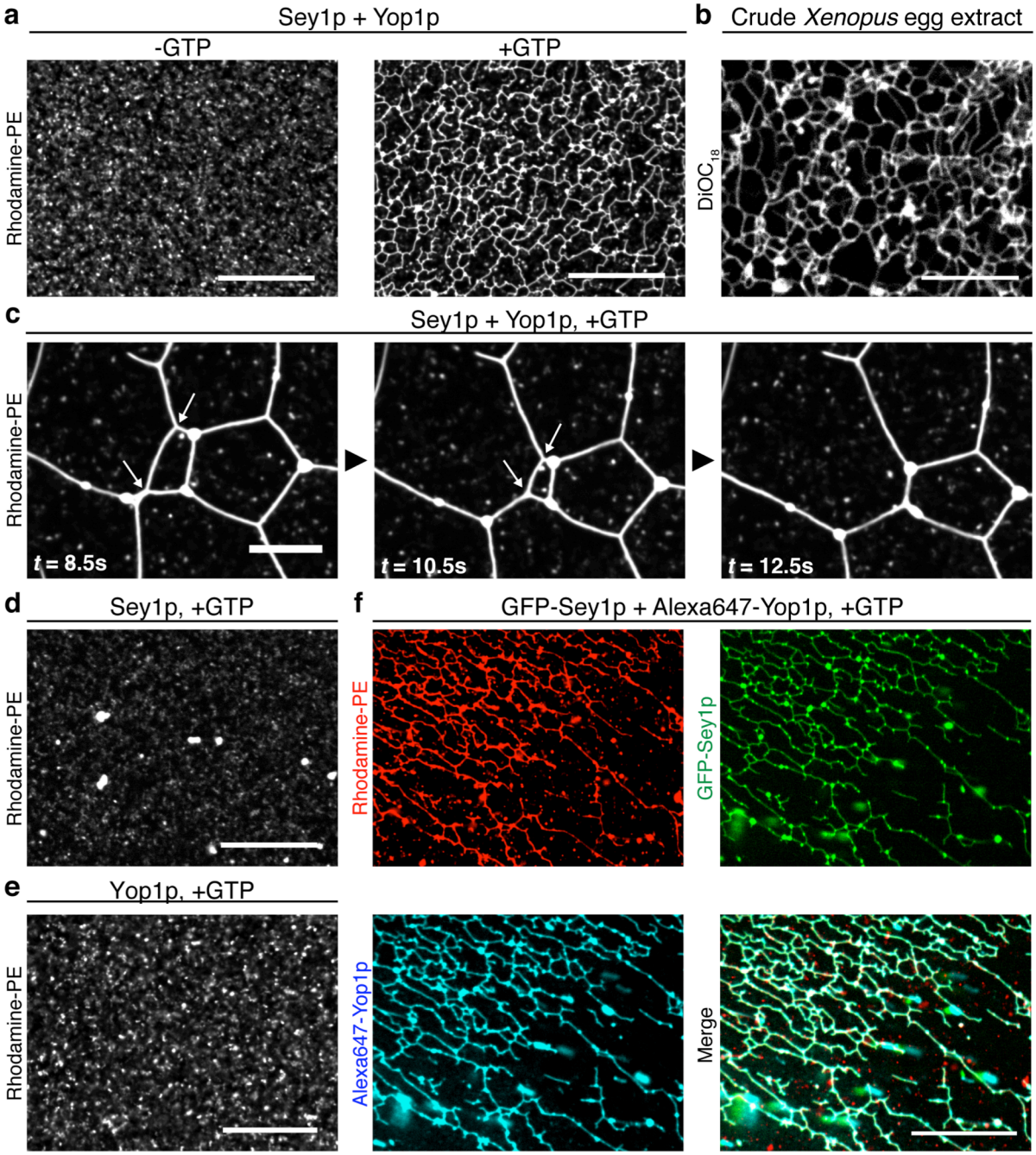

Figure 2.1 Co-reconstituted Sey1p and Yop1p form GTP-dependent tubular networks
A) *S. cerevisiae* Sey1p and Yop1p were co-reconstituted into rhodamine-PE labeled liposomes at protein:lipid ratios of 1:500 and 1:35, respectively, incubated without (left) or with (right) 2 mM GTP, and visualized by fluorescence microscopy. **B)** An ER network was formed with crude interphase *Xenopus* egg extract and fluorescently stained with $DiOC_{18}$. **C)** Time-lapse images of the reconstituted network (see also Supplementary Video 1). White arrows indicate sliding or fusing junctions. **D)** Proteoliposomes formed with Sey1p alone (protein:lipid ratio of 1:500) were incubated with 2 mM GTP. **E)** As in **D**, but with proteoliposomes formed with Yop1p alone (protein:lipid ratio of 1:35). **F)** As in **A**, but with GFP-labeled Sey1p and Alexa647-labeled Yop1p. Scale bars = 20 μm, except in c where scale bars = 10 μm.

and Yop1p was labeled at lysine residues with Alexa647 dye. The labeled proteins were co-reconstituted into liposomes that also contained rhodamine-PE. Upon GTP addition, a network was formed that contained all three fluorescent labels (Figure 2.1F). Both Sey1p and Yop1p distributed throughout the network. An even distribution of Yop1p is expected, but Sey1p is typically enriched at three-way junctions *in vivo* (Hu et al., 2009; Yan et al., 2015). The difference might be due to a higher Sey1p concentration in our *in vitro* system or to the absence of unknown factors that localize to junctions in cells. However, the Sey1p ortholog ATL1 is uniformly distributed throughout tubules *in vivo* (Wang et al., 2016), indicating that the fusion proteins need not be enriched at junctions.

The addition of GTPγS to a preformed network resulted in its rapid fragmentation (Figure 2.2A). Within a few minutes, the network converted into small vesicles, although some larger structures were also observed. Intermediates of the fragmentation process were difficult to visualize, but we observed several cases in which long tubules broke into smaller ones (Figure 2.2B; Supplementary Video 2). In addition, tubules probably shorten by shedding vesicles from their tips. These results show that network formation requires continuous membrane fusion by Sey1p to counterbalance fragmentation into small vesicles. This behavior is similar to that of ER networks generated in *Xenopus* egg extracts and tissue culture cells (Wang et al., 2016), which disassemble when ATL is inhibited.

To examine the reconstituted ER network in more detail, Sey1p and Yop1p were directly incorporated into unlabeled liposomes and the samples were analyzed by negative-stain electron microscopy (EM). When the proteoliposomes were incubated with GTP, small areas of a tubular network were seen (Figures 2.3A,B; Figure A.9A, Appendix A). No network was observed in the

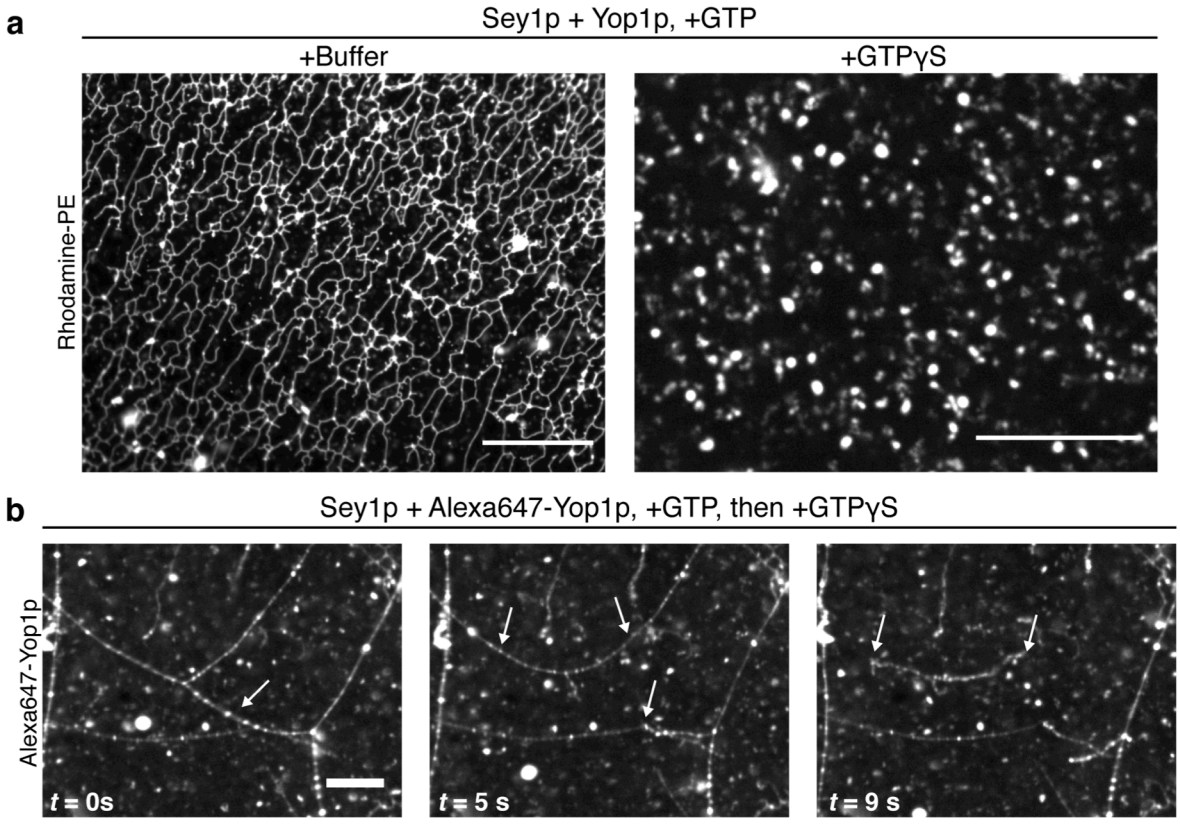

Figure 2.2 Network maintenance requires continuous GTP hydrolysis by Sey1p
A) *S. cerevisiae* Sey1p and Yop1p were co-reconstituted into rhodamine-PE labeled liposomes at protein:lipid ratios of 1:500 and 1:35, respectively. Network was formed by incubating proteoliposomes with 2 mM GTP. After addition of buffer (left) or 2 mM GTPγS (right), the samples were immediately analyzed. **B)** Time-lapse images after addition of 1 mM GTPγS to a preformed network formed with Sey1p and Alexa647-labeled Yop1p (see also Supplementary Video 2). Alexa647-labeled Yop1p is visualized. White arrows indicate fragmentation points. Scale bars = 20 μm for **A** and 10 μm for **B**.

absence of GTP or when one of the two proteins was omitted (Figures 2.3A–D). The areas of the network were much less extensive than those seen in the light microscope, likely because they only partially survived the harsh negative-staining protocol. The two bilayers and the lumen of the reconstituted tubules were clearly visible, confirming that three-way junctions indeed consist of fused, rather than simply tethered, membrane tubules. Most of the reconstituted tubules had a diameter of ~16 nm, similar to those formed with Yop1p alone (Hu et al., 2008). They are significantly narrower than the tubules in normal cells, likely because the concentration of Yop1p is higher in the proteoliposomes than *in vivo*, an assumption supported by the observation

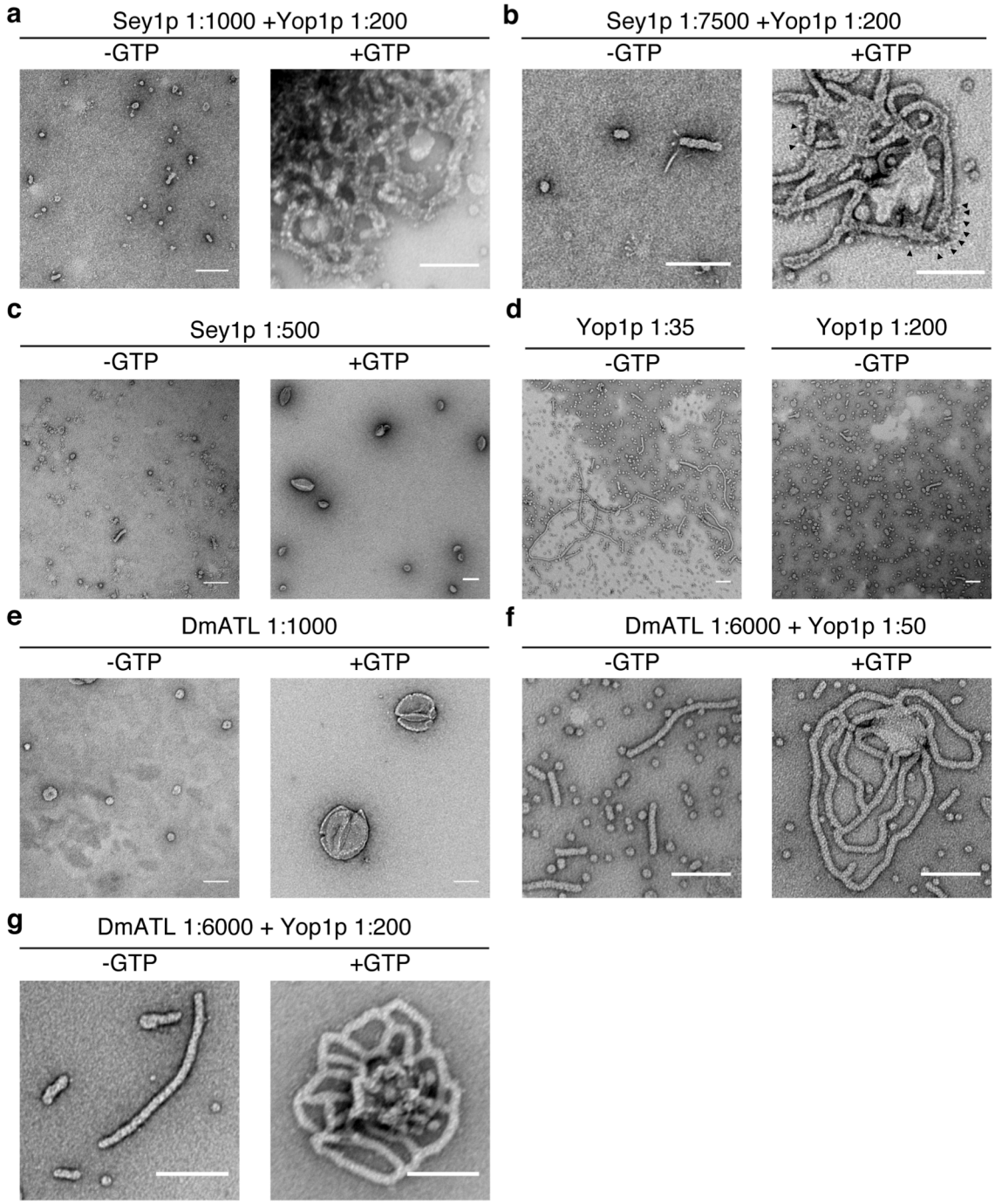

Figure 2.3 Visualization of reconstituted networks with negative-stain EM

A) *S. cerevisiae* Sey1p and Yop1p were co-reconstituted into liposomes at protein:lipid ratios of 1:1000 and 1:200, respectively. The samples were incubated with or without 1 mM GTP and visualized by EM after uranyl acetate staining. The figure shows a magnification of the network in Extended Data Fig. 7. **B)** As in **A**, but with Sey1p and Yop1p at protein:lipid ratios of 1:7500 and 1:200, respectively. Black arrowheads indicate Sey1p molecules. **C**) As in **A**, but with Sey1p alone at a protein:lipid ratio of 1:500. **D**) As in **A**, but with Yop1p alone at protein:lipid ratios of 1:35 and 1:200 in the absence of GTP. **E**) As in **A**, but with *D. melanogaster* ATL alone at a protein:lipid ratio of 1:1000. **F)** As in **A**, but with ATL and Yop1p co-reconstituted into liposomes at protein:lipid ratios of 1:6000 and 1:50, respectively. **G)** As in **A**, but with ATL and Yop1p at protein:lipid ratios of 1:6000 and 1:200, respectively. Scale bars = 100 nm.

that overexpression of curvature-stabilizing proteins in cells constricts ER tubules (Hu et al., 2008). In the reconstituted tubules, Sey1p molecules were visible as small, globular objects that extended approximately 18 nm from the bilayer and were connected to the membrane via a thin stalk (Figure 2.3B; Figures A.9B,C, Appendix A), features and dimensions that are in agreement with the crystal structure of Sey1p (Yan et al., 2015). Sey1p was distributed throughout the entire network, consistent with its localization in light microscopy.

Next, we tested whether Sey1p could form networks with other curvature-stabilizing proteins of the Rtn and DP1/Yop1p families. Indeed, networks were observed when Sey1p was combined with Rtn1p from *S. cerevisiae* (Figure 2.4a), Rtnl1 from *D. melanogaster* (Figure 2.4B), a REEP5 (DP1) homolog from *D. melanogaster* (CG8331; Figure 2.4C), and REEP4 or REEP5 from *X. laevis* (Figures 2.4D,E). In all these cases, network formation was only seen in the presence of GTP (Figure A.10, Appendix A). Small, GTP-dependent networks were also seen when proteoliposomes containing Sey1p and *Drosophila melanogaster* Rtnl1 were analyzed by negative-stain EM (Figure A.9D). Taken together, these results indicate that proteins of the Rtn and REEP/Yop1p families are functionally equivalent in shaping the ER network. Furthermore, given that these proteins are derived from evolutionarily distant organisms, network formation probably does not require a specific physical interaction between Sey1p and curvature-stabilizing proteins.

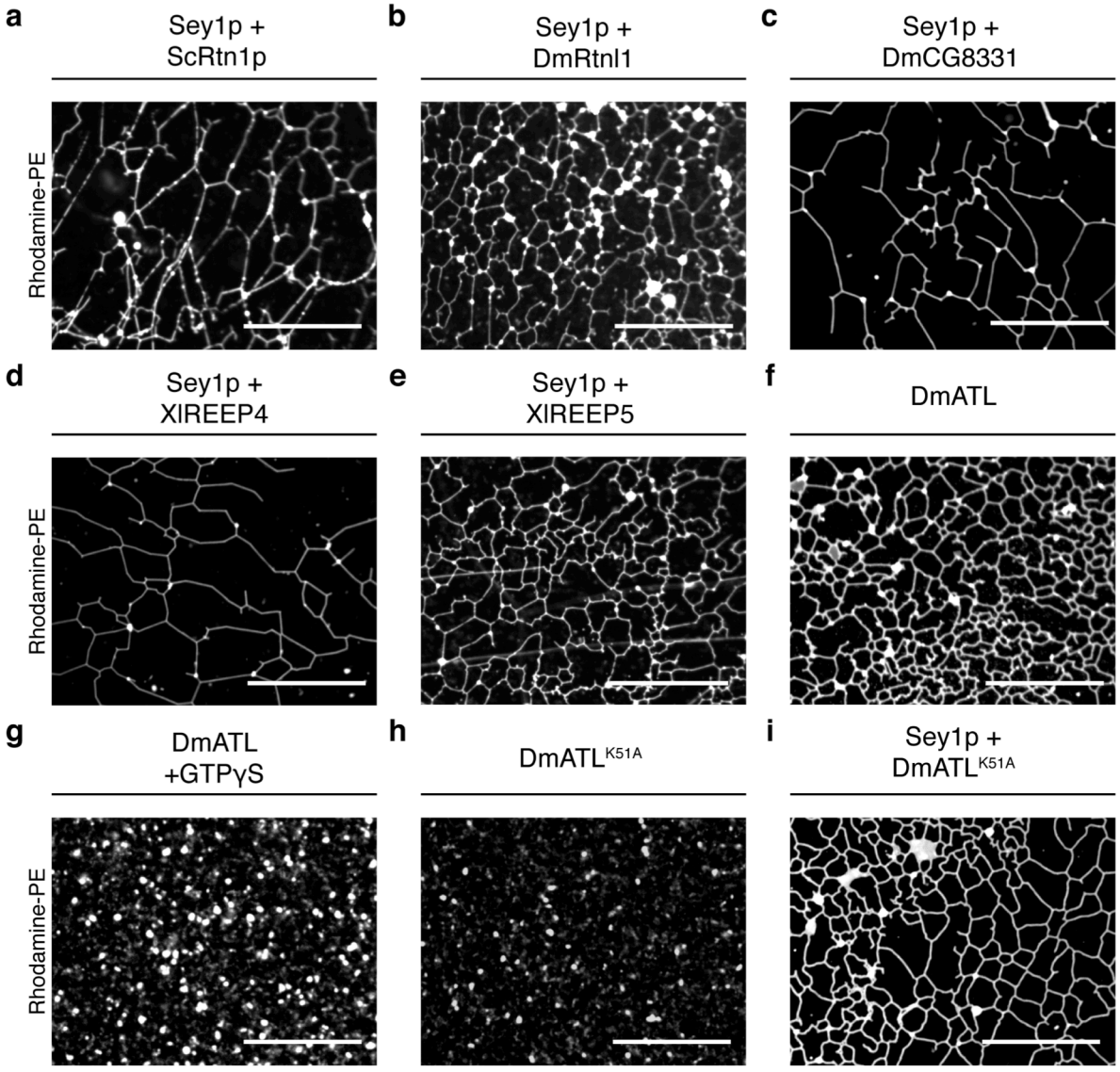

Figure 2.4. Networks formed with different membrane-fusing and curvature-stabilizing proteins
A) *S. cerevisiae* Sey1p was co-reconstituted with *S. cerevisiae* Rtn1p into rhodamine-PE labeled liposomes at protein:lipid ratios of 1:500 and 1:50, respectively. The proteoliposomes were incubated with 2 mM GTP and visualized by fluorescence microscopy. **B)** As in **A** but with Sey1p and *D. melanogaster* Rtnl1. **C)** As in **A**, but with Sey1p and *D. melanogaster* REEP-homolog CG8331. **D)** As in **A**, but with Sey1p and *X. laevis* REEP4. **E)** As in a, but with Sey1p and *X. laevis* REEP5 (protein:lipid ratio of 1:200). **F)** Proteoliposomes formed with *D. melanogaster* ATL alone at a protein:lipid ratio of 1:1000 in the presence of 2 mM GTP. **G)** As in **F**, but 2 mM GTPγS was added after network formation. **H)** Proteoliposomes formed with fusion-defective *D. melanogaster* ATL^{K51A} alone at a protein:lipid ratio of 1:100 in the presence of 2 mM GTP. **I)** *S. cerevisiae* Sey1p and fusion-defective *D. melanogaster* ATL^{K51A} co-reconstituted at protein:lipid ratios of 1:500 and 1:100, respectively, incubated in the presence of 2 mM GTP. Scale bars = 20 μm.

Finally, we tested whether ATL, the metazoan ortholog of Sey1p, can also mediate network formation. Surprisingly, proteoliposomes containing purified Drosophila ATL alone formed an elaborate network upon GTP addition (Figure 2.4F and Figure A.10F, Appendix A). Network formation was not observed in a previous study, likely because the sample was too dilute (Liu et al., 2015). As before, network maintenance required continuous membrane fusion; when GTPγS was added to a preformed network, it rapidly disassembled (Figure 2.4G). Lowering the ATL concentration reduced network formation, but did not make it dependent on curvature-stabilizing proteins (not shown). These results suggest that ATL not only mediates fusion, but also stabilizes high membrane curvature. To test this idea, we used a fusion-defective ATL mutant (ATL^{K51A}) (Orso et al., 2009) that on its own no longer formed a network (Figure 2.4H). However, when co-reconstituted with Sey1p, ATL^{K51A} supported GTP-dependent network formation, indicating that it retained its curvature-stabilizing activity (Figure 2.4I). *In vivo*, ATL probably only mediates fusion, while the more abundant Rtn and REEP/Yop1p proteins stabilize curvature. Because Sey1p cannot form networks on its own, it might have a lower curvature-stabilizing activity than ATL. However, it is also possible that it does not reach sufficiently high concentrations in our reconstituted vesicles, as flotation experiments show it is less efficiently incorporated into liposomes (Figures A.3M,N, Appendix A). Interestingly, the network formed with ATL alone could not be visualized by EM, likely because the tubules did not survive the harsh negative-staining protocol (Figure 2.3E). In contrast, networks were visible when the proteoliposomes contained both ATL and *S. cerevisiae* Yop1p (Figures 2.3F,G) or ATL and *D. melanogaster* Rtnl1 (Figure A.9, Appendix A). Thus, the presence of high concentrations of curvature-stabilizing proteins makes the tubules more mechanically robust.

2.4 Discussion

Our results show that a tubular ER network can be reconstituted with a surprisingly small set of membrane proteins. The network corresponds to a steady state of continuous membrane fusion and fragmentation. Fusion is mediated by the membrane-bound GTPases ATL or Sey1p, whereas fragmentation is likely caused by the curvature-stabilizing proteins of the Rtn and REEP/Yop1p families, which seem to prefer the higher membrane curvature of small vesicles to that of tubules. In a steady state network, fusion by the GTPases appears to be faster than the breakage of tubules or the shedding of small vesicles by the curvature- stabilizing proteins, explaining why tubule fission is a rare event *in vivo*. Our *in vitro* results are in agreement with recent experiments in mammalian cells, which demonstrate that ATL inactivation or overexpression of Rtn4a results in ER fragmentation (Wang et al., 2016). Our results also show that, as in intact cells, the reconstituted network is dynamic, consisting of sliding and fusing three-way junctions. *In vivo*, these movements are caused by the attachment of the ER to the cytoskeleton or molecular motors, whereas *in vitro*, they may be due to thermal convection in conjunction with focal attachment of the network to the cover slip. We speculate that both the continuous formation and disassembly of the ER network and the dynamics of tubular junctions may allow the rapid adaptation of ER shape to different conditions. For example, it may contribute to the conversion of tubules to sheets during the cell cycle and may explain changes of ER morphology during cell differentiation. We propose that other organelles are shaped by similar principles as the ER, representing a steady state between formation and disassembly mediated by a small set of proteins.

2.5 Materials and Methods

2.5.1 Plasmids

Codon-optimized *D. melanogaster* (Dm) ATL (NM_001300577.1) and *S. cerevisiae* SEY1 (NM_001183584.1) were cloned into pGEX-6P-1 and pGEX-4T-3 as described previously (Anwar et al., 2012; Bian et al., 2011). Site-directed mutagenesis was used to generate the mutant DmATL^{K51A}.To generate a GFP-SEY1 fusion protein, SEY1 was cloned into the pET28b vector engineered with an N-terminal streptavidin binding protein (SBP) tag followed by a tobacco etch virus (TEV) protease cleavage site and super-folder GFP. *S. cerevisiae* (Sc) YOP1 (NM_001184125.1) and ScRTN1 (NM_001180541.3) were both cloned into the pRS426 vector with a Gal1 promoter and a CYC1 terminator. The vector also contains a N-terminal His_{14} tag and a TEV protease cleavage site. Both genes are tagged with a C-terminal sortase sequence. *D. melanogaster* reticulon-like1 (Rtnl1; NM_001169405), *X. laevis* REEP4 (codon optimized for *E. coli*; NM_001093429), and *X. laevis* REEP5 (NM_001096221.1) were cloned into the NdeI and XhoI restriction sites of a modified pET21b vector that included a C-terminal 3C protease site followed by a His_{10} tag. The *D. melanogaster* REEP homolog CG8331 (AY069293.1) was cloned into the pFastBac1 vector with a TEV protease site and a (SBP) tag at the C-terminus.

2.5.2 Protein expression and purification

ScYop1p and ScRtn1p were expressed and purified as C-terminal sortase fusion proteins in *S. cerevisiae*. Cells were first grown in synthetic complete media selecting for the appropriate plasmid to stationary phase to deplete glucose at 30 °C. Galactose was then added to 2% to induce the expression of the proteins at room temperature for 16 hrs. Cells were collected, washed once in water and resuspended in lysis buffer (20 mM Tris pH 7.5, 300 mM NaCl, 10%

glycerol, 20 mM imidazole, 1 mM phenylmethylsulfonyl fluoride (PMSF) and protease inhibitors). Cells were lysed in a bead beater for 30 min at 4 °C. The lysate was centrifuged at low speed to clear cellular debris and unbroken cells and then at 100,000 g for 1 hr to sediment the membranes. Membranes were washed twice with lysis buffer and then solubilized in lysis buffer containing 1% n-dodecyl-b-maltoside (DDM) for 1 hr at 4 °C. Insoluble material was removed by centrifugation at 100,000 g for 1 hr and the resulting supernatant was incubated with Ni-NTA resin (Qiagen) for 1-2 hrs. Proteins were eluted using lysis buffer containing 250 mM imidazole and 0.03% DDM and incubated with TEV protease overnight at 4 °C to remove the His_{14} tag. Proteins were further purified by size-exclusion chromatography on a Superdex200 column (GE Healthcare) and concentrated by ultrafiltration (Amicon Ultra, EMD Millipore). Absorbance at 280 nm was used to determine concentrations of the proteins purified using DDM.

D. melanogaster ATL, *S. cerevisiae* Sey1p, GFP-Sey1p, *D. melanogaster* Rtnl1, *X. laevis* REEP4, and *X. laevis* REEP5 were expressed in *E. coli* BL21-CodonPlus (DE3)-RIPL (Agilent). Expression was induced at OD_{600} ~ 0.6-1.0 with 250 μM isopropyl-β-D-thiogalactopyranoside (IPTG) at 16 °C for 16-18 hrs. The lysis buffer used for GFP-Sey1p did not contain glycerol, which interferes with the binding of SBP tag to the streptavidin agarose resin. Cells were lysed either by sonication or through high-pressure homogenization in an M-110P microfluidizer (Microfluidics). The subsequent purification steps were similar to what was described for ScYop1p and ScRtn1p purification with some minor differences. Membranes were washed once with buffer and then solubilized for 1 hr with 1% DDM, except for DmATL, which was solubilized with 1% Triton X-100 (TX-100). The clarified supernatant was passed over the appropriate affinity-resin for 1-2 hrs to bind the tagged protein—Ni-NTA resin in the case of REEP4, REEP5, and DmRtnl1; glutathione agarose in the case of Sey1p and DmATL;

streptavidin agarose resin in the case of GFP-Sey1p. The proteins were eluted from the affinity-resin by on-column cleavage of the affinity tags. 3C protease was used to cut off all tags except in the case of Sey1p and GFP-Sey1p, for which thrombin and TEV protease was used, respectively. All proteins were further purified by size-exclusion chromatography. For DmATL, which was purified in TX-100, protein concentration was measured using a 660 nm Protein Assay (Thermo Scientific Pierce).

The pFastBac1 vector containing the CG8331-SBP gene was first transformed into DH10Bac cells to obtain the recombinant bacmid. The isolated bacmid was used to infect Sf9 insect cells and P0 virus was collected after 4-5 days. The viral stock was amplified to the P3 virus stage. The expression of the fusion protein was examined after each amplification step by immunostaining the infected Sf9 cells with a SBP antibody (Millipore). The P3 virus was used to infect 500 ml of Sf9 insect cells and cells were collected 48 hrs post-infection at 1,000 g for 10 min. Cells were broken by passing them through a dounce homogenizer fifty times and the homogenate was centrifuged at 5,000 rpm for 15 min to remove unbroken cells and debris. The subsequent purification steps were performed in TX-100 and the SBP tag was removed by on-column TEV cleavage, as described above.

2.5.3 Labeling of *S. cerevisiae* Yop1p with Alexa Fluor 647 dye

Purified ScYop1p was mixed with Alexa Fluor 647 NHS ester dye (Thermo Fischer Scientific) at a 1:1 protein:dye molar ratio and incubated at room temperature for 1 hr. The labeling reaction was quenched by addition of 100 mM Tris pH 8.0. After an incubation of 1 hr at 4 °C, excess dye was removed by passing the sample over Sephadex G-50 resin (GE healthcare). The labeled protein was collected and concentrated by ultrafiltration using a 50,000 MW cut-off filter (Amicon Ultra, EMD Millipore). The labeling efficiency was ~50%, as

calculated by comparing the absorbance of the protein at 280 nm and the absorbance of the dye using the pre-configured "Proteins & Labels" function on a Nano Drop 2000c Spectrophotometer (Thermo Scientific).

2.5.4 Preparation of liposomes

All lipids were obtained as chloroform stocks from Avanti Polar Lipids. For fusion assays, donor and acceptor liposomes had a lipid composition as described previously (Faust et al., 2015) with minor modification. Donor liposomes consisted of 65:17:15:1.5:1.5 mole percent of 1-palmitoyl-2-oleoyl-sn-glycero-3-phosphocholine (POPC): 1,2-dioleoyl-*sn*-glycero-3-phosphoethanolamine (DOPE): 1,2-dio-leoyl-sn-glycero-3-phosphoserine (DOPS): NBD-1,2-dipalmitoyl-sn-glycero-3-phosphoethanolamine (NBD-DPPE): rhodamine-DPPE. Acceptor liposomes consisted of 65:18.5:15:1.5 mole percent of POPC:DOPE:DOPS:dansyl-DPPE. For confocal fluorescence microscopy experiments, synthetic liposomes consisting of 65:18.5:15:1.5 mole percent of POPC:DOPE:DOPS: 1,2-dioleoyl-*sn*-glycero-3-phosphoethanolamine-N-[lissamine rhodamine B sulfonyl] (Rh-PE), or *E. coli* extract liposomes consisting of 98.5:1.5 mole percent of *E. coli* Polar Lipid Extract:Rh-PE, or *S. cerevisiae* extract liposomes consisting of 98.5:1.5 mole percent Yeast Polar Lipid Extract (*S. cerevisiae*):Rh-PE were used. For electron microscopy experiments, liposomes consisting of 60:33.4:6.6 mole percent of 1,2-dioleoyl-*sn*-glycero-3-phosphocholine (DOPC):DOPE:DOPS were used.

All chloroform lipid mixtures were first dried under a nitrogen stream and then under vacuum overnight to yield a thin lipid film. These lipid films were hydrated in A100 buffer (25 mM HEPES, pH 7.5, 100 mM KCl, 10% glycerol, 1 mM EDTA, 2 mM b-mercaptoethanol) and subjected to 10 freeze-thaw cycles in liquid N_2 and water at room temperature. For the fusion assay and confocal fluorescence microscopy experiments, liposomes were extruded 21 times

through polycarbonate filters of 100 nm pore size using a mini-extruder (Avanti Polar Lipids) at room temperature. For the EM experiments, the liposomes were used without extrusion.

2.5.5 Reconstitution of protein into liposomes

Detergent-mediated reconstitution was used to integrate all proteins into liposomes as previously described (Bian et al., 2011; Orso et al., 2009; Rigaud and Levy, 2003). Briefly, liposomes and protein were incubated together at the desired protein:lipid ratio in A100 buffer. This mixture was supplemented with DDM such that the final estimated detergent concentration was ~0.1%. The mixture was incubated at room temperature for 30 min. The detergent was then removed by four successive additions Bio-Beads SM-2 Resin (Bio-Rad) over the course of 4 hrs. Insoluble aggregates were removed by centrifugation. To examine the reconstitution efficiency, an aliquot was floated in a 0-40% w/v Nycodenz step-gradient and fractions were collected and analyzed by SDS-PAGE. To determine the orientation of proteins inserted into liposomes, equal volumes (5 μl) of proteoliposomes were incubated with a decreasing amounts of trypsin (0.2, 0.04, 0.008 and 0.0016 μg) in the absence or presence of 0.2% Triton-X 100 for 30 min at room temperature. Reactions were stopped by PMSF and SDS-containing protein loading dye, and analyzed by SDS-PAGE.

2.5.6 Lipid-mixing fusion assay

Fusion assays were performed as previously described (Bian et al., 2011) with the modifications of the lipid compositions of donor and acceptor liposomes described above. Briefly, Sey1p and Yop1p were reconstituted at the indicated protein:lipid ratios into donor and acceptor liposomes in the presence of A100 buffer containing 0.1% DDM at room temperature. Donor vesicles contained NBD-PE and rhodamine-PE. After detergent removal by Bio-Beads SM-2 Resin (Bio-Rad), samples were spun once to remove insoluble material. Lipid

concentration was determined based on rhodamine or dansyl fluorescence. Donor and acceptor liposomes were mixed in a 1:3 ratio in the presence of A100 buffer containing 5 mM $MgCl_2$. Data were subsequently collected every minute using a Flexstation III (Molecular Devices) at 37 °C. Pre-fusion data were collected during the first 10 min. The average of the pre-fusion data was set as the baseline fluorescence value. Buffer or 1 mM GTP was added to the reactions and the dequenching of NBD fluorescence data caused by the fusion of donor and acceptor vesicles was followed for 40 min. Triton-X 100 was then added to a final concentration of 2.5% and the reactions further incubated for 10 min to determine maximum fluorescence. The difference between the average of the maximum fluorescence data and the baseline value is defined as "total fluorescence". The difference between the fusion data and the baseline value was then expressed as the percentage of the total fluorescence.

2.5.7 Imaging of reconstituted networks by confocal fluorescence microscopy

To test for network formation, a proteoliposome solution was supplemented with 5 mM $MgCl_2$ prior to addition of any nucleotide. Then, either 2 mM GTP, 2 mM GTPγS, or A100 buffer was added to the proteoliposome solution and the reaction was incubated for 1-2 min at room temperature. Three μl of sample was placed between two PEG-passivated No. 1.5 coverslips, which were mounted onto a metal slide and sealed with VALAP (1:1:1 mixture of vaseline, lanolin and paraffin). The coverslips were passivated with 5,000 MW polyethylene glycol (PEG) as previously described (Wang et al., 2013). After mounting, the samples were incubated at room temperature for 10-20 min prior to imaging. All fluorescence microscopy samples were visualized using a spinning disk confocal head (CSU-X1; Yokogawa Corporation of America) with Borealis modification (Spectral Applied Research) and a quad bandpass 405/491/561/642 dichroic mirror (Semrock). The confocal was mounted on a Ti motorized

inverted microscope (Nikon) equipped with a 60× Plan Apo NA 1.4 oil immersion objective or a 40x Plan Fluor NA 1.3 oil immersion objective and the Perfect Focus System for continuous maintenance of focus (Nikon). Green fluorescence images were collected using a 488-nm solid-state laser, controlled with an AOTF (Spectral Applied Research) and ET525/50 emission filter (Chroma Technology Corp.). Red fluorescence images were collected using a 561-nm solid-state laser controlled with an AOTF and ET620/60 emission filter. Far-red fluorescence images were collected using a 642-nm solid-state laser controlled with an AOTF and ET700/75 emission filter. The laser lines are combined in an LMM5 laser merge module (Spectral). All images were acquired with a cooled CCD camera (ORCA R2; Hamamatsu Photonics) controlled with MetaMorph software (version 7.0; Molecular Devices) and archived using ImageJ (National Institutes of Health). In some cases, linear adjustments were applied to enhance the contrast of images.

For network disassembly, reconstituted networks were first formed using GTP and spotted onto a passivated coverslip. GTPγS at the desired concentration was added to the solution on the coverslip immediately prior to sandwich-sealing the sample with VALAP and imaging. The time between GTPgS addition and taking the first image was about 1.5 min.

2.5.8 Imaging of reconstituted networks by negative-stain electron microscopy

For negative stain electron microscopy analysis, samples were prepared as previously described (Hu et al., 2008). Briefly, 5 µl of proteoliposome solution was mixed with 7.5 µl of buffer A100 supplemented with 5 mM $MgCl_2$. Buffer or 1 mM GTP were then added and the reactions incubated for 20 min at room temperature. Subsequently, 0.5 µl of sample was mixed with 4.5 µl of buffer A100 and added to a glow-discharged carbon-coated copper grid (Pelco, Ted Pella Inc.) for 1 min. Excess sample was then blotted off with filter paper, the grids washed

twice with deionized water, and then stained twice with freshly prepared 1% uranyl acetate. Images were collected at room temperature using a conventional transmission electron microscope JEOL 1200EX equipped with a Tungsten filament and operated at an acceleration voltage of 80 kV. All images were acquired using an AMT 2kCCD camera.

2.5.9 ER network formation with *Xenopus* egg extracts

The interphase ER network was formed using the crude *Xenopus* egg extracts as described previously (Wang et al., 2013). The network was stained with $DiOC_{18}$ and visualized by a spinning-disk confocal microscope.

2.5.10 Representative images

Images shown are representative of all images collected. For Figure 2.1, images are representative of **A,** 98 (left) and 108 (right), **B,** 15, **C,** 108 **D,** 30 **E,** 10, **F,** 30 total images captured. For Figure 2.2, images are representative of **A,** 18 (left) and 30 (right), **B,** total 36 images captured. For Figure 2.3, Images are representative of **A,** 21 (left) and 25 (right), **B,** 7 (left) and 17 (right), **C,** 12 (left) and 15 (right), **D,** 78 (left) and 52 (right), **E,** 10 (left) and 10 (right), **F,** 9 (left) and 23 (right), **G,** 5 (left) and 20 (right) total images captured. For Figure 2.4, images are representative of **A,** 20, **B,** 23, **C,** 21, **D,** 27, **E,** 15, **F,** 20, **G,** 20, **H,** 18, **I,** 32 total images captured. For Figure A.5, images are representative of 108 total images captured. For Figure A.6, images are representative of **A,** 11 (left) and 10 (right), **B,** 15 and **C,** 10 total images captured. For Figure A.7, images are representative of **A,** 15 (left) and 25 (right), **B,** 13 (left) and 20 (right) total images captured. For Figure A.8, images are representative of **A,** 10 (left) and 25 (right), **B,** 12 (left) and 34 (right) total images captured. For Figure A.9, images are representative of **A,** 25, **B,** 17 **C,** 17 **D,** 6 (left) and 12 (right), **E,** 5 (left) and 6 (right) total

images captured. For Figure A.10, images are representative of **A,** 18, **B,** 10, **C,** 14, **D,** 17, **E,** 13, **F,** 11, **G,** 12, **H,** 10 total images captured.

2.6 Acknowledgements

We thank Hanna Tukachinsky for help with protein purifications, Misha Kozlov for stimulating discussions, Andrea Daga for material, the Nikon Imaging Center at Harvard Medical School, the Harvard Medical School EM facility, and the ICCB Longwood Screening Facility for help. We thank Misha Kozlov, Junjie Hu, and Hanna Tukachinsky for critical reading of the manuscript. R.E.P. is supported by NIGMS T32 GM008313 training grant. S.W. is supported by a fellowship from the Charles King Trust. T.A.R. is a Howard Hughes Medical Institute Investigator.

2.7 Author contributions

R.E.P. and S.W. performed all experiments. Initial tests of Sey1p and Yop1p co-reconstitution were performed by T.Y.L. R.E.P., S.W., and T.A.R. designed the experiments and wrote the paper. T.A.R. supervised the project. The authors declare no competing interests.

3

Towards a structure of a curvature-stabilizing protein of the tubular ER network

3.1 Abstract

The reticulon and Yop1/REEP proteins generate and stabilize positive membrane curvature within the tubular endoplasmic reticulum network. These integral membrane proteins contain wedge-shaped transmembrane domains, which force the outer membrane leaflet to expand, as well as a C-terminal amphipathic helix—two characteristics that are believed to induce membrane curvature. However, a lack of an atomic-resolution structure of any of these proteins has left their exact mechanism of curvature generation and stabilization unknown. Unfortunately, given their small size and lack of hydrophilic surfaces, the reticulons and Yop1/REEP proteins represent a difficult target for structural studies. To this end, I sought to use new tools that have been adapted for membrane protein crystallization to attempt to obtain a structure of REEP5. These tools included lipidic cubic phase crystallization (LCP) techniques, as well as nanobody-aided crystallization. While initial LCP crystallization experiments failed to

yield any crystals, I successfully isolated a large number of nanobodies that bind to REEP5 with high affinity using an *in vitro* yeast display system. These nanobodies will be useful in future crystallization as well as *in vitro* biochemical experiments aimed at understanding REEP5 function.

3.2 Introduction

Despite the overwhelming *in vivo* and *in vitro* evidence that the reticulon and Yop1/REEP proteins stabilize high curvature (Hu et al., 2008; Voeltz et al., 2006; Westrate et al., 2015), how this stabilization is actually accomplished at the molecular level is still not completely understood. The reticulon and Yop1/REEP proteins are characterized by two extended hydrophobic segments, approximately 35 amino acids in length (Hu et al., 2008; Voeltz et al., 2006). This domain, known in the reticulon proteins as the reticulon homology domain (RHD), has been proposed to constitute hydrophobic hairpins that fail to traverse the membrane completely and that form a wedge-like structure (Hu et al., 2008; Shibata et al., 2010; Figure 3.1). This wedge would cause expansion of the outer leaflet of the membrane, leading to the generation of positive curvature (Hu et al., 2011). However, recent NMR experiments have suggested that there are enough hydrophobic and helical residues to span the membrane four times (Brady et al., 2015). Furthermore, a conserved C-terminal amphipathic helix has also been identified as necessary for the generation and stabilization of curvature by reticulon and Yop1/REEP proteins (Brady et al., 2015; Breeze et al., 2016). Finally, the reticulon and Yop1/REEP are known to form higher-order oligomers (Hu et al., 2008; Shibata et al., 2008). These oligomers could potentially create arc-like scaffolds that function to curve the membrane (Hu et al., 2011).

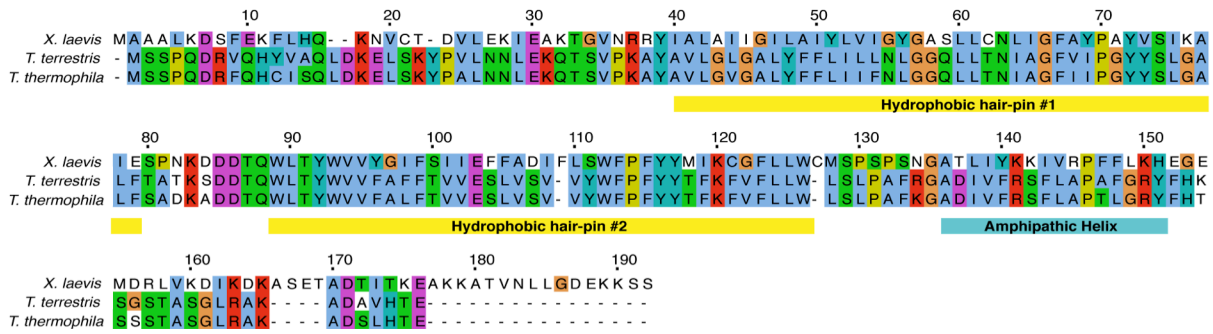

Figure 3.1 Sequence alignment of REEP5 constructs used for crystallization
Sequence alignment of *X. laevis*, *T. terrestris*, and *T. thermophila* REEP5 proteins. Boxes indicate specific sequence features including the two transmembrane hairpin domains and the C-terminal amphipathic helix.

Clearly, there is a lack of structural information about these proteins that prevents an understanding of the mechanism by which they generate membrane curvature. Unfortunately, the relatively small size of these proteins (~20-50 kDa) demands an x-ray crystallographic approach to obtaining high-resolution structural information. Given the nature of these membrane proteins, particularly the lack of a large cytosolic or luminal domain, obtaining a crystal is difficult. To help overcome these challenges and begin to work towards solving a crystal structure, I sought to use new tools available for membrane protein crystallography. These tools included the use of lipidic cubic phase crystallization (LCP) techniques (Cherezov, 2011), as well as nanobody-aided crystallization.

LCP is a lipidic mesophase into which integral membrane proteins can be directly reconstituted for crystallization (Cherezov, 2011). LCP provides a membrane-like environment that can help to stabilize otherwise difficult membrane proteins. Furthermore, since reconstituted protein is free to diffuse within the membrane, type I crystal packing can occur, creating contacts between both the hydrophilic and the hydrophobic portions of the protein, leading to superior crystal order and diffraction (Ishchenko et al., 2017). The most common lipids used for LCP are monoacylglycerols (MAGs) that consist of a hydrophilic glycerol headgroup linked to a

hydrophobic monounsaturated fatty acid chain (Ishchenko et al., 2017). Monoolein has proved the most successful MAG for LCP crystallization. While MAGs are not typically found in native membranes, MAGs can be doped with native lipids, including phospholipids, to further help stabilize membrane proteins for crystallization (Ishchenko et al., 2017).

LCP has been successfully used to determine the crystal structures of several different classes of membrane proteins that previously proved recalcitrant to crystallization using traditional methods (Cherezov, 2011; Ishchenko et al., 2017). Most famously, this has included the GPCR family of membrane proteins (reviewed in Ishchenko et al., 2017; Xiang et al., 2016; Yin et al., 2014). LCP has also been used to determine the structure of a tetraspanin (Zimmerman et al., 2016), a member of a class of proteins that are topologically reminiscent of the reticulon and Yop1/REEP proteins.

Nanobodies have been used to stabilize and increase the available packing surface of various membrane proteins, aiding in their crystallization (Geertsma et al., 2015; Hassaine et al., 2014; Li et al., 2016; Rasmussen et al., 2011a, 2011b; Smirnova et al., 2014). Conventional antibodies comprise two heavy chains and two light chains. Present within each chain is a variable domain (V_H, heavy chain and V_L, light chain) that determines the binding specificity of the antibody. However, the antibodies in camelids comprise only of heavy chains. The antigen specificity of camelid antibodies is determined by a single variable domain called the V_{HH} (Hamers-Casterman et al., 1993; McMahon et al., 2018; Muyldermans, 2013). Single, isolated V_{HH} domains can be easily expressed and purified from *E coli*, making them an attractive tool for both biochemistry and clinical applications (McMahon et al., 2018; Muyldermans, 2013). Typically, to obtain a nanobody specific towards a particular target protein, it was necessary immunize camelid species—a time consuming and expensive endeavor. Excitingly, McMahon

et al. have recently developed a yeast library that displays upwards of 10^8 unique nanobodies and an accompanying protocol that allows for the enrichment of nanobodies against protein targets *in vitro* using standard cell sorting techniques (McMahon et al., 2018). Each nanobody contains a constant scaffold and three variable loops (CDR1, CDR2, and CDR3) that create specificity in target binding. McMahon et al. (2018) demonstrated that the library can be used to isolate conformational-specific nanobodies with high binding affinity to both soluble and membrane protein targets.

Informed by my network reconstitution experiments, I decided to pursue *Xenopus laevis* REEP5 as a target for crystallization based on its superior behavior during protein purification and network formation. In this chapter, I detail my initial experiments towards obtaining a structure of REEP5. These experiments include isolating nanobodies that bind to REEP5 with high affinity and using these nanobodies in preliminary LCP and vapor diffusion experiments. Furthermore, I also demonstrate that REEP5 homologues derived from thermophilic yeast species can be obtained from *E. coli* in large amounts with high purity. Informed by my experiences with *X. laevis* REEP5, I also isolated nanobodies that bind to these thermophilic homologues with high affinity, and demonstrated that particular sets of these nanobodies can bind simultaneously to REEP5. These nanobodies will undoubtedly prove useful in future crystallographic and biochemical experiments.

3.3 Results

3.3.1 Isolating nanobodies that bind to *Xenopus laevis* REEP5

To isolate nanobodies that specifically bind to *X. laevis* REEP5 using the yeast display protocol of McMahon et al. (2018), I first generated fluorescently labeled *X. laevis* REEP5. I labeled two aliquots of *X. laevis* REEP5, which was solubilized using the detergent n-Dodecyl-β-

D-Maltoside (DDM) and purified using a C-terminal HIS_{10} tag. One aliquot was labeled using an N-Hydroxysuccinimide (NHS) conjugated Alexa 647 fluorophore ($REEP5_{647}$) and the other aliquot was labeled with an NHS conjugated Fluorescein isothiocyanate (FITC) fluorophore ($REEP5_{FITC}$). The NHS conjugated fluorophores can label REEP5 at the nineteen lysine residues present along the length of the protein.

Using $REEP5_{647}$ and $REEP5_{FITC}$, I performed two consecutive rounds of magnetic activated cell sorting (MACS) with magnetic beads conjugated to antibodies against each fluorophore. To reduce potential enrichment of nanobodies directed against Alexa-647, I preformed the initial selection using 1 µM of $REEP5_{FITC}$, followed by a subsequent selection using 1 µM $REEP5_{647}$.

Unfortunately, after these two rounds of selection, fluorescent flow cytometry analysis revealed a high level of nonspecific binding between REEP5 and yeast cells that were not expressing nanobodies on the cell surface (Figure 3.2A). Further control experiments revealed a nonspecific interaction between uninduced yeast cells and $REEP5_{FITC}$ (Figures 3.2B,C). This nonspecific binding makes it impossible to enrich yeast cells expressing nanobodies that bind

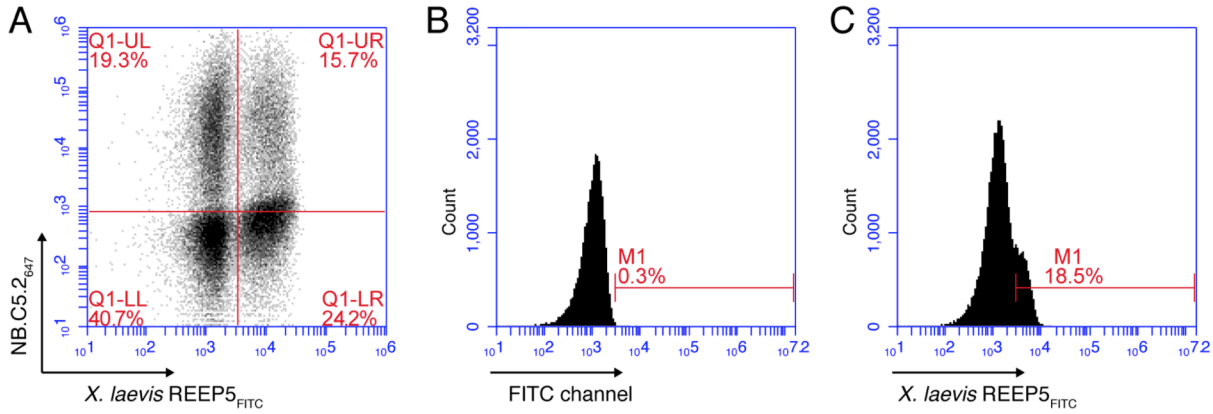

Figure 3.2 *X. laevis* $REEP5_{FITC}$ nonspecifically binds to yeast cells
Fluorescent flow cytometry analysis of **(A)** induced yeast stained with a Alexa 647-labeled anti-HA antibody ($anti\text{-}HA_{647}$) and a FITC-labeled *X. laevis* REEP5 ($REEP5_{FITC}$), **(B)** unstained, uninduced yeast, and **(C)** uninduced yeast stained with $REEP5_{FITC}$.

specifically to *X. laevis* REEP5. This nonspecific interaction was not observed for REEP5-647.

At the same time, I began to test the purification of REEP5 using the detergent Lauryl Maltose Neopentyl Glycol (LMNG). LMNG has an extremely low critical micelle concentration (CMC), which makes it useful for LCP experiments, as too much detergent can prevent successful reconstitution of protein into LCP. More generally, LMNG and other neopentyl glycol detergents have also been shown to improve the purification and stability of particular membrane proteins (Sadaf et al., 2015). Furthermore, I also started to test the purification of a *X. laevis* REEP5 construct with a C-terminal streptavidin binding protein (SBP) tag preceded by a TEV cleavage site (REEP5-SBP) to try to improve the overall purity and yield of the prep.

My tests demonstrated that I could solubilize and purify REEP5-SBP using LMNG ($REEP5_{LMNG}$) (Figure 3.3). I further incorporated an ATP wash that helped to remove contaminating chaperones. I was able to elute the REEP5-SBP one of two ways: 1) by adding biotin to the streptavidin column and then adding TEV protease to remove the tag or 2) cleaving the protein off the column by overnight incubation with TEV protease. The protease, which contains a HIS-tag, can then be removed using Ni^{2+} resin.

I then generated a fluorescently labeled $REEP5_{LMNG}$ by labeling the purified protein with NHS-FITC ($REEP5_{LMNG}$ -FITC). Surprisingly, unlike $REEP5_{FITC}$ purified using DDM, $REEP5_{LMNG}$ -FITC did not nonspecifically bind to uninduced yeast (Figure 3.4). Therefore, I restarted the nanobody isolation using $REEP5_{LMNG}$-FITC and $REEP5_{647}$. I performed an initial round of MACS using 1 μM $REEP5_{LMNG}$ -FITC followed by a second round of MACS using 0.5 μM $REEP5_{647}$.

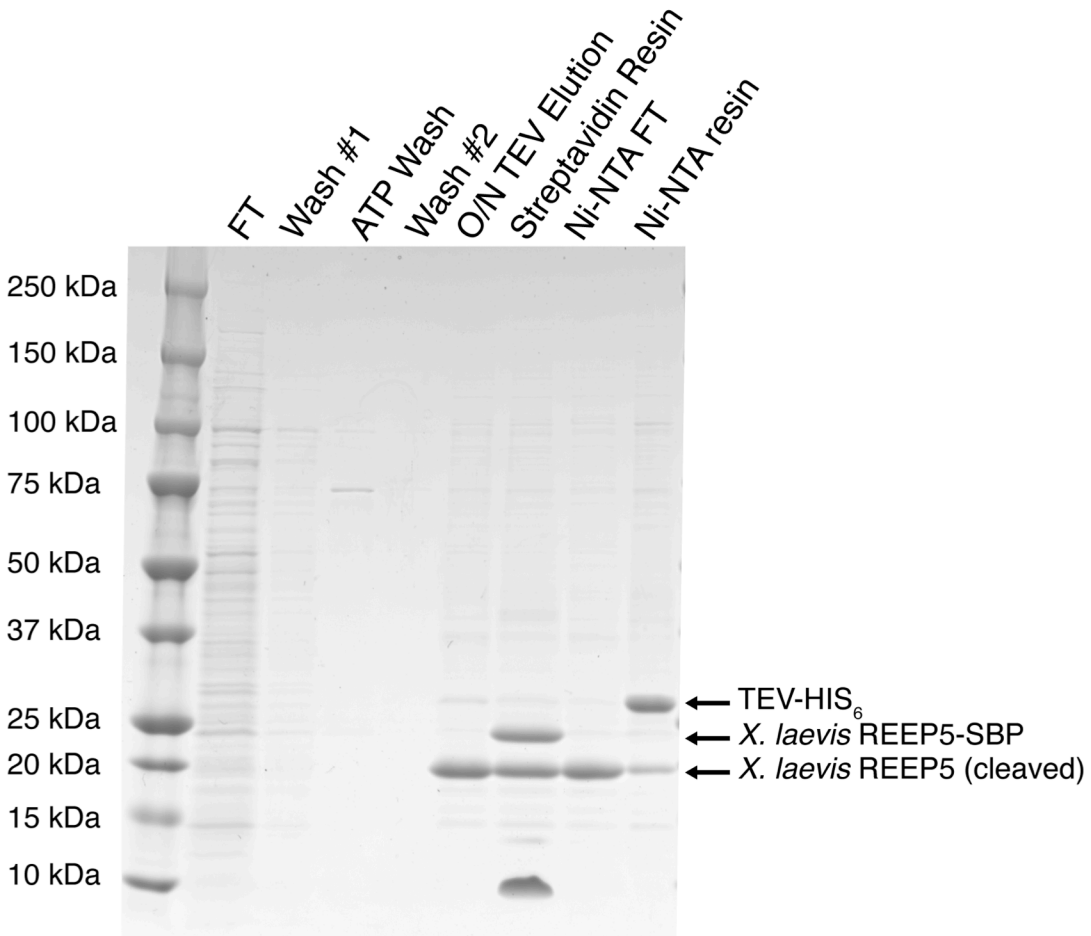

Figure 3.3 Purification of LMNG-solubilized *X. laevis* REEP5-SBP using LMNG
SDS-PAGE analysis of streptavidin-affinity purification of *X. laevis* REEP5-SBP solubilized in LMNG. His-tagged TEV was used to cleave REEP5 off the streptavidin column and then was subsequently removed using Ni-NTA resin.

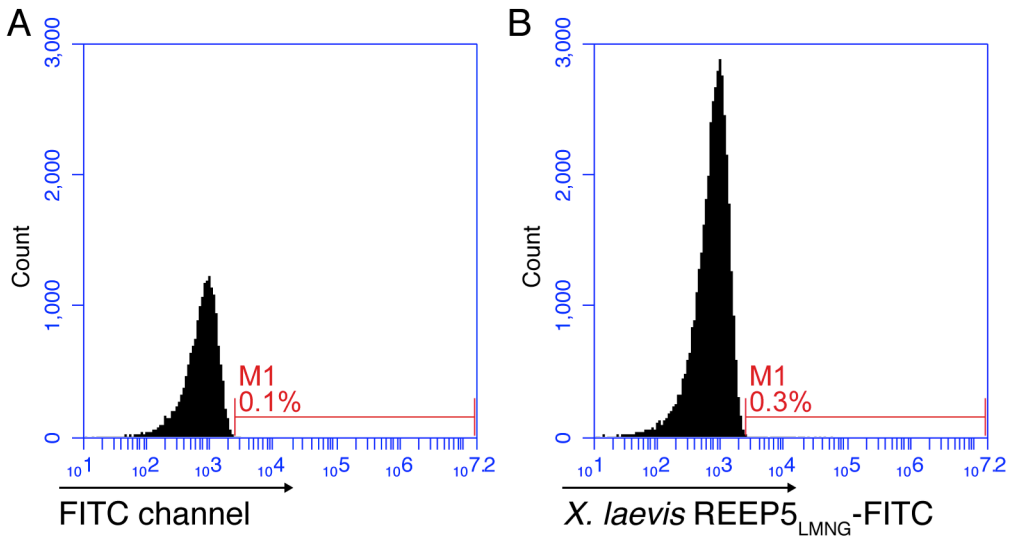

Figure 3.4 $REEP5_{LMNG}$-FITC does not nonspecifically bind to yeast cells
Fluorescent flow cytometry analysis of **(A)** uninduced yeast and **(B)** uninduced yeast stained with $REEP5_{LMNG}$-FITC demonstrates that $REEP5_{LMNG}$-FITC does not bind to uninduced yeast.

However, after these two rounds of MACS, fluorescent flow cytometry analysis using both $REEP5_{LMNG}$ -FITC and $REEP5_{647}$ revealed appreciable binding only to $REEP5_{647}$ (Figures 3.5A,B). This was concerning due to the observation that the nanobodies within the yeast library have a natural proclivity for binding to Alexa fluorophores (A. Kruse, personal communication). To further test whether I had enriched nanobodies that were specifically binding to *X. laevis* REEP5, I purified REEP5-SBP using LMNG, but did not cleave off the tag ($REEP5_{LMNG}$-SBP). I labeled this protein by incubating it with Phycoerythrin (PE)-labeled streptavidin. Using fluorescent flow cytometry, I was able to observe binding of induced yeast to this labeled protein, indicating that I had enriched nanobodies specific to *X. laevis* REEP5 (Figure 3.5C). The lack of signal for $REEP5_{LMNG}$-FITC binding could have been due to the relatively low brightness of the FITC dye.

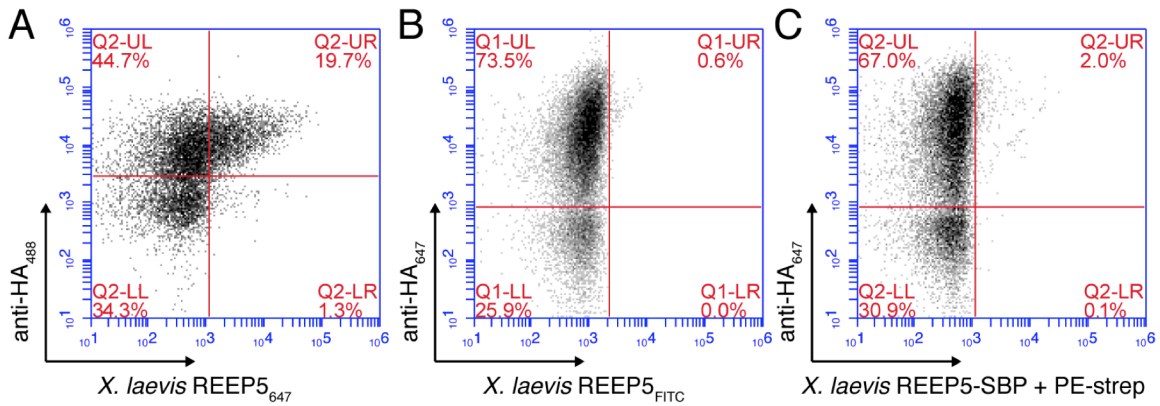

Figure 3.5 Fluorescent flow cytometry results after 2nd MACS round for *X. laevis* REEP5
Induced yeast cells were stained with a combination of either **(A)** a Alexa 488-labeled anti-HA antibody (anti-HA_{488}) and Alexa 647-labeled *X. laevis* REEP5 ($REEP5_{647}$), **(B)** a Alexa 647-labeled anti-HA antibody (anti-HA_{647}) and *X. laevis* $REEP5_{LMNG}$-FITC, or **(C)** anti-HA_{647} and *X. laevis* REEP5-SBP stained with PE-labeled streptavidin (PE-strep), and analyzed using fluorescent flow cytometry.

To ensure enrichment of REEP5 specific nanobodies and to try to eliminate any Alexa-binding nanobodies, I performed a third MACS round using 0.1 µM $REEP5_{LMNG}$-SBP and streptavidin magnetic beads. Fluorescent flow cytometry analysis after this round of MACS revealed robust binding of *X. laevis* REEP5 to induced yeast (Figure 3.6).

I then performed two rounds of fluorescence-activated cell sorting (FACS) to further enrich the nanobodies that bound with high affinity to REEP5. In the first FACS round, I stained induced yeast with a fluorescent anti-HA antibody (to visualize nanobody expression), 0.01 µM $REEP5_{LMNG}$-SBP labeled with PE-streptavidin, and a cytosolic fragment of *D. melanogaster* atlastin labeled using NHS-Alexa 647. By triple staining the yeast, I was able to perform a negative selection against Alexa 647 as another means of avoiding nanobodies that potentially bound to the Alexa dye. I collected only the yeast that showed the strongest HA and $REEP5_{LMNG}$-SBP staining and that did not display Alexa 647 staining.

In the second round of FACS, I stained the yeast with a fluorescent HA antibody and $REEP5_{LMNG}$-SBP labeled with PE-streptavidin, collecting the yeast with the strongest staining in both channels, and sorting single cells into a 96-well plate. I then performed yeast colony PCR

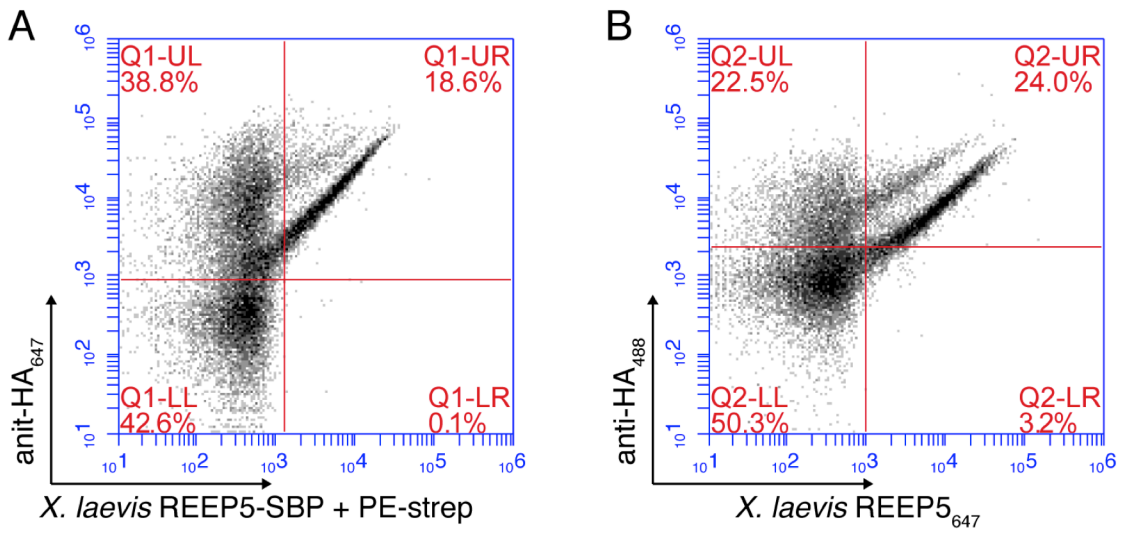

Figure 3.6 Fluorescent flow cytometry results after 3rd MACS round for *X. laevis* REEP5
Induced yeast cells were stained with a combination of either (**A**) a Alexa 647-labeled anti-HA antibody (anti-HA_{647}) and *X. laevis* REEP5-SBP stained with PE-labeled streptavidin (PE-strep) or (**B**) a Alexa 488-labeled anti-HA antibody (anti-HA_{488}) and Alexa 647-labeled *X. laevis* REEP5 ($REEP5_{647}$). During staining, a final concentration of 0.01 μM REEP5 was used.

for each well in the 96-well plate to obtain the sequences of the enriched nanobodies. I identified 5 unique sequences (Nb01-Nb05) (Figure 3.7), which I subsequently cloned into the pet26 plasmid for periplasmic expression in *E. coli* and purification via a HIS-tag.

	CDR1	CDR2	CDR3
NB01	GNISAYYSM	RELVAGIGQGGTTNYA	A--VLPS--------SWDV----FYY
NB02	GSISDFDVM	REFVAAIAYGTTTNYA	A--AYRA--------SWYLWDATHAY
NB03	GNISYIYSM	REFVAAITFGSNTYYA	A--ALFR--------YWSV----YHY
NB04	GSISPYGRM	RELVAAITYGATTNYA	AVDVDPW--------SWYVW--RFLY
NB05	GNIFRYVDM	RELVATITAGTSTYYA	A--VYYWDSIAQGLVYWDF----HTY

Figure 3.7 Sequence alignment of nanobodies isolated against *X. laevis* REEP5
Sequence alignment of CDR1 (left), CDR2 (middle), and CDR3 (right) of nanobodies isolated against *X. laevis* REEP5.

3.3.2 Solution binding tests of nanobodies isolated against *X. laevis* REEP5

To test whether the isolated nanobodies could bind to *X. laevis* REEP5 with high affinity in solution, I performed small-scale expression tests for NB01-NB05. Briefly, *E. coli* cells expressing the nanobodies were osmotically shocked to break open the periplasm and release the nanobody into solution. After removing cellular debris, the periplasmic solution was applied to

Ni^{2+} resin. The Ni^{2+} resin was extensively washed with high salt buffer and the nanobodies were eluted using a high imidazole buffer. Unfortunately, NB03 and NB04 were recalcitrant to purification, as the two proteins precipitated on the Ni^{2+} resin after addition of imidazole (Figure 3.8). I was able to obtain large amounts of NB01, NB02, and NB05. I performed small-scale binding experiments by incubating purified, LMNG-solubilized *X. laevis* REEP5 with a 5 molar excess of NB01, NB02, or NB05. The REEP5-nanobody mixture was then analyzed using analytical size exclusion chromatography (SEC) and SDS-PAGE. While NB01 did not co-elute with *X. laevis* REEP5 (Figure 3.9), NB02 (Figure 3.10) and NB05 (Figure 3.11) displayed strong binding.

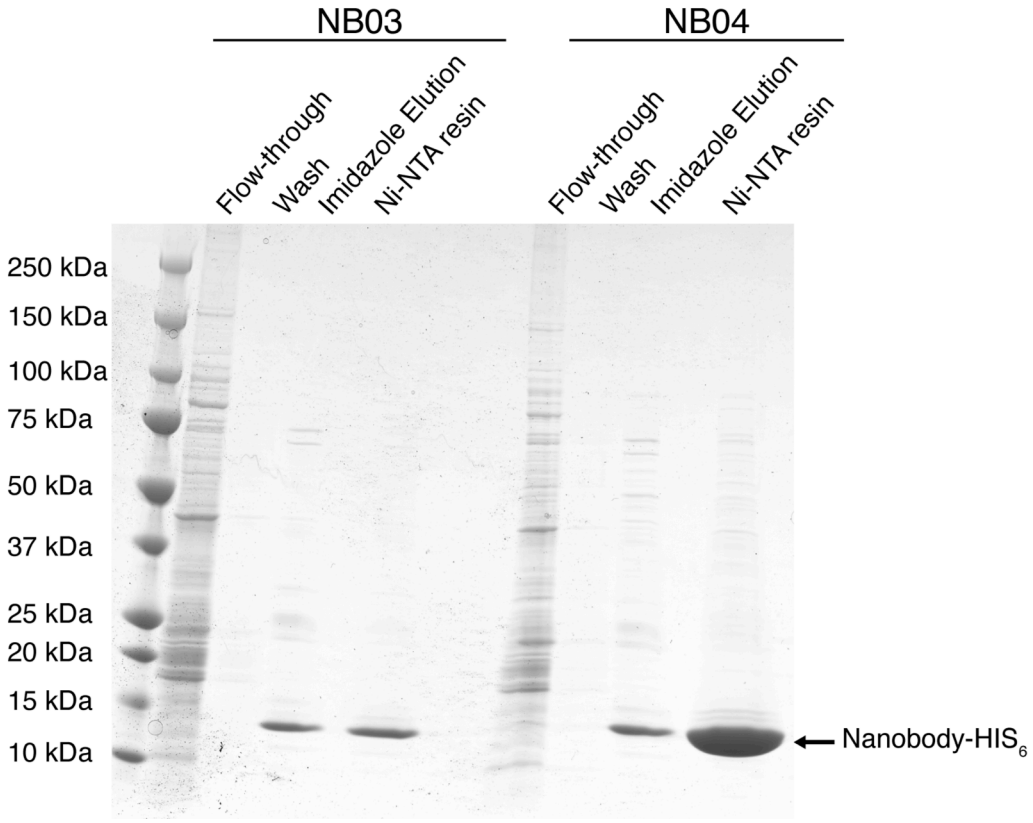

Figure 3.8 NB03 and NB04 are recalcitrant to purification from *E. coli*
SDS-PAGE analysis of a test purification of NB03 and NB04 from *E. coli*.

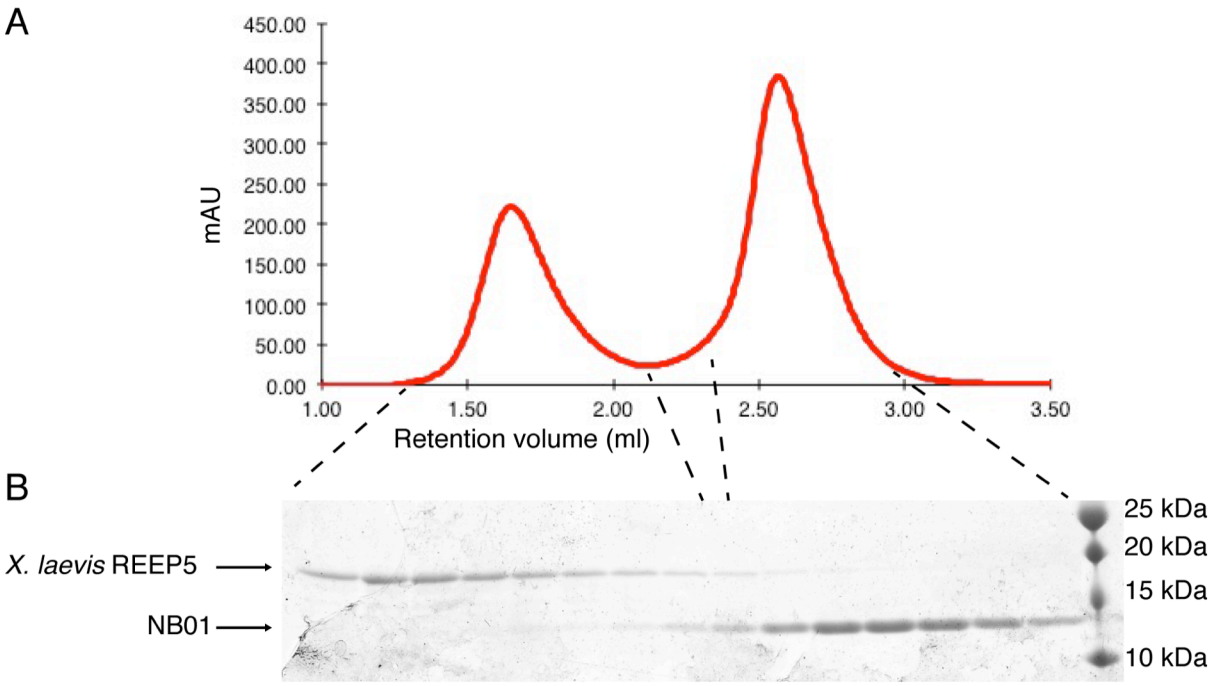

Figure 3.9 NB01 does not bind to *X. laevis* REEP5 in solution

A) Chromatogram of analytical SEC using a Superdex200 column to test the binding of NB01 to *X. laevis* REEP5. The first peak (highlighted) was analyzed using SDS-PAGE analysis (**B**) to determine if NB01 co-eluted with *X. laevis* REEP5 during analytical SEC, indicating binding of the nanobody to REEP5.

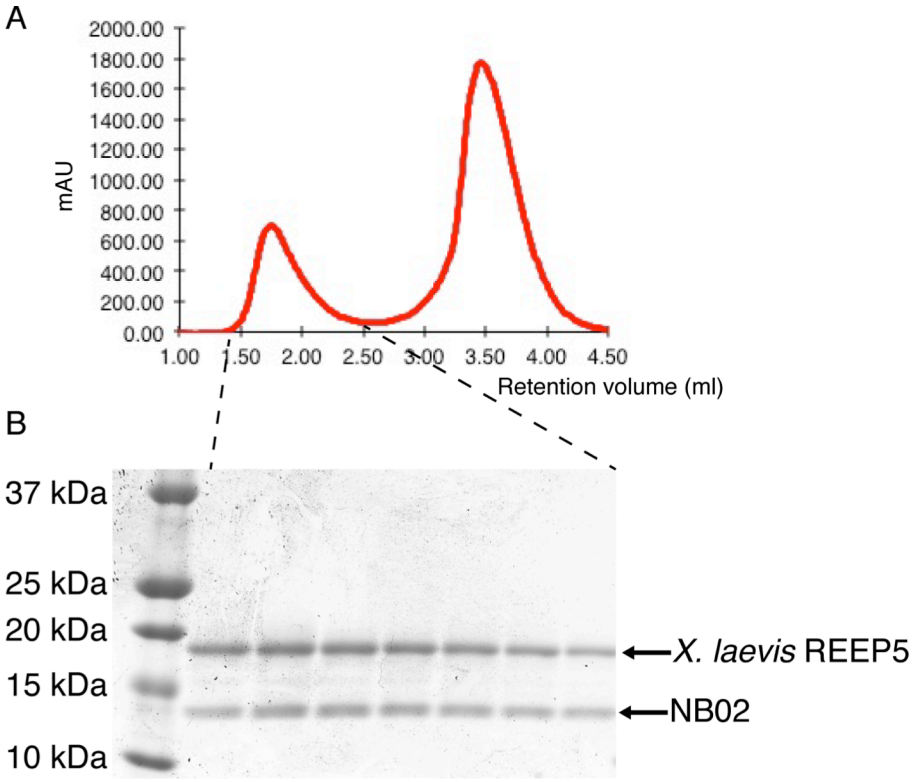

Figure 3.10 NB02 binds to *X. laevis* REEP5 in solution with high affinity
A) Chromatogram of analytical SEC using a Superdex200 column to test the binding of NB02 to *X. laevis* REEP5. The first peak (highlighted) was analyzed using SDS-PAGE analysis (**B**) to determine if NB02 co-eluted with *X. laevis* REEP5 during analytical SEC, indicating binding of the nanobody to REEP5.

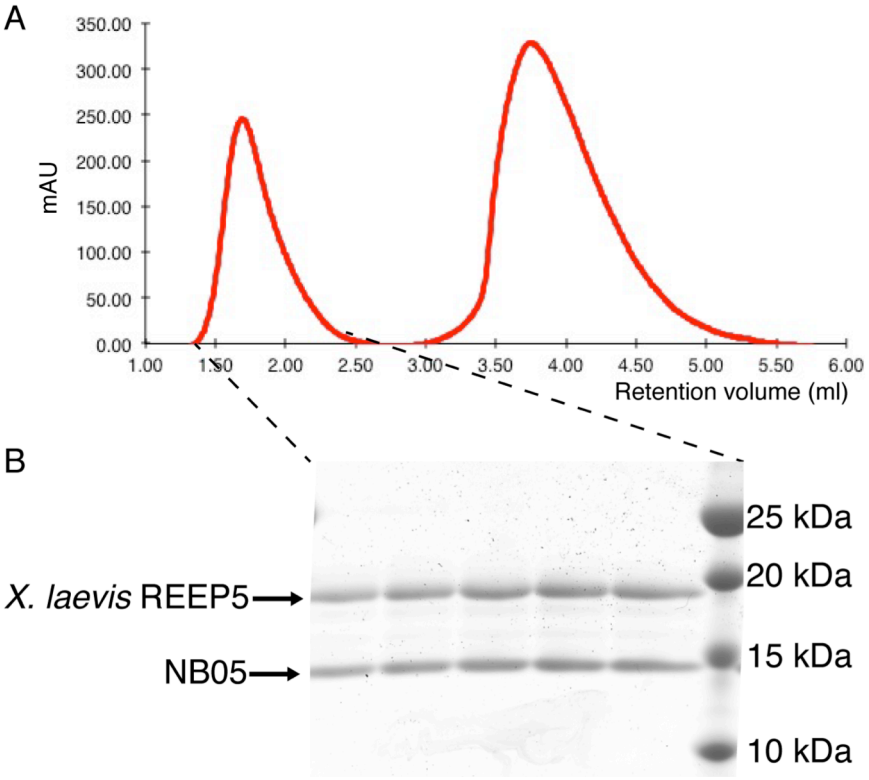

Figure 3.11 NB05 binds to *X. laevis* REEP5 in solution with high affinity
A) Chromatogram of analytical SEC using a Superdex200 column to test the binding of NB05 to *X. laevis* REEP5. The first peak (highlighted) was analyzed using SDS-PAGE analysis (**B**) to determine if NB05 co-eluted with *X. laevis* REEP5 during analytical SEC, indicating binding of the nanobody to REEP5.

3.3.3 Preliminary crystallization experiments with *X. laevis* REEP5

Given these positive results, I scaled up the purification of the NB02-REEP5 complex and the NB05-REEP5 complex to obtain protein amounts suitable for crystallographic trials. I purified the nanobodies and REEP5 separately using affinity chromatography and then incubated the two proteins together prior to final SEC purification (Figures 3.12 and 3.13). After SEC, I concentrated the purified nanobody-REEP5 complexes to ~40 mg/ml and mixed the protein with monoolein to reconstitute the complex into LCP. I then prepared a large number of LCP crystallization experiment using sparse matrix screens. I also preformed vapor diffusion crystallization experiments with the detergent solubilized complexes. Unfortunately, these crystallization trials have yet to produced any protein crystals.

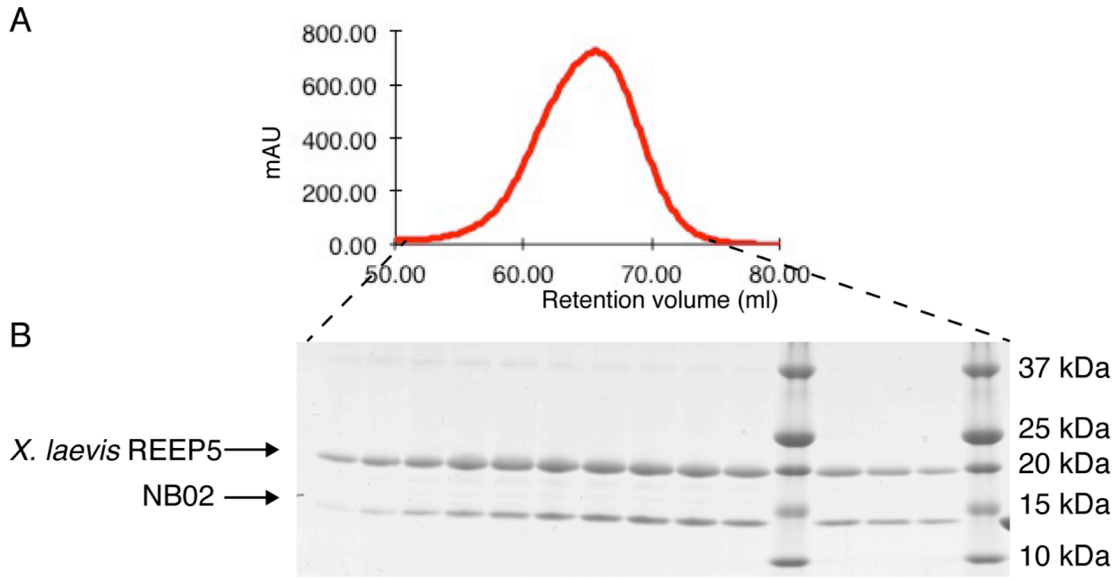

Figure 3.12 Large-scale purification of NB02-*X. laevis* REEP5 complex for crystallography
A) Chromatogram and **B)** SDS-PAGE analysis of the SEC purification using a Superdex200 column of the NB02-*X. laevis* REEP5 complex for crystallography. REEP5 was solubilized in LMNG, affinity purified, and incubated with a ~5 molar excess of NB02 prior to SEC purification.

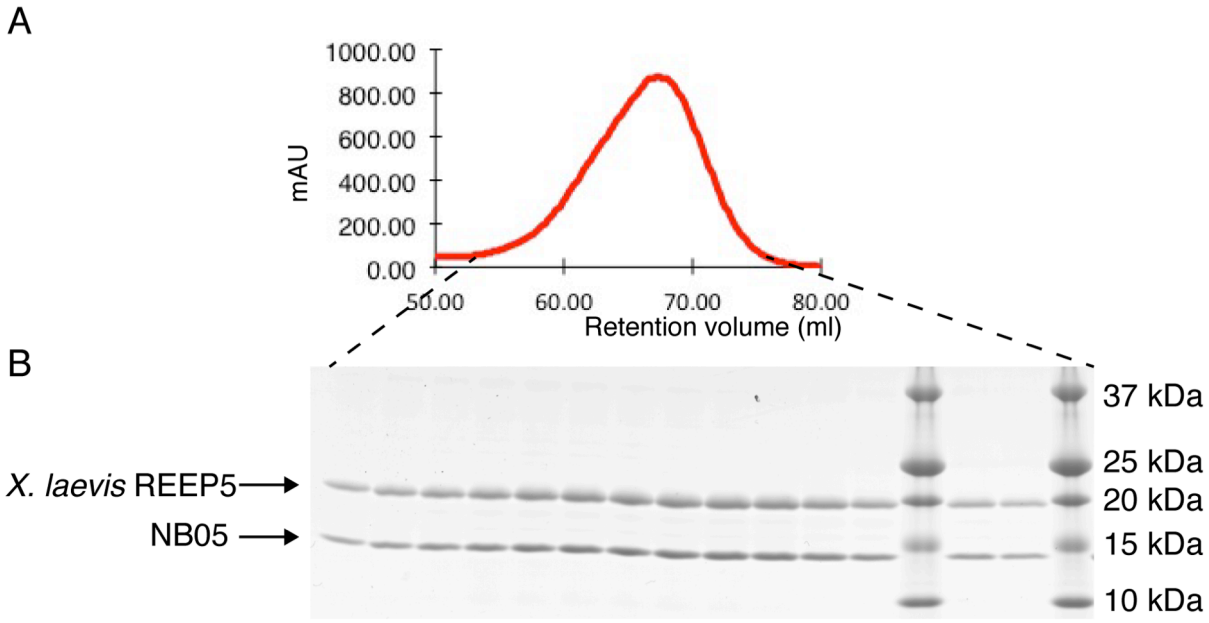

Figure 3.13 Large-scale purification of NB05-*X. laevis* REEP5 complex for crystallography
A) Chromatogram and **B)** SDS-PAGE analysis of the SEC purification using a Superdex200 column of the NB05-*X. laevis* REEP5 complex for crystallography. REEP5 was solubilized in LMNG, affinity purified, and incubated with a ~5 molar excess of NB05 prior to SEC purification.

3.3.4 Purification of thermophilic REEP5 constructs

In addition to my experiments with *Xenopus laevis* REEP5, I also sought to produce REEP5 proteins derived from thermophilic organisms with the aim of identifying a REEP5 construct that could be purified in larger amounts, that was more suitable for *in vitro* manipulation, and more amenable to crystallization. To this end, I cloned REEP5 derived from the thermophilic yeasts *Thielavia terrestris* and *Thermothelomyces thermophila* (Figure 3.1) into suitable expression vectors for purification from *E. coli*. For both species I generated a construct with a C-terminal SBP-tag (REEP5-SBP) and a construct with a C-terminal FLAG tag (REEP5-FLAG). In both cases, the affinity tags were preceded by a 3C protease cleavage site to allow for removal of the tag prior to crystallization.

Following the same purification protocols as used for *X. laevis* REEP5, I performed small-scale expression tests of *T. terrestris* and *T. thermophila* REEP5. These tests revealed that *T. terrestris* REEP5-SBP and *T. thermophila* REEP5-SBP could both be solubilized and purified from *E. coli* using LMNG. Accordingly, I scaled up purification of both the SBP and FLAG-tagged constructs for both species. I first purified the SBP and FLAG constructs without cleaving the tags to use for the isolation of nanobodies (Figures 3.14-3.17). I then purified aliquots of the SBP-tagged constructs, with the tag cleaved, for crystallization trials. Both *T. terrestris* and *T. thermophila* REEP5 were concentrated to ~40 mg/ml and mixed with monoolein to reconstitute the proteins into LCP. I performed extensive sparse matrix screening for suitable crystallization conditions, including screens designed specifically for use with LCP. Unfortunately, I was unable to obtain any crystals, which motivated me to isolate nanobodies against the thermophilic REEP5 proteins.

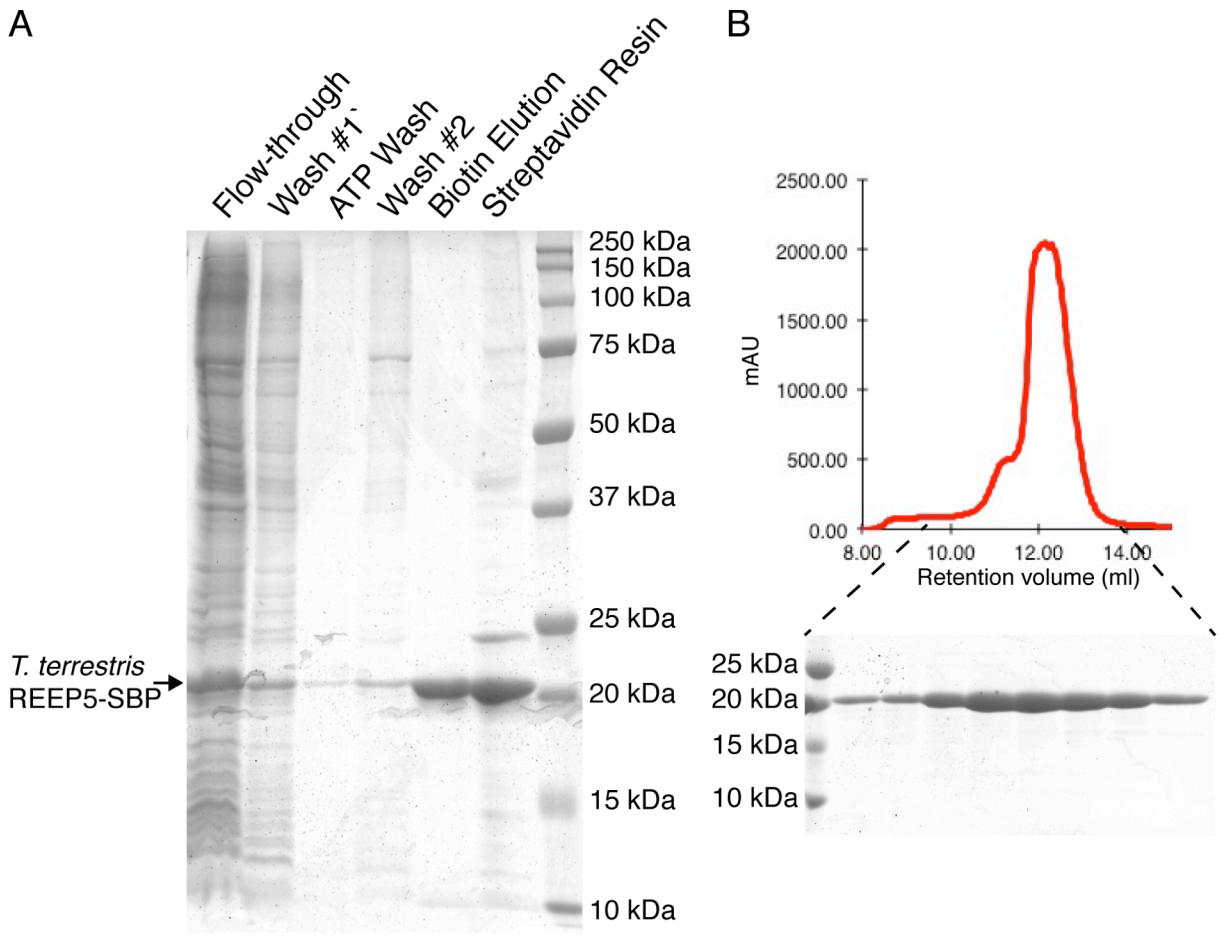

Figure 3.14 Purification of LMNG-solubilized *T. terrestris* REEP5-SBP
A) SDS-PAGE analysis of the streptavidin-affinity purification of *T. terrestris* REEP5-SBP solubilized in LMNG. **B)** Chromatogram (top) and SDS-PAGE analysis (bottom) of the subsequent SEC purification of LMNG-solubilized *T. terrestris* REEP5-SBP using a Superdex200 column.

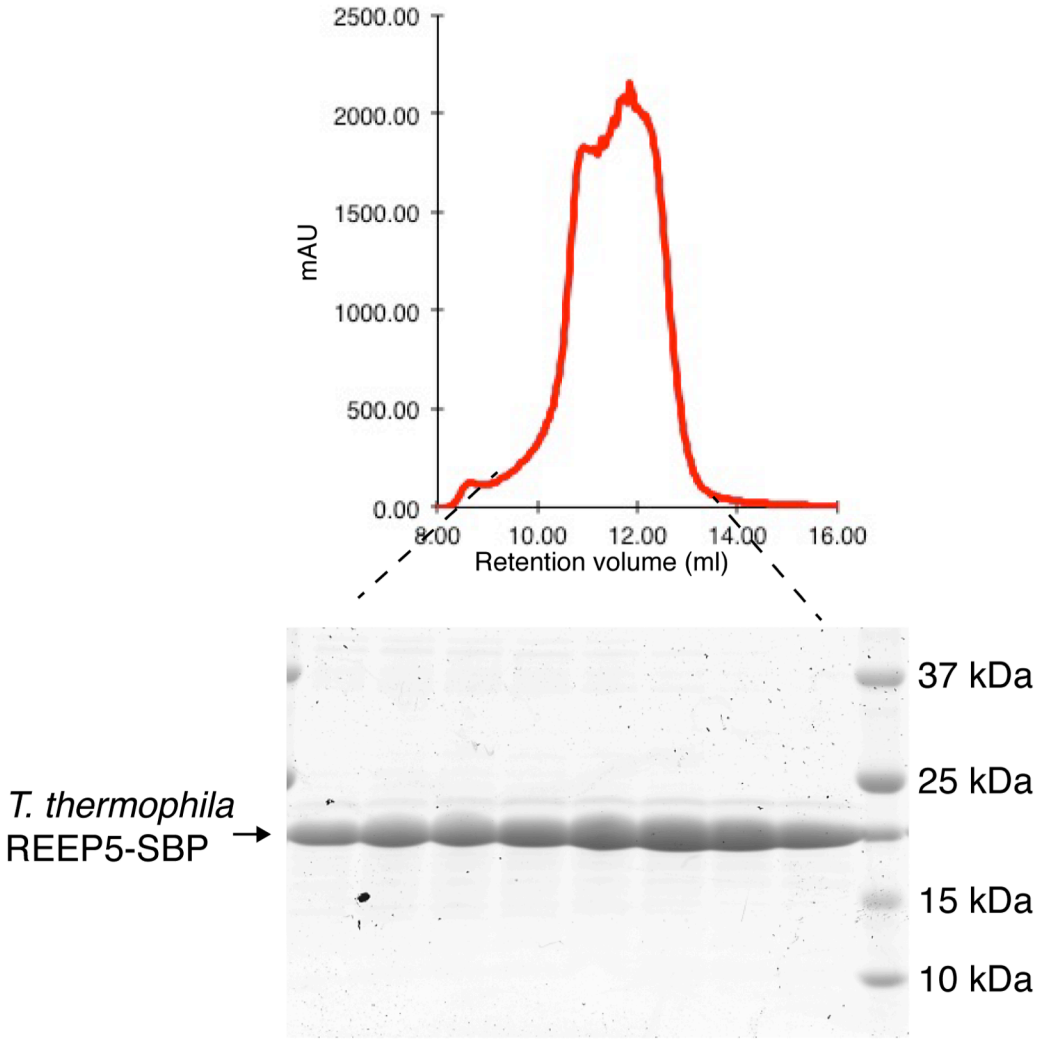

Figure 3.15 Purification of LMNG-solubilized *T. thermophila* REEP5-SBP
Chromatogram (top) and SDS-PAGE analysis (bottom) from the SEC purification of *T. thermophila* REEP5-SBP solubilized in LMNG using a Superdex200 column.

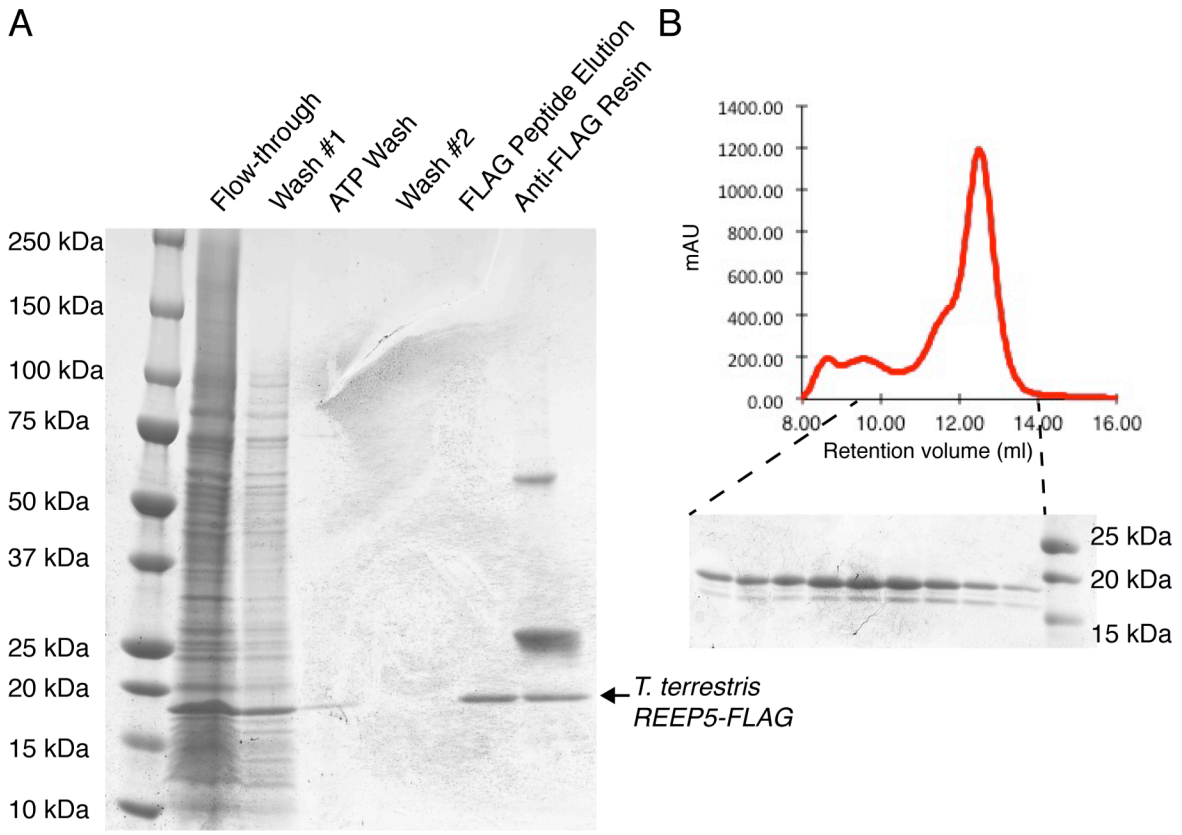

Figure 3.16 Purification of LMNG-solubilized *T. terrestris* REEP5-FLAG
A) SDS-PAGE analysis of the FLAG-affinity purification of *T. terrestris* REEP5-FLAG solubilized in LMNG. **B)** Chromatogram (top) and SDS-PAGE analysis (bottom) of the subsequent SEC purification of LMNG-solubilized *T. terrestris* REEP5-FLAG using a Superdex200 column.

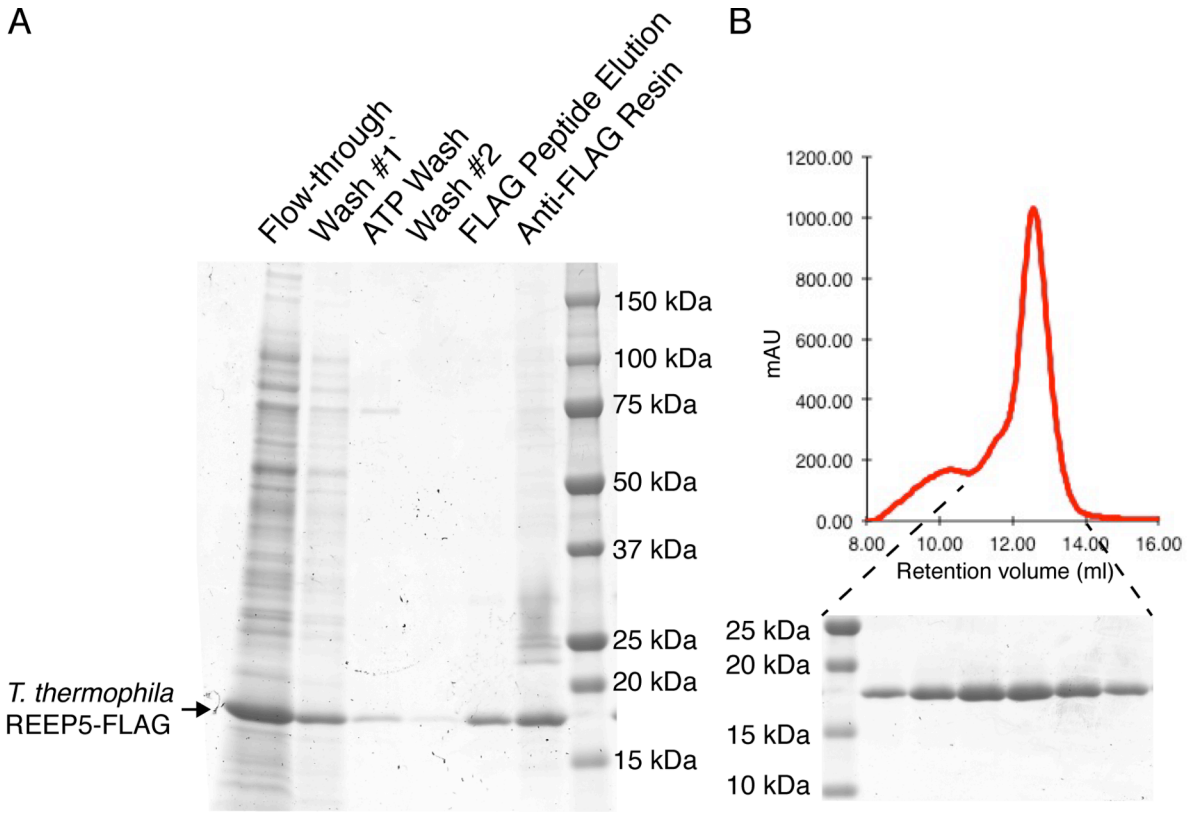

Figure 3.17 Purification of LMNG-solubilized *T. thermophila* REEP5-FLAG
A) SDS-PAGE analysis of the FLAG-affinity purification of *T. thermophila* REEP5-FLAG solubilized in LMNG. **B)** Chromatogram (top) and SDS-PAGE analysis (bottom) of the subsequent SEC purification of LMNG-solubilized *T. thermophila* REEP5-FLAG using a Superdex200 column.

3.3.5 Isolating nanobodies that bind to *T. terrestris* and *T. thermophila* REEP5

To isolate nanobodies specific to *T. terrestris* and *T. thermophila* REEP5, I again used the yeast display library and protocol developed by McMahon et al. (2018). Informed by my experience with *X. laevis* REEP5, I decided to forgo using fluorescently labeled protein and instead use the REEP5-SBP and REEP5-FLAG constructs that I purified (see above). To enrich for more nanobodies, I also performed the selections at higher protein concentrations than I used during the enrichment of nanobodies against *X. laevis* REEP5.

I performed an initial round of MACS using 1 μM of the SBP-tagged proteins and streptavidin magnetic beads followed by a second round of MACS using 1 μM of the FLAG-tagged proteins and magnetic beads conjugated to an anti-FLAG antibody. Fluorescent flow cytometry after these two MACS rounds revealed a good enrichment of REEP5-binding nanobodies (Figure 3.18). I then performed two successive rounds of FACS. The first round was performed using a protein concentration of 0.5 μM while the second round was using a protein concentration of 0.1 μM. For both FACS rounds, I stained the induced yeast cells with an Alexa 647-labeled anti-HA antibody and REEP5-SBP labeled with PE-streptavidin. For the second FACS round, I sorted single cells into 96 well plates for subsequent screening using colony PCR.

I obtained 17 unique sequences for nanobodies selected against *T. thermophila* REEP5 (Figure 3.19). None of the CDR sequences were repeated amongst the different nanobodies, and each well of the 96 well plate yielded only one nanobody sequence. The sequencing of nanobodies raised against *T. Terrestris* REEP5 proved more difficult as the sequencing results were consistently difficult to interpret. Although I eventually obtained 10 nanobody sequences, some nanobodies shared the same CDR sequences and the sequencing of individual wells yielded more than one nanobody sequence (Figure 3.20).

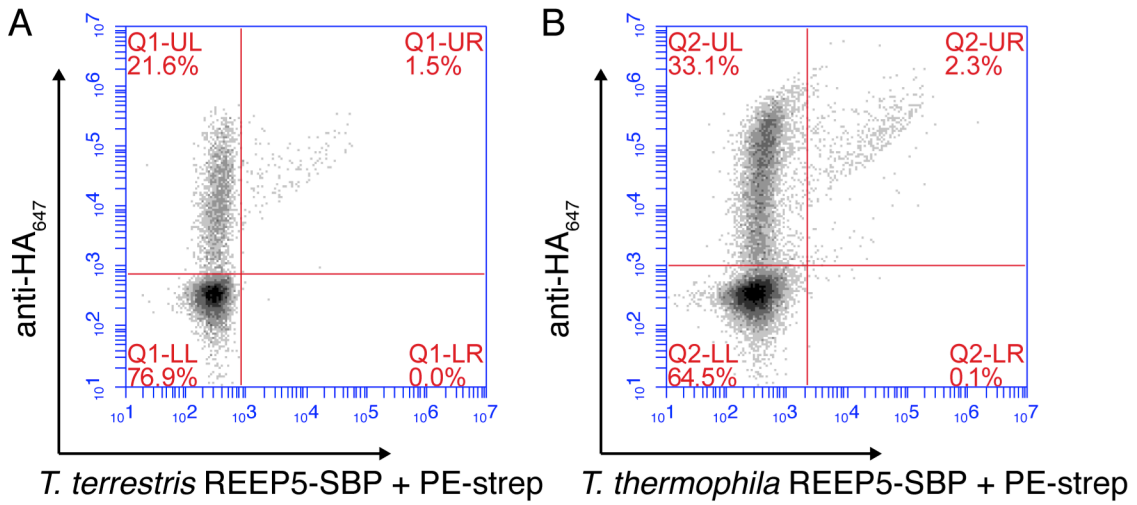

Figure 3.18 Fluorescent flow cytometry results after 2nd MACS round for thermophilic REEP5 constructs
Induced yeast cells were stained with a Alexa 647-labeled anti-HA antibody (anti-HA_{647}) and either **(A)** *T. terrestris* REEP5-SBP stained with PE-labeled streptavidin (PE-strep) or **(B)** *T. thermophila* REEP5-SBP stained with PE-strep. Cells were subsequently analyzed using fluorescent flow cytometry. During staining, a final concentration of 0.5 µM REEP5 was used.

	CDR1	CDR2	CDR3
NB.E7.2	GSIFRWWSM	EFVASIADGATTYYA	CAADTFAV--WPDLYYHYY
NB.C9.2	GTIFGYYVM	ELVAAINYGGTTYYA	CAVLNGVT--SDGQIIYGY
NB.E5.2	GTISDDQSM	EFVATINYGGTTNYA	CAAGDDWW--ITYAGYFDY
NB.C1.2	GNISHHFDM	EFVATIDLGGITYYA	CAA--DYWAVAPAPVYLVY
NB.A7.2	GNISSVFGM	EFVATIADGTTTNYA	CAVAVYWY--TA----FNY
NB.G8.2	GNISYVGWM	EFVATIADGTTTNYA	CAVTSGYW--GL----FQY
NB.A3.2	GNISTFYDM	EFVASIDDGGNTNYA	CAAAPSWY--EA----HSY
NB.D6.2	GTIFRDDSM	EFVASIDSGTTTNYA	CAVHPSYL--FW----LDY
NB.D8.2	GTISYRDIM	EFVATIDGGTTTNYA	CAAYDDWW--PW---TLGY
NB.C5.2	GYIFTGEVM	EFVAGINYGGNTNYA	CAVYHPAY--VP----HTY
NB.F5.2	GTIFEDDLM	EFVASIDYGANTNYA	CAVYEDFY--SYWFDYYYY
NB.F2.2	GYIFWLVDM	EFVATIDIGGSTNYA	CAA--DYG--SD--TTFDY
NB.C2.2	GTIFTEDAM	EFVATIDDGGSTNYA	CAADLIVY------DFYYY
NB.A8.2	GNISRTYDM	ELVASINDGTITYYA	CAANSWLY--WW----HVY
NB.G6.2	GNISRVGDM	ELVASIGPGASTNYA	CAAFDDRW--YDVRFFYAY
NB.E6.2	GNISYPNGM	ELVAGISVGTNTYYA	CAVYDPST-------YYYY
NB.F7.2	GNISRWYAM	ELVATISGGATTYYA	CAAAIYWY------DYYKY
	* * *	*:** * * * **	**. *

Figure 3.19 Sequence alignment of nanobodies isolated against *T. thermophila* REEP5
Sequence alignment of CDR1 (left), CDR2 (middle), and CDR3 (right) of nanobodies isolated against *T. thermophila* REEP5.

```
                CDR1            CDR2                CDR3
NB.H6.1         GTISQVVYM       ELVAAIGYGASTYYA      CAADTPYD-----WLDDILHDY
NB.H2.1         GSIFRWWSM       EFVASIADGATTYYA      CAADTFAV-----WPDLYYHYY
NB.E5.1         GNISRWYAM       ELVATISGGATTYYA      CAAAIY-------WYD--YYKY
NB.H8.1         GSIFESDYM       EFVATIDDGTITNYA      CAAVRQDK-----W----WLDY
NB.D10.1        GNISEYDWM       ELVATIAQGSNTNYA      CAADYLDLA----WFPA-YYEY
NB.G4.1         GNISEYDWM       ELVAAITAGGTTNYA      CAADDVTSFYNW-WFGDGGFEY
NB.G12.1        GSISDSLSM       EFVAGIALGGTTNYA      CAVDYFYPPLVYDWYGG-YFVY
NB.C12.1        GNISEYDWM       ELVAAITAGGTTNYA      CAVDYFYPPLVYDWYGG-YFVY
NB.A7.1         GNISEYDWM       ELVAAITAGGTTNYA      CAVVHQTIP---------WVSY
NB.E8.1         GNISEYDWM       EFVAGIALGGTTNYA      CAVVHQTIP---------WVSY
                *.*     *       *:** *   *   * **    **.                 *
```

Figure 3.20 Sequence alignment of nanobodies isolated against *T. terrestris* REEP5
Sequence alignment of CDR1 (left), CDR2 (middle), and CDR3 (right) of nanobodies isolated against *T. terrestris* REEP5.

3.3.6 Solution binding tests of *T. terrestris* and *T. thermophila* REEP5 nanobodies

Following the cloning of the enriched nanobodies into a suitable expression vector for periplasmic expression in *E. coli*, I performed small-scale expression and purification tests that demonstrated that all of enriched nanobodies could be successfully expressed and purified. The overall purity along with the ability to be concentrated did vary slightly from nanobody to nanobody (Figures 3.21 and 3.22). To test whether the purified nanobodies could bind to their respective REEP5 targets in solution, I performed binding experiments using analytical SEC. Each nanobody was incubated with its respective REEP5 target at a ratio of 2:1, nanobody:REEP5, weight:weight. This roughly equates to a molar ratio of 3.5:1, nanobody:REEP5. The samples were then analyzed with analytical SEC. I used SDS-PAGE to determine whether the nanobody and the REEP5 target co-eluted during SEC.

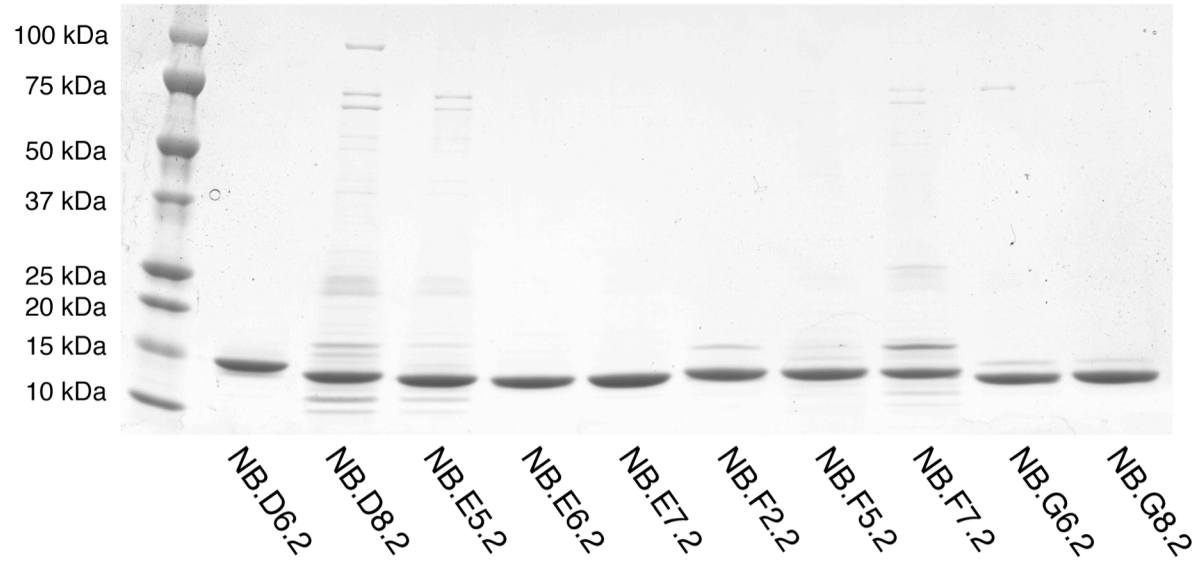

Figure 3.21 Expression and purification of nanobodies isolated against *T. terrestris* REEP5
SDS-PAGE analysis of test expression and purification of nanobodies isolated against *T. terrestris* REEP5.

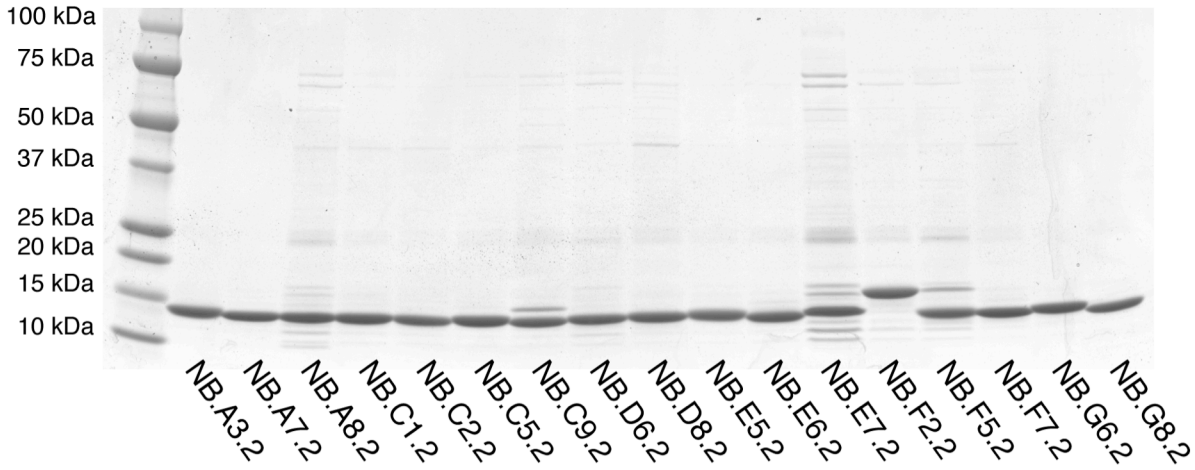

Figure 3.22 Expression and purification of nanobodies isolated against *T. thermophila* REEP5
SDS-PAGE analysis of test expression and purification of nanobodies isolated against *T. thermophila* REEP5.

I observed a large variability in the amount of nanobody that co-eluted with REEP5, both for the nanobodies isolated against *T. terrestris* REEP5 and *T. thermophila* REEP5. For some of the nanobodies, very little to no nanobody was observed to co-elute with REEP5, indicating the binding of the nanobody to REEP5 was not sufficiently strong enough to survive dilution during SEC (Figures 3.23 and 3.24). However, for both REEP5 species, there was a subset of nanobodies that showed strong co-elution with REEP5 and therefore bind with high affinity (Figures 3.25 and 3.26). These nanobodies are the most suitable for use in crystallographic trials. I also tested whether the nanobodies that were raised against and bound with high affinity to *T. thermophila* REEP5 were able to bind to *T. terrestris* REEP5. I observed that a subset of the *T. thermophila* REEP5 nanobodies were able to bind to *T. terrestris* REEP5 with high affinity (Figure 3.27).

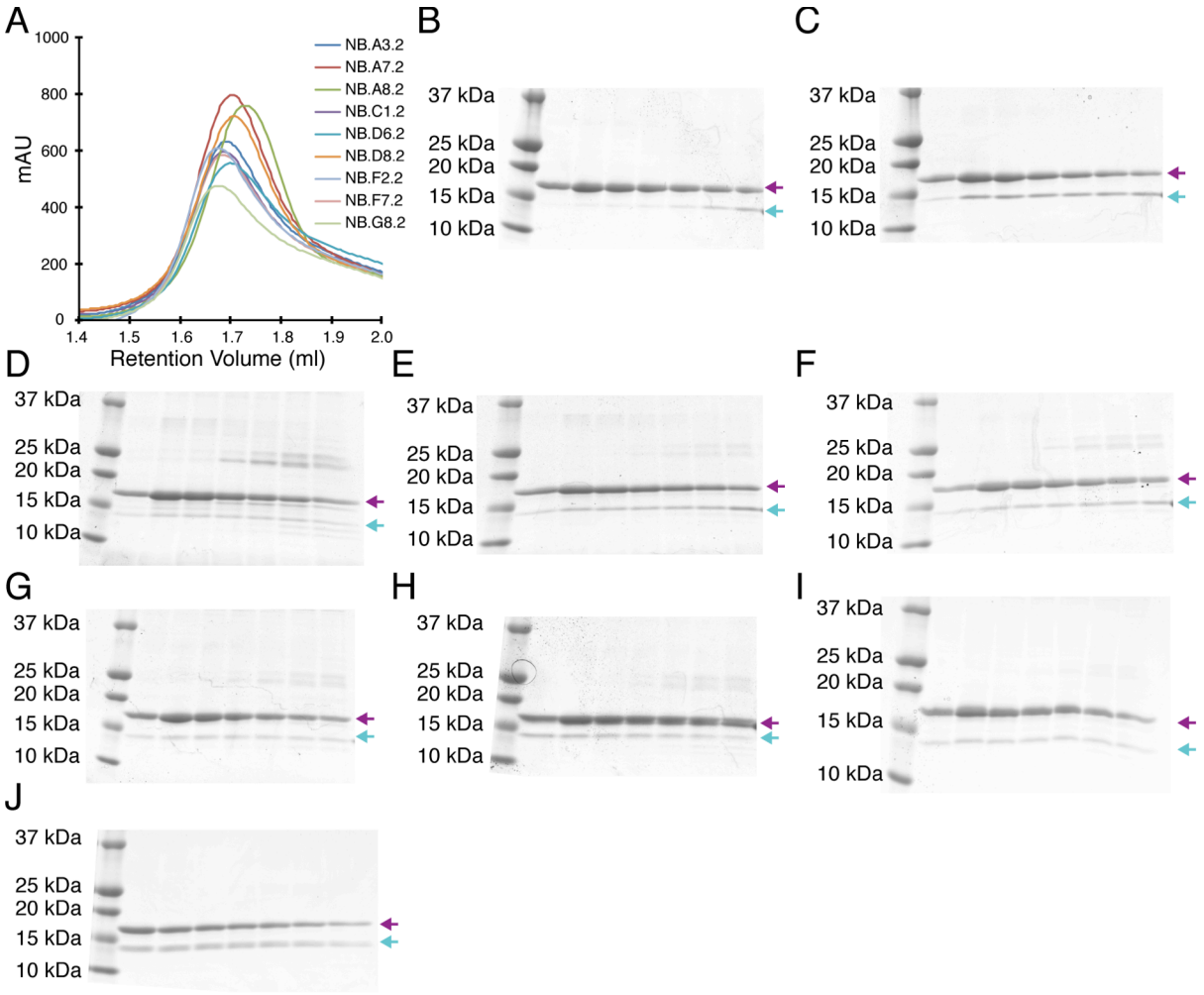

Figure 3.23 A subset of nanobodies isolated against *T. thermophila* REEP5 do not bind to REEP5 with high affinity in solution

A) Chromatogram of analytical SEC using a Superdex200 to test the binding of nanobodies to *T. thermophila* REEP5. The first peak (highlighted) was analyzed using SDS-PAGE in panels **B**-**J**. SDS-PAGE analysis to determine if **B)** NB.A3.2, **C)** NB.A7.2, **D)** NB.A8.2, **E)** NB.C1.2, **F)** NB.D6.2, **G)** NB.D8.2, **H)** NB.F2.2, **I)** NB.F7.2, and **J)** NB.G8.2 co-eluted with *T. thermophila* REEP5 during analytical SEC. Magenta arrow indicates REEP5 and cyan arrow indicates nanobody.

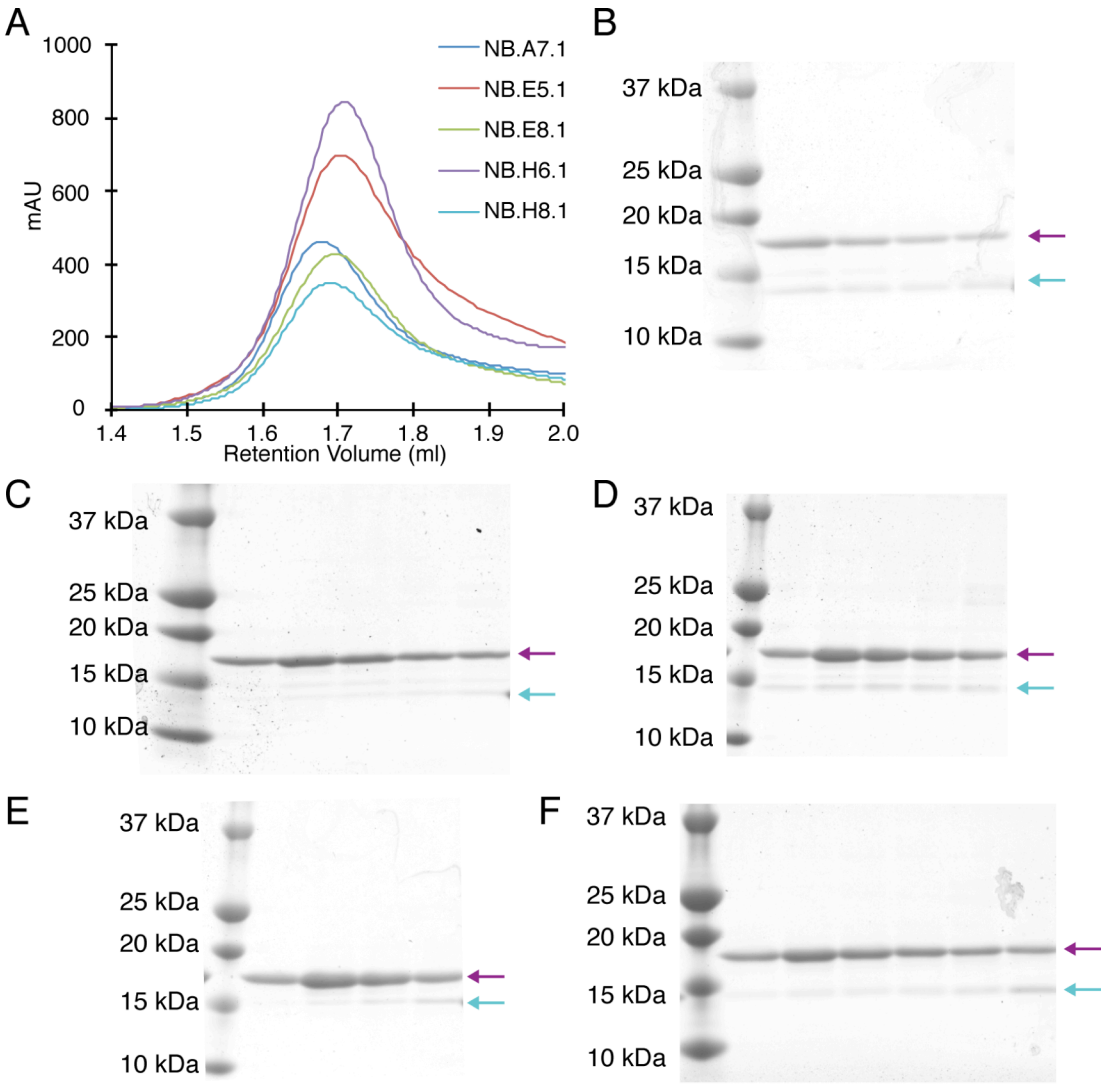

Figure 3.24 A subset of nanobodies isolated against *T. terrestris* REEP5 do not bind to REEP5 with high affinity in solution

A) Chromatogram of analytical SEC using a Superdex200 to test the binding of nanobodies to *T. terrestris* REEP5. The first peak (highlighted) was analyzed using SDS-PAGE in panels **B**-**F**. SDS-PAGE analysis to determine if **B)** NB.A7.1, **C)** NB.E8.1, **D)** NB.E5.1, **E)** NB.H6.1, and **F)** NB.H8.1 co-eluted with *T. terrestris* REEP5 during analytical SEC. Magenta arrow indicates REEP5 and cyan arrow indicates nanobody.

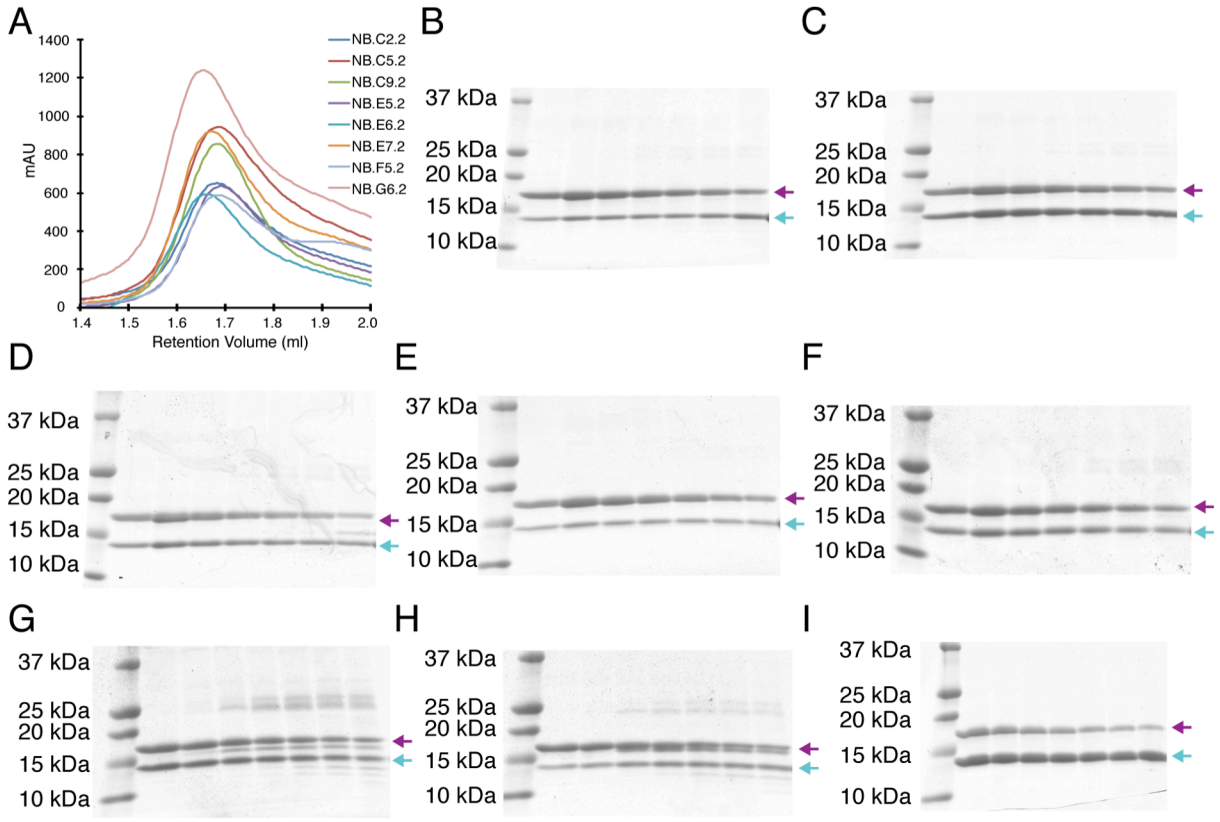

Figure 3.25 A subset of nanobodies isolated against *T. thermophila* REEP5 bind to REEP5 with high affinity in solution

A) Chromatogram of analytical SEC using a Superdex200 column to test the binding of nanobodies to *T. thermophila* REEP5. The first peak (highlighted) was analyzed using SDS-PAGE in panels **B-I**. SDS-PAGE analysis to determine if **B)** NB.C2.2, **C)** NB.C5.2, **D)** NB.C9.2, **E)** NB.E5.2, **F)** NB.E6.2, **G)** NB.E7.2, **H)** NB.F5.2, and **I)** NB.G6.2 co-eluted with *T. thermophila* REEP5 during analytical SEC. Magenta arrow indicates REEP5 and cyan arrow indicates nanobody.

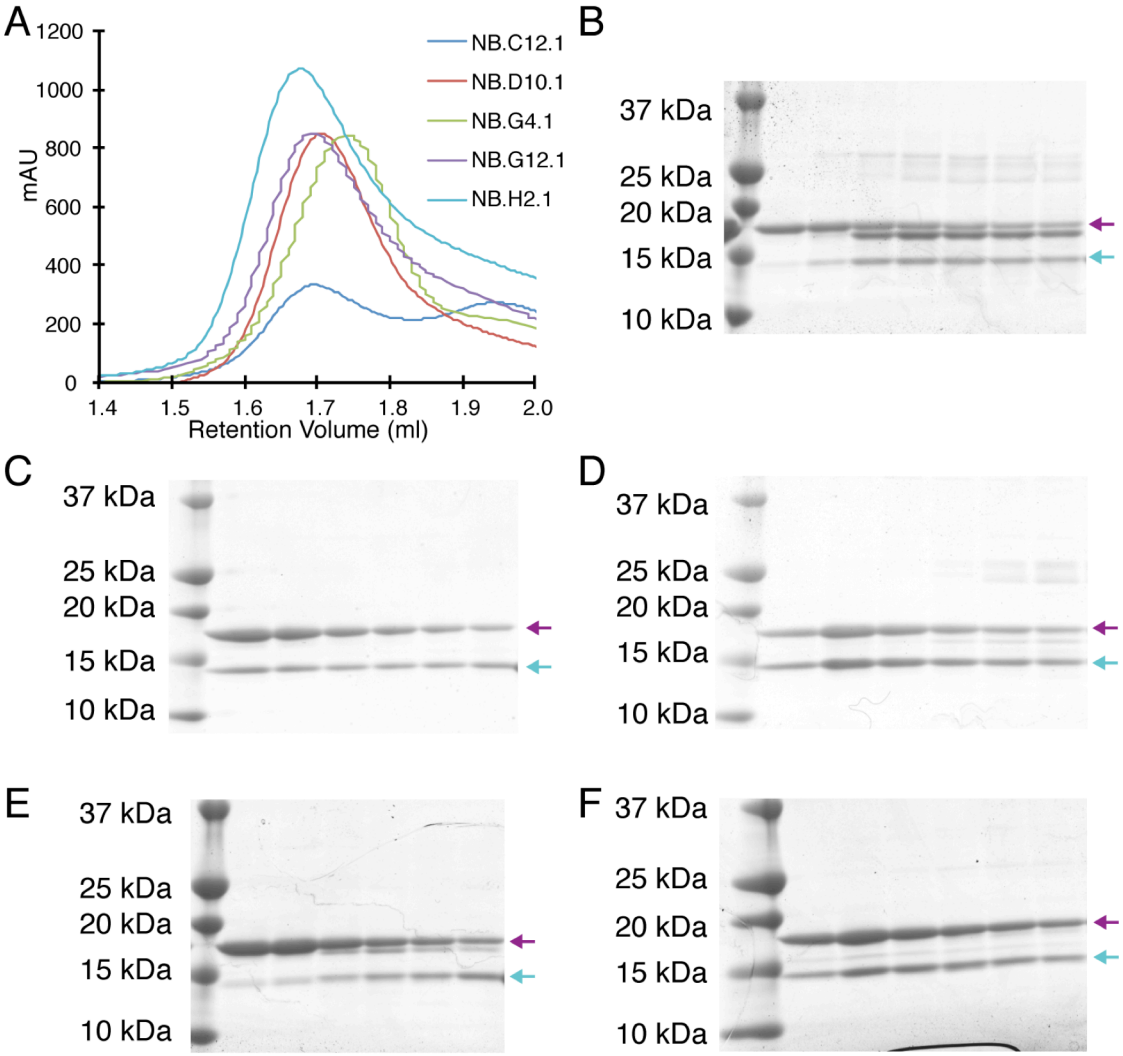

Figure 3.26 A subset of nanobodies isolated against *T. terrestris* REEP5 bind to REEP5 with high affinity in solution

A) Chromatogram of analytical SEC using a Superdex200 column to test the binding of nanobodies to *T. terrestris* REEP5. The first peak (highlighted) was analyzed using SDS-PAGE in panels **B**-**F**. SDS-PAGE analysis to determine if **B)** NB.C12.1, **C)** NB.D10.1 **D)** NB.H2.1 **E)** NB.G4.1, and **F)** NB.G12.1 co-eluted with *T. terrestris* REEP5 during analytical SEC, indicating binding of the nanobody to REEP5. Magenta arrow indicates REEP5 and cyan arrow indicates nanobody.

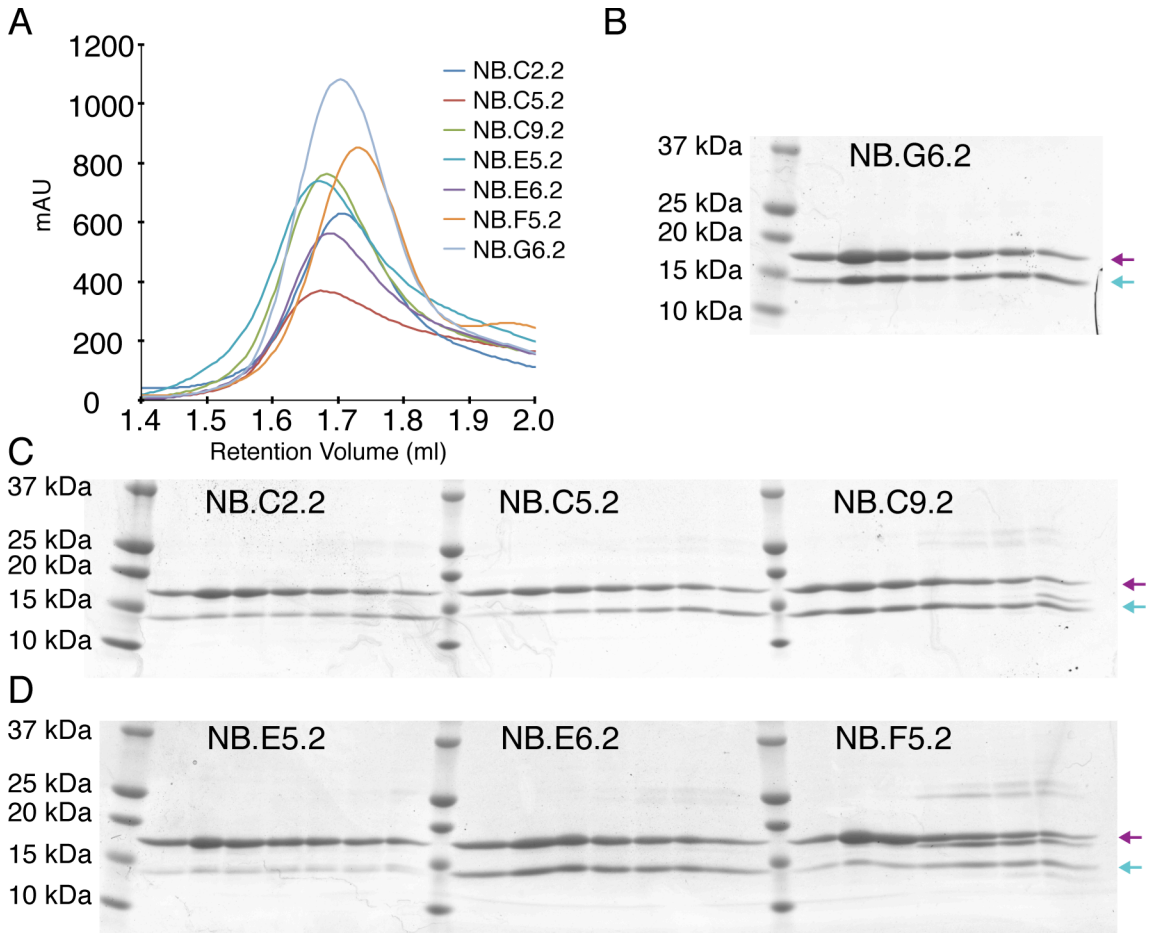

Figure 3.27 Nanobodies that bind to *T. thermophila* REEP5 also bind to *T. terrestris* REEP5
A) Chromatogram of analytical SEC using a Superdex200 column to test if nanobodies isolated against *T. thermophila* REEP5 can bind to *T. terrestris* REEP5 the binding of nanobodies isolated against *T. thermophila* REEP5. The first peak (highlighted) was analyzed using SDS-PAGE in panel **B-D**. Magenta arrow indicates REEP5 and cyan arrow indicates nanobody.

3.3.7 Developing a nanobody co-binding assay

To further increase the hydrophilic surface area available for crystal packing, it would be advantageous to simultaneously bind two different nanobodies to a single REEP5 protein, creating an NB_1-NB_2-REEP5 complex. The most beneficial arrangement might be to have one nanobody bind on the luminal side of REEP5 and the other nanobody to bind to the cytosolic side of REEP5, thereby creating packing surfaces on either side of the membrane. To this end, I sought to develop an assay that could be used to test whether two nanobodies could simultaneously bind to REEP5.

I designed the assay as follows: detergent solubilized REEP5 protein containing an SBP tag is incubated with both fluorescently labeled streptavidin and a fluorescently labeled nanobody. The labeled streptavidin protein should bind to the SBP tag while the single labeled nanobody should bind to its specific binding site on REEP5. This REEP5-labeled streptavidin-labeled nanobody complex is then incubated with yeast cells expressing one species of nanobody that is also known to bind REEP5. If the two nanobodies are able to bind simultaneously, then yeast cells should stained by both the labeled streptavidin and the soluble, labeled nanobody. If the two nanobodies cannot bind simultaneously, then the yeast cells should be either stained with the labeled streptavidin or not stained at all, depending on the kinetics of nanobody exchange and the relative binding affinities of the soluble and yeast bound nanobodies.

Informed by the results of the expression and solution-binding tests, I selected NB.C5.2 as the first nanobody to label and test. NB.C5.2 was both highly expressed, making production of protein for labeling easy, and bound to *T. thermophila* REEP5 with high affinity. To label NB.C5.2, I incubated the purified protein with an N-Hydroxysuccinimide (NHS) conjugated Alexa 647 fluorophore that can label at the four lysine residues present in the nanobody. After

incubation, I quenched and removed any free dye using standard chromatographic techniques. Subsequent SDS-PAGE analysis revealed only a small amount of unreacted free dye was present in the sample.

To test for co-binding, I prepared two separate aliquots of REEP5. One aliquot was incubated with PE-streptavidin alone (REEP5-$Strep_{PE}$) while the other aliquot was incubated with PE-streptavidin and 20 x molar excess of 647-labeled NB.C5.2 (REEP5-$Strep_{PE}$-$NBC5_{647}$). Aliquots of *S. cerevisiae* cells expressing one of each of the eight nanobodies that displayed appreciable binding to *T. thermophila* REEP5 during SEC were incubated either with REEP5-$Strep_{PE}$ and an Alexa 647-labeled ant-HA antibody or with REEP5-$Strep_{PE}$-$NBC5_{647}$. The cells were then washed and analyzed using flow cytometry.

For each of the eight different yeast strains, the cells incubated with REEP5-$Strep_{PE}$ and the Alexa 647-labeled anti-HA antibody displayed strong co-staining for both REEP5-$Strep_{PE}$ and the HA antibody, indicating strong expression of the nanobody and tight binding of REEP5 (Figure 3.28). These results confirm the results of the solution binding experiments.

If the assay does work as designed, pre-bound, soluble $NB.C5.2_{647}$ should bind to REEP5 with high affinity and occlude the binding of the NB.C5.2 expressed on the surface of the yeast. This was indeed what I observed. In the case of the yeast strain expressing NB.C5.2, cells that were incubated with the REEP5-$Strep_{PE}$-$NBC5_{647}$ complex displayed little to no staining for REEP5-$Strep_{PE}$ or for $NB.C5.2_{647}$ (Figure 3.29B). A similar result was obtained with yeast cells expressing NB.C9.2 and NB.E6.2 (Figures 3.29C,E), indicating that these nanobodies are not able to co-bind with NB.C5.2 to REEP5. Conversely, yeast cells expressing NB.C2.2, NB.E5.2, NB.E7.2, NB.F5.2, and NB.G6.2 showed a strong staining for REEP5-$Strep_{PE}$, and, in the case of the cells most strongly stained by REEP5-$Strep_{PE}$, also displayed staining for $NB.C5.2_{647}$

(Figures 3.29A,D, F-H). These preliminary results indicate that these nanobodies are able to co-bind with NB.C5.2 to *T. thermophila* REEP5 and could be used in combination with NB.C5.2 during crystallographic trials.

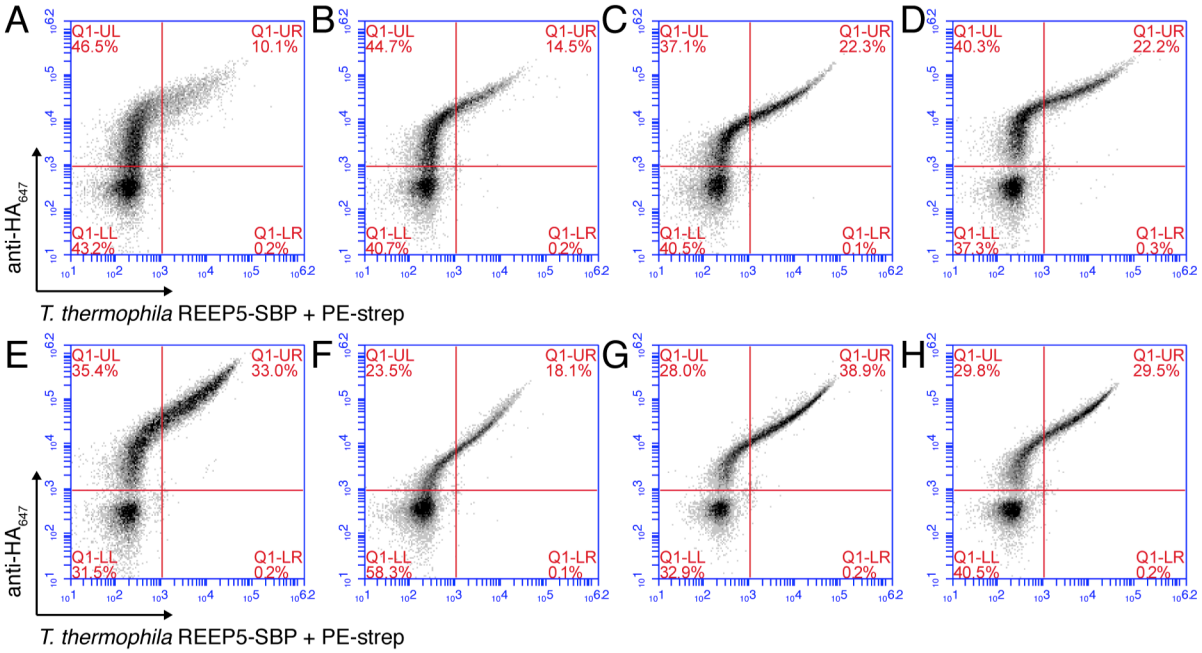

Figure 3.28 Fluorescent flow cytometry results for nanobodies that bind to *T. thermophila* REEP5 with high affinity in solution

Yeast cells expressing **A)** NB.C2.2, **B)** NB.C5.2, **C)** NB.C9.2, **D)** NB.E5.2, **E)** NB.E6.2, **F)** NB.E7.2, **G)** NB.F5.2, and **H)** NB.G6.2 with stained with an Alexa 647-labeled anti-HA antibody (anti-HA_{647}) and *T. thermophila* REEP5-SBP stained with PE-labeled streptavidin (PE-strep). Cells were subsequently analyzed using fluorescent flow cytometry. During staining, a final concentration of 0.5 µM REEP5 was used.

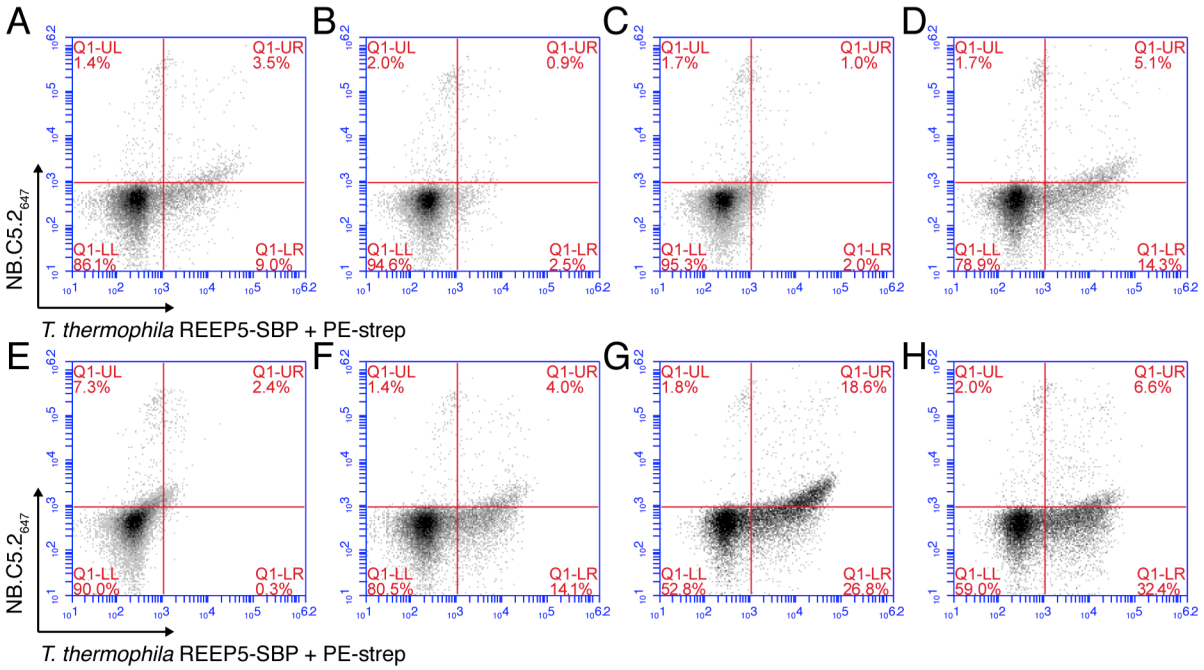

Figure 3.29 Testing co-binding of *T. thermophila*-specific nanobodies
Yeast cells expressing **A)** NB.C2.2, **B)** NB.C5.2, **C)** NB.C9.2, **D)** NB.E5.2, **E)** NB.E6.2, **F)** NB.E7.2, **G)** NB.F5.2, and **H)** NB.G6.2 were stained with *T. thermophila* REEP5 that was pre-stained with PE-labeled streptavidin (PE-strep) and pre-bound to soluble, Alexa 647-labeled NB.C5.2 ($NB.C5.2_{647}$).

3.4 Discussion

Understanding how the reticulon and Yop1/REEP5 proteins stabilize curvature at a molecular level remains one of the most vexing and important questions in the field of ER morphology. The results presented in this chapter represent important initial steps toward obtaining a high-resolution structure of a curvature-stabilizing protein of the tubular ER network. REEP5, along with the other members of the reticulon and Yop1/REEP families, are inherently difficult structural targets. The small size of these proteins lends them to analysis via x-ray crystallography, yet their lack of extensive hydrophilic surfaces makes the formation of crystals much more difficult. In this chapter I have presented and applied several new membrane protein crystallography strategies to the study of REEP5.

Most notably, I was able to isolate a large number of nanobodies that bind with high affinity to REEP5 constructs derived from a variety of different species including *Xenopus laevis*, *Thielavia terrestris*, and *Thermothelomyces thermophila*. The thermophilic REEP5 constructs displayed highly favorable purification behavior, indicating that these proteins may prove useful in a variety of different *in vitro* experiments in the future.

For *X. laevis* REEP5, I isolated two nanobodies, NB02 and NB05, which bound with high affinity to REEP5. I performed large-scale purification of both NB02-REEP5 and NB05-REEP5 complexes and obtained amounts suitable for crystallization trials. Although extensive LCP and vapor diffusion crystallization trials of these two complexes proved unsuccessful, there are still many different strategies that could be used to try to obtain crystals of the complexes. This includes reconstituting the complexes into different lipids for LCP, such as lipids with different acyl-chain characteristics and lipid mixtures with additives such as cholesterol (Ishchenko et al., 2017). Modifying the lipid composition has proved important in the crystallization of other

membrane proteins. Furthermore, crystallization trials using lipidic bicelles can be performed. Lipidic bicelles are lipid filled discs usually composed of two different types of lipids—one that forms a bilayer in the middle of the disc and one that assembles into a monolayer-like structure on the edge of the bilayer (Ishchenko et al., 2017).

Needless to say, initial crystallization trials should be performed with the nanobodies isolated against the thermophilic REEP5 proteins. I was able to obtain several, high affinity nanobodies for both *T. terrestris* and *T. thermophila* using the lessons learned from isolating nanobodies using *X. laevis* REEP5. Thus, there are a large number of possible nanobody-REEP5 complexes to test in crystallization trials. In addition, I also developed an assay to test for pairs of nanobodies that can simultaneously bind to REEP5. Using this assay, I identified nanobodies that could co-bind with NB.C5.2 to REEP5. The remaining nanobodies can be labeled and tested using this assay to generate a comprehensive list of the possible dual nanobody-REEP5 complexes to use in crystallization trials.

Moving beyond just crystallography, the isolated nanobodies could also prove useful as reagents in other types of experiments. For example, the nanobodies that bind to *X. laevis* REEP5 can be tested in a *X. laevis* egg extracts to determine if the nanobodies can inactivate REEP5 and disrupt network formation and maintenance. Labeled nanobodies could also be used to probe the specific location and mobility of REEP5 within the *X. laevis* ER networks.

3.5 Materials and Methods

3.5.1 Cloning of expression constructs

X. laevis REEP5-HIS_{10} was generated by cloning *X. laevis* REEP5 (NM_001096221.1) into the NdeI and XhoI restriction sites of a modified pET21b vector that included a C-terminal 3C protease site followed by a HIS_{10} tag.

X. laevis REEP5-SBP was generated by cloning *X. laevis* REEP5 (NM_001096221.1) into the NdeI and XhoI restriction sites of a modified pET21b vector that included a C-terminal TEV protease site followed by a SBP tag (MDEKTTGWRGGHVVEGLAGELEQLRARLEHHPQGQREP).

T. terrestris REEP5-SBP, *T. thermophila* REEP5-SBP were generated by cloning *T. terrestris* REEP5 (XM_003649133.1, codon optimized for *E. coli* expression) and *T. thermophila* REEP5 (XM_003661605.1, codon optimized for *E. coli expression*) into the NdeI and XhoI restriction sites of a modified pET21b vector that included a C-terminal 3C protease site followed by a SBP tag.

T. terrestris REEP5-FLAG and *T. thermophila* REEP5-FLAG expression constructs were generated by cloning *T. terrestris* REEP5 (XM_003649133.1, codon optimized for *E. coli* expression) and *T. thermophila* REEP5 (XM_003661605.1, codon optimized for *E. coli expression*) into the NdeI and XhoI restriction sites of a modified pET21b vector that included a C-terminal 3C protease site followed by a FLAG tag (DYKDDDD).

Nanobody expression constructs for periplasmic expression in *E. coli* were generated by cloning isolated nanobodies into the NcoI and XhoI sites of a pET26b vector that included an N-terminal signal sequence and a C-terminal His_6tag. The isolated nanobodies were amplified from the genomic DNA of sorted yeast cells (see below).

3.5.2 Purification of REEP5 proteins

X. laevis REEP5-HIS_{10}, *X. laevis* REEP5-SBP, *T. terrestris* REEP5-SBP, *T. terrestris* REEP5-FLAG, *T. thermophila* REEP5-SBP, and *T. thermophila* REEP5-FLAG were expressed in *E. coli* BL21-CodonPlus (DE3)-RIPL (Agilent). Expression was induced at OD_{600} ~ 0.6-1.0 with 250 μM isopropyl-β-D-thiogalactopyranoside (IPTG) at 16 °C for 16-18 hrs.

Cells were lysed through high-pressure homogenization in an Emulsiflex C3 (Avestin) in a buffer containing 20 mM Tris pH 7.5, 300 mM NaCl, 1mM phenylmethylsulfonyl fluoride (PMSF), and protease inhibitors. In the case of *X. laevis* REEP5-HIS_{10}, the lysis buffer was supplemented with 20 mM imidazole. The lysate was centrifuged at 20,000 x g for 20 minutes to clear cellular debris and unbroken cells and then at 100,000 x g for 1 hr to sediment the membranes. Membranes were washed once with lysis buffer and then solubilized in lysis buffer containing either 1% n-dodecyl-β-maltoside (DDM) or Lauryl Maltose Neopentyl Glycol (LMNG) for 1-2 hrs at 4 °C. Insoluble material was removed by centrifugation at 100,000 x g for 1 hr and the resulting supernatant was incubated with either Ni-NTA resin (Qiagen) in the case of *X. laevis* REEP5-HIS_{10}, streptavidin agarose resin (Thermo Fisher) in the case of *X. laevis* REEP5-SBP, *T. terrestris* REEP5-SBP, and *T. thermophila* REEP5-SBP, or anti-FLAG M2 affinity gel (Sigma Aldrich) in the case of *T. terrestris* REEP5-FLAG and *T. thermophila* REEP5-FLAG. The affinity resin was washed with 2.5 CV of lysis buffer, 2.5 CV of ATP-wash buffer (20 mM Tris pH 7.5, 200 mM NaCl, 100 mM KCl, 2 mM $MgCl_2$, and 2 mM ATP) to remove any bound chaperones, and 2.5 CV of lysis buffer to remove excess nucleotide. Proteins were eluted from the affinity resin by on-column cleavage of the affinity tags using the appropriate protease. 3C protease was used to cut off all tags except in the case of *X. laevis* REEP5-HIS_{10}, for which TEV protease was used. In the cases where the affinity tag was to be kept attached to the protein (for example, for nanobody isolation), the REEP5 protein was eluted using a competitive ligand. *X. laevis* REEP5-HIS_{10} was eluted using lysis buffer supplemented with 250 mM imidazole. *T. terrestris* REEP5-SBP and *T. thermophile* REEP5-SBP were eluted using holding buffer (20 mM HEPES 7.5, 150 mM KCl) supplemented with 2 mM biotin. *T. terrestris* REEP5-FLAG and *T. thermophila* REEP5-FLAG were eluted using holding buffer

supplemented with 0.2 mg/ml poly FLAG-peptide (DYKDDDDK repeated 3 times; Bimake). Proteins were further purified by size-exclusion chromatography on a Superdex200 column (GE Healthcare) and concentrated by ultrafiltration using a 100,000 MWCO filter (Amicon Ultra, EMD Millipore). Absorbance at 280 nm was used to determine concentrations of the all the purified REEP5 proteins. REEP5 proteins were frozen in small aliquots for storage at -80° C.

3.5.3 Text Expression of Nanobodies

All nanobodies were expressed in *E. coli* BL21-CodonPlus (DE3)-RIPL (Agilent). For test expressions, 200 ml of cell culture was used. Expression was induced at OD_{600} ~ 0.6-1.0 with 750 µM isopropyl-β-D-thiogalactopyranoside (IPTG) at 25° C for 16-18 hrs. Cells were pelleted and resuspended in 15 ml of sucrose buffer (0.5 M sucrose, 0.2 M Tris pH 8, 0.5 mM EDTA). After a 1 hour incubation at 4° C, the cells were osmotically shocked to release periplasmic nanobodies by the addition of 30 ml of H_2O. The solution was incubated with stirring for 1 hour at 4° C, after which various salts were added to final concentrations of 150 mM NaCl, 2 mM MgCl2, and 20 mM imidazole. Cellular debris was pelleted by centrifugation at 20,000 x g for 20 minutes at 4° C. The supernatant was then incubated with 0.5 ml of Ni^{2+}-NTA resin (Qiagen) in batch for 1-2 hrs at 4° C. After incubation, the resin was washed extensively with high salt buffer (20 mM HEPES pH 7.5, 500 mM NaCl, 20 mM imidazole), followed by low salt buffer (20 mM HEPES pH7.5, 100 mM NaCl, 20 mM imidazole). Finally, the nanobodies were eluted using a high imidazole buffer (20 mM HEPES pH7.5, 100 mM NaCl, 400 mM imidazole). The nanobodies were concentrated by ultrafiltration using a 10,000 MW cut-off filter (Amicon Ultra, EMD Millipore) and purity was assessed using SDS-PAGE. The nanobodies were frozen in small aliquots for storage at -80° C.

3.5.4 Labeling of *X. laevis* REEP5

Purified *X. laevis* REEP5 was mixed with either Alexa Fluor 647 NHS ester dye (Thermo Fisher Scientific) or Fluorescein isothiocyanate NHS ester dye (Thermo Fisher Scientific) at a 1:20, protein:dye molar ratio and incubated at room temperature for 1 hr. The labeling reaction was quenched by addition of 100 mM Tris pH 8.0. After an incubation of 1 hr at 4 °C, excess dye was removed by passing the sample over Sephadex G-50 resin (GE healthcare). The labeled protein was collected and concentrated by ultrafiltration using a 100,000 MW cut-off filter (Amicon Ultra, EMD Millipore). Protein concentration and labeling efficiency was calculated by comparing the absorbance of the protein at 280 nm and the absorbance of the dye using the pre-configured "Proteins & Labels" function on a Nano Drop 2000c Spectrophotometer (Thermo Scientific).

3.5.5 Labeling of NB.C5.2

To obtain NB.C5.2 for labeling, the nanobody was purified using the same protocol as the test expression except that 2 liters of cell culture were harvested to increase the final amount of nanobody obtained. To release the nanobodies from the periplasm, the cell pellets were resuspended in 75 ml of sucrose buffer and 150 ml of H_2O was added after incubation. Following elution from the Ni^{2+}-NTA resin, the protein was concentrated and further purified by SEC using a Superdex200 column and a buffer containing 20 mM HEPES pH 7.5 and 150 mM KCl. Following SEC, the protein was concentrated and frozen in small aliquots for storage at -80° C.

For labeling, 0.5 mg of purified NB.C5.2 was thawed and incubated with a three molar excess of N-Hydroxysuccinimide (NHS) conjugated Alexa 647 fluorophore (Thermo Fisher Scientific) at room temperature for 1 hour. The reaction was then quenched by the addition of

TRIS pH 8.0 to a final concentration of 100 mM. Excess dye was removed by passing the sample over Sephadex G-50 resin (GE healthcare). The labeled protein was collected and concentrated by ultrafiltration using a 10,000 MW cut-off filter (Amicon Ultra, EMD Millipore). The final protein sample was analyzed by SDS-PAGE, using an Amersham Imager 600RGB (GE Healthcare Life Sciences) to visualize labeled protein and free dye. The protein concentration was measured using the pre-configured "Proteins & Labels" function on a Nano Drop 2000c Spectrophotometer (Thermo Scientific).

3.5.6 Crystallography

To purify the NB02-*Xenopus* REEP5 and NB05-*Xenopus* REEP5 complexes for crystallography, the nanobodies were purified from *E. coli* as described above. *X. laevis* REEP5-SBP was also purified as described above with tag cleavage, but prior to SEC, REEP5 was mixed with a 5 molar excess of either NB02 or NB05. The complexes were purified by SEC on a Superdex200 column to remove excess free nanobody and concentrated to ~40 mg/ml by ultrafiltration using a 10,000 MW cut-off filter (Amicon Ultra, EMD Millipore).

For LCP crystallization trials, purified protein was reconstituted into LCP by mixing the protein solution with monoolein (Sigma Aldrich) at a ratio of 1.5:1.0 by mass using the coupled syringe reconstitution method. Samples were mixed at least 100 times to ensure homogeneity of the reconstitution. The resulting phase was dispensed in 50 nl drops onto a glass plate and overlaid with 500 nl of precipitant solution using a Gryphon LCP robot (Art Robbins Instruments). For vapor diffusion experiments, hanging drop crystallization trials were set up using a mosquito crystal robot (ttplabtech) in which 100 nl of protein solution was mixed with 100 nl of precipitant solution over a reservoir of 50 ul of precipitant solution.

3.5.7 Isolation of Nanobodies from yeast library

Isolation of nanobodies was performed as previously described (McMahon et al., 2017) with some modifications. Magnetic beads, LD and LS columns, and MACS magnet were all purchased from Miltenyi Biotec. Labeled anti-HA antibodies and labeled streptavidin was purchased from BioLegend.

MACS selections were performed as follows: The desired number of yeast cells were collected from culture (10-fold over estimated library diversity, never less than 1 x 10^7 cells), pelleted, and washed with selection buffer (20 mM HEPES pH 7.5, 150 mM NaCl, 0.1% bovine serum albumin, 5 mM maltose and either 0.1% DDM or 0.1% LMNG depending on the detergent used to purify the target protein). To remove any yeast cells expressing nanobodies that bind to the magnetic beads, the yeast cells were resuspended in 4.5 ml of selection buffer and 0.5 ml of magnetic beads that bind to the fluorophore or tag attached to the target protein were added to the suspension. After incubation for 40 minutes at 4° C, the cells were washed and resuspended in 5 ml of selection buffer. The cells were then flowed through a pre-equilibrated LD column on a MACS magnet to remove any yeast cells bound to the magnetic beads. The cells in the flow-through were collected, washed, and resuspended in 5 ml of selection buffer. The target protein was then added to the cells at the desired concentration and incubated for 1 hour at 4° C. The cells were then washed with selection buffer, resuspended in 4.5 ml of selection buffer, and incubated with 0.5 ml of magnetic beads for 20 minutes at 4° C. After incubation, the cells were washed, resuspended in 3 ml of selection buffer, and flowed through a pre-equilibrated LS column on a MACS magnet. The column was washed while on the MACS magnet with selection buffer. The column was then removed from the MACS magnet and the

captured yeast cells eluted using selection buffer. These cells were collected, pelleted, resuspended in media, and grown at 30° C for recovery.

FACS selections were performed as follows: For samples to be used in selection, 6 x 10^7 cells were collected, pelleted, and washed with selection buffer supplemented with the appropriate detergent. For compensation samples, 1 x 10^7 cells were collected, pelleted, and washed with selection buffer. The selection samples were resuspended in 6 ml of selection buffer and the compensation samples were resuspended in 1 ml of selection buffer. Labeled target proteins and/or antibodies were then added to the samples to the desired concentration. After incubation for 1 hr at 4° C, the selection and compensation samples were washed and resuspended in 3 ml and 0.5 ml of selection buffer respectively. The FACS was performed using a Sony SH800Z cell sorter. The compensation samples were used along with the built-in compensation wizard to generate a compensation matrix prior to cell sorting. Cells were collected in either 15 ml falcon tubes or 96-well plates depending on the experiment.

For isolation of nanobodies against *X. laevis* REEP5, the following selections were performed:

1) 1st round of MACS: 1 μM $REEP5_{LMNG}$-FITC
2) 2nd round of MACS: 0.5 μM REEP5-647
3) 3rd round of MACS: 0.1 μM REEP5-SBP
4) 1st round of FACS: yeast cells were stained with 0.01 μM $REEP5_{LMNG}$ -SBP pre-bound to PE-streptavidin, FITC-labeled anti-HA antibody, and 0.75 μM Alexa 647-labeled cytosolic fragment of Atlastin. Yeast cells were selected for high HA, high REEP5, and low 647-Atlastin staining and bulk sorted into a 15 ml falcon tube.

5) 2nd round of FACs: yeast cells were stained with 0.01 μM $REEP5_{LMNG}$ -SBP pre-bound to PE-streptavidin and FITC-labeled anti-HA antibody. Yeast cells were selected for high HA and high REEP5 staining. Individual cells were sorted into 96 well plates.

For isolation of nanobodies against *T. terrestris* REEP5 and *T. thermophila* REEP5, the following selections were performed:

1) 1st round of MACS: 1 μM SBP-tagged constructs
2) 2nd round of MACS: 1 μM FLAG-tagged constructs
3) 1st round of FACS: yeast cells were stained with 0.5 μM SBP-tagged constructs pre-bound to PE-streptavidin and Alexa 647-labeled HA antibody. Yeast cells were selected for high HA and high REEP5 staining and bulk sorted into a 15 ml falcon tube
4) 2nd round of FACS: yeast cells were stained with 0.1 μM SBP-tagged constructs pre-bound to PE-streptavidin and Alexa 647-labeled HA antibody. Yeast cells were selected for high HA and high REEP5 staining. Individual cells were sorted into 96 well plates.

Following sorting into 96 well plates, unique nanobody sequences were screened for by colony PCR. From liquid culture, 3 x 10^6 cells were collected, washed, and resuspended in 30 μl of 0.2% SDS. The samples were vortexed and heated at 90° C for 4 minutes. Cellular debris was removed by centrifugation and 0.5-2 μl of the sample was used in a 50 μl, standard PCR reaction.

Analytical fluorescent flow cytometry was performed using a BD Accuri C6 Plus (BD Biosciences). For each experiment, 1 x 10^6 cells were stained.

4

Concluding discussion

Organelles display characteristic shapes that are intimately tied to their cellular function. Thus, the question as to how organelle morphology is generated and maintained is a fundamental question in cell biology. The endoplasmic reticulum (ER) is a particularly powerful model system for studying organelle morphology, as the ER is composed of a continuous, interconnected network of tubules and sheets. While previous studies have demonstrated that the tubular ER is primarily shaped by the curvature-stabilizing activity of the reticulon and Yop1/REEP proteins (Hu et al., 2008; Voeltz et al., 2006) and the membrane fusing activity of the atlastin/Sey1 proteins (Anwar et al., 2012; Hu et al., 2009; Orso et al., 2009), how these proteins cooperate to give rise to the tubular ER network was unclear. Furthermore, not only had the minimal set of components needed to form and maintain a tubular ER network not been identified, it was unclear whether these components would allow for the ER dynamics observed *in vivo*. In this chapter I will summarize the novel and exciting insights that my thesis has

provided into how ER morphology is generated, and how these insights may be extendable to other organelle morphologies. I will also review the progress that I have made towards obtaining a structure of a curvature-stabilizing protein and suggest future experiments that leverage the tools that I have developed.

4.1 Reconstitution of the tubular ER network using a minimal set of proteins

In Chapter 2, I demonstrated that the tubular ER can be reconstituted using a minimal set of proteins consisting of a curvature-stabilizing protein and a membrane-fusing protein. When *S. cerevisiae* Yop1p and *S. cerevisiae* Sey1p were co-reconstituted into liposomes, the addition of GTP resulted in the formation of tubular networks that were nearly indistinguishable from those formed by the extracts of *Xenopus laevis* eggs. Network formation required the presence of both proteins, and both proteins were found distributed across the entire network. While this is in contradiction to some previous results that indicate that Sey1p is typically located at three-way junctions (Yan et al., 2015), the high protein concentration used in the reconstitution could force Sey1p to localize throughout the network. Furthermore, some atlastin proteins have been shown to localize throughout the entire ER network, not just at three-way junctions (Wang et al., 2016).

Atlastin had been previously shown to tether liposomes together (Liu et al., 2015; Saini et al., 2014). However, closer inspection of the reconstituted network by electron microscopy (EM) revealed that the networks were composed of fused junctions. Unfortunately the networks visualized by EM were much smaller than the networks observed using light microscopy, possibly due to the harsh conditions of staining. Future experiments could include using cryo-electron microscopy to analyze the reconstituted network, as the freezing procedure may preserve more of the network. Techniques such as tomography could then be used to more closely analyze the network architecture.

One of the most exciting observations was that the integrity of the reconstituted network was dependent upon continuous GTP hydrolysis by Sey1p. The addition of GTPγS lead to rapid disassembly of the network. This result is consistent with prior *in vitro* and *in vivo* experiments that show that inactivation of atlastin results in ER fragmentation in both *Xenopus laevis* egg extracts and in tissue culture cells (Wang et al., 2016).

Finally, I showed that the reconstituted tubular ER could also be formed using other purified curvature stabilizing proteins, including other members of the reticulon and Yop1/REEP families. This included proteins from other species, indicating that interaction between the curvature-stabilizing and the membrane-fusing proteins may not be necessary. Interestingly, *Drosophila melanogaster* atlastin formed tubular ER networks when reconstituted alone, demonstrating that in addition to its membrane-fusion activity, its hairpin transmembrane domain has an intrinsic ability to promote membrane curvature.

4.2 Model of tubular ER network formation and disassembly

Based on my results I construct the following model for the generation and maintenance of the ER tubular network. Small vesicles containing both a membrane-fusing protein and a curvature-stabilizing protein are fused together in a GTP hydrolysis-dependent manner to yield small tubules. As fusion continues, a larger network of interconnected tubules is formed, giving rise to the stereotypical polygonal ER network. However, due to the stress induced on the membrane by the curvature-stabilizing proteins, the tubules within the network are susceptible to fragmentation. This fragmentation is counteracted by the continuous activity of the membrane-fusing proteins, which can rapidly repair any breaks in the network. Upon inactivation of the membrane-fusing protein, the curvature-stabilizing proteins proceed to fragment the network, first into smaller tubules, and finally into small vesicles and/or stable, small "proto-networks".

Thus, the coordinated activity of the two proteins not only causes the tubular ER to assume its characteristic shape, but also allows the network to be highly dynamic.

The fact that inactivation of Sey1p leads to rapid fragmentation of the reconstituted network suggests that the reticulon and Yop1/REEP proteins may have a preference for the high curvature of small vesicles. Furthermore, the small size of the vesicles may indicate that these proteins mainly generate curvature by hydrophobic insertion (Hu et al., 2008, 2011) or through their C-terminal amphipathic helices (Brady et al., 2015; Breeze et al., 2016). Oligomerization of the proteins may occur at higher concentrations, explaining why both tubules and small vesicles can be visualized using EM with reconstituted yeast Yop1p or Rtn1p, and why oligomerization mutants are defective in tubule formation (Park et al., 2010; Shibata et al., 2008).

I speculate that both the continuous formation and disassembly of the ER network and the dynamics of tubular junctions may allow the rapid adaptation of ER shape to different conditions. For example, it may contribute to the conversion of tubules to sheets during the cell cycle (Friedman and Voeltz, 2011; Westrate et al., 2015) and may explain changes of ER morphology during cell differentiation (Park and Blackstone, 2010). The intrinsic dynamics of the ER network is likely further affected by other factors, including molecular motors, ribosome binding, and other morphogenic proteins. I propose that other organelles are shaped by similar principles as the ER, and represent a steady state between formation and disassembly that is mediated by a small set of proteins.

4.3 Physiological significance of the reconstituted ER network

The importance of the both the curvature-stabilizing and membrane-fusing proteins in tubular ER formation is underscored by the fact that mutations in many of these proteins cause the genetic neurological disease heredity spastic paraplegia (HSP) (Blackstone, 2018;

McCorquodale et al., 2011; Park and Blackstone, 2010). HSP is characterized by progressive lower limb-spasticity and weakness. This weakness appears to be due to axonal degeneration within motor neurons (Blackstone, 2018). Amongst the most commonly mutated genes in HSP patients are *ATL1* and *REEP1*, indicating that loss of the integrity of the tubular ER network in neurons may be an underlying cause of HSP. ATL1 is ubiquitously expressed, but is particularly enriched in brain tissue (Rismanchi et al., 2008; Zhu et al., 2003). The loss of ATL1 in cultured cortical neurons resulted in an axonal elongation defect (Zhu et al., 2006). This is consistent with my observation that the reconstituted network requires continuous GTP hydrolysis to maintain integrity.

Likewise, cortical neurons derived from REEP1 knockout mice show defects in the tubular ER (Beetz et al., 2013). The reconstituted network, like previous reconstitutions, required a relatively high concentration of the curvature-stabilizing proteins. The result is that the tubules in the reconstituted systems display a diameter of ~16 nm, which is significantly smaller than the ~60 nm often observed in tissue culture cells. However, a recent study using serial section electron microscopy has demonstrated that the tubular ER found in neurons is extremely thin, with tubules that have a diameter of 20-30 nm (Terasaki, 2018). Thus, the reconstituted network, with its apparently very thin tubules, may actually be a closer approximation to the axonal tubular ER than was first appreciated. It would be interesting to try to reconstitute some of the HSP-causing mutants, particularly the REEP1 mutants, to see what effect they have on the formation, integrity, and dynamics of the reconstituted network.

4.4 Future uses of the reconstituted ER network

The reconstituted network will also prove a valuable tool to test the activity of other proteins that are thought to shape the ER. First of all, it would be interesting to try to purify and

co-reconstitute proteins that are thought to promote the formation of ER sheets, like CLIMP-63, with Yop1p and Sey1p. One could test if CLIMP-63 is indeed sufficient to promote sheet formation. Furthermore, one could analyze protein localization and see if the curvature-stabilizing proteins do indeed localize to the edges of sheets and whether there is any other type of segregation between the three different protein classes.

One particularly enigmatic protein that could be studied using the reconstituted network is the protein called Lunapark. Lunapark is an ER-localized membrane protein that is present in all eukaryotic cells. Lunapark has been shown to localize to three-way junctions and was originally proposed to stabilize these junctions, thereby stabilizing the entire tubular network (Chen et al., 2012, 2015; Wang et al., 2016). Clearly, Lunapark is not required for network formation, but its exact function remains a mystery. Most recently, it was shown that the *in vitro* reconstitution of Lunapark into vesicles results in the formation of stacked bilayer discs (Wang et al., 2018). The incorporation of Lunapark and previously studied Lunapark mutants into the reconstituted network may begin to offer further insights into the function of the protein.

4.5 Initial progress towards the structure of a Yop1/REEP protein

Exactly how the reticulon and Yop1/REEP proteins stabilize positive membrane curvature on the molecular level is one of the most important, yet seemingly most difficult questions to answer, in the field of ER morphology. In Chapter 3, I presented a number of initial steps I took towards obtaining an atomic-resolution structural model of a curvature-stabilizing protein using x-ray crystallography. I chose *Xenopus laevis* REEP5 as my crystallization target as I was able to easily purify a large amount of the protein while performing my reconstitution experiments. I refined the *X. laevis* REEP5 purification protocol and determined that the protein could be efficiently solubilized and purified using LMNG, a detergent that is useful for lipidic

cubic phase (LCP) crystallization experiments. Given that REEP5 lacks any extensive hydrophilic surfaces for crystal packing, I used an *in vitro* yeast display system (McMahon et al., 2018) to isolate two nanobodies that bind to *X. laevis* REEP5 with high affinity for use as crystallization chaperones. I used both nanobodies in co-crystallization experiments with REEP5. I performed large scale screening for crystals using both LCP crystallization techniques and standard vapor diffusion methods.

While my preliminary experiments failed to yield crystals, there are a seemingly endless number of strategies that could be pursued to obtain initial crystals of the nanobody-*Xenopus* REEP5 complex. This includes reconstituting the complexes into different lipid compositions for LCP crystallization experiments. Modulating the lipid composition, particularly the length of the MAG and the presence of certain lipid additives, has proved indispensible for the crystallization of other membrane proteins (Ishchenko et al., 2017; Li et al., 2011). Furthermore, other membrane protein crystallization techniques could be pursued, including bicelle-mediated crystallization (Ishchenko et al., 2017).

In addition to attempting to crystallize *X. laevis* REEP5, I also cloned and purified REEP5 proteins derived from the thermophilic yeasts *Thielavia terrestris* and *Thermothelomyces thermophila*. Thermophilic proteins have proved a useful tool in crystallography, and both *T. terrestris* and *T. thermophila* REEP5 displayed superior behavior during protein purification. Using the lessons I learned working with *X. laevis* REEP5, I isolated a large number of nanobodies that bound with high affinity to *T. terrestris* REEP5 and *T. thermophila* REEP5. These nanobodies can be used in future crystallization experiments. Given the number of nanobodies I was able to isolate, I hope that I have sufficiently increased the probability of obtaining initial crystal hits that can be refined for structure determination.

I also developed an assay to test if two different nanobodies can bind to their target protein simultaneously. I used this assay to demonstrate that several of the *T. thermophila* REEP5-specific nanobodies can in fact co-bind to REEP5. These pairs of nanobodies can be used simultaneously in future experiments should crystallization with a single nanobody fail to yield high quality crystals. To increase the throughput of this assay, instead of labeling the soluble nanobody with an NHS-conjugated fluorophore, nanobodies with a genetically encoded, high affinity protein tag could be cloned, expressed, and purified. The soluble nanobody could then be labeled using commercially available, fluorescently labeled reagents that bind to that specific tag. For example, nanobodies with FLAG-tags could be labeled with a fluorescently conjugated anti-FLAG antibody. This is analogous to how I labeled the REEP5-SBP constructs using Phycoerythrin-labeled streptavidin. This would dramatically increase throughput and also remove the concern of free dye obscuring the experimental results. The assay could then be used to rapidly determine all of the pairs of nanobodies that can co-bind to REEP5 so that more crystallization experiments can be designed and tested.

4.6 Beyond a REEP5 structure: future experiments

If a structure of REEP5 can be obtained, there are numerous follow-up experiments that could be pursued to better understand how the protein stabilizes curvature. First, molecular dynamics simulations have been used to probe how certain proteins, including integral membrane proteins, are able to bend membranes (Davies et al., 2012; Hsin et al., 2009; Yu and Schulten, 2013). The structure of REEP5 could be used in conjugation with all-atom and coarse grain simulation to observe how REEP5 behaves within a lipid environment and how it may be able to shape the membrane. The structure of REEP5 could also be used to design mutants for use in further *in vitro* and *in vivo* experiments. This could include expressing, purifying, and

reconstituting these mutants to see if they are able to convert liposomes into tubules and to form a network in cooperation with a membrane-fusing protein.

Furthermore, although this type of assay has not yet been used to study reticulon/Yop1/REEP proteins, I propose the curvature-stabilizing activity of these proteins may be tested by overexpressing the proteins in *E. coli* and then visualizing the cells' membranes. Such an approach has been used to study caveolin, the protein responsible for forming pits in the surface of eukaryotic cells known as caveolae (Walser et al., 2012). EM analysis revealed that caveolin overexpression in *E. coli* led to the formation of caveolin-containing cytoplasmic vesicles. These vesicles were formed through a membrane budding process, and mutants of caveolin that are unable to form caveolae in mammalian cells were not able to drive vesicle formation in *E. coli*. It is possible that the reticulon and Yop1/REEP proteins could generate enough positive curvature to deform the *E. coli* membrane, possibly forming tubules or vesicles. If so, this would provide a relatively high through-put assay to study different REEP5 mutants as one would only have to overexpress the protein in *E. coli* rather than purify and reconstitute it.

4.7 Concluding thoughts

The results I have presented in this thesis represent a major step towards an understanding of the molecular mechanisms underlying ER morphology. I have demonstrated that a minimal set of proteins consisting of a membrane-fusing protein and a curvature-stabilizing protein can generate a dynamic tubular ER network. I have also generated a large set of tools for future crystallization experiments aimed at obtaining a structure of the curvature-stabilizing protein REEP5.

More broadly, my results demonstrate that organelle morphologies, such as the tubular network of the peripheral ER, can be generated using a surprisingly limited set of proteins. These

few proteins not only produce the general shape of a particular organelle, but can also account for seemingly complex morphological dynamics. In fact, the regulation of a single protein, Sey1p in the case of the reconstituted ER network, can cause drastic and rapid changes in morphology. The principles put forth by my model of ER morphology could be generalized to the study of other organelles, such as the nucleus and the golgi apparatus, both of which undergo significant remodeling during the cell cycle.

References

Anderson, D.J., and Hetzer, M.W. (2008). Reshaping of the endoplasmic reticulum limits the rate for nuclear envelope formation. J. Cell Biol. *182*, 911–924.

Anwar, K., Klemm, R.W., Condon, A., Severin, K.N., Zhang, M., Ghirlando, R., Hu, J., Rapoport, T.A., and Prinz, W.A. (2012). The dynamin-like GTPase Sey1p mediates homotypic ER fusion in S. cerevisiae. J. Cell Biol. *197*, 209–217.

Bannai, H., Inoue, T., Nakayama, T., Hattori, M., and Mikoshiba, K. (2004). Kinesin dependent, rapid, bi-directional transport of ER sub-compartment in dendrites of hippocampal neurons. J. Cell Sci. *117*, 163–175.

Baumann, O., and Walz, B. (2001). Endoplasmic reticulum of animal cells and its organization into structural and functional domains. Int. Rev. Cytol. *205*, 149–214.

Beetz, C., Koch, N., Khundadze, M., Zimmer, G., Nietzsche, S., Hertel, N., Huebner, A.-K., Mumtaz, R., Schweizer, M., Dirren, E., et al. (2013). A spastic paraplegia mouse model reveals REEP1-dependent ER shaping. J. Clin. Invest. *123*, 4273–4282.

Behrens, M., Bartelt, J., Reichling, C., Winnig, M., Kuhn, C., and Meyerhof, W. (2006). Members of RTP and REEP gene families influence functional bitter taste receptor expression. J. Biol. Chem. *281*, 20650–20659.

Bernales, S., McDonald, K.L., and Walter, P. (2006). Autophagy counterbalances endoplasmic reticulum expansion during the unfolded protein response. PLoS Biol. *4*, e423.

Bian, X., Klemm, R.W., Liu, T.Y., Zhang, M., Sun, S., Sui, X., Liu, X., Rapoport, T. a, and Hu, J. (2011). Structures of the atlastin GTPase provide insight into homotypic fusion of

endoplasmic reticulum membranes. Proc. Natl. Acad. Sci. U. S. A. *108*, 3976–3981.

Bjork, S., Hurt, C.M., Ho, V.K., and Angelotti, T. (2013). REEPs are membrane shaping adapter proteins that modulate specific g protein-coupled receptor trafficking by affecting ER cargo capacity. PLoS One *8*, e76366.

Blackstone, C. (2018). Hereditary spastic paraplegia. Handb. Clin. Neurol. *148*, 633–652.

Boevink, P., Oparka, K., Santa Cruz, S., Martin, B., Betteridge, A., and Hawes, C. (1998). Stacks on tracks: the plant Golgi apparatus traffics on an actin/ER network. Plant J. *15*, 441–447.

Bola, B., and Allan, V. (2009). How and why does the endoplasmic reticulum move? Biochem. Soc. Trans. *37*, 961–965.

Brady, J.P., Claridge, J.K., Smith, P.G., and Schnell, J.R. (2015). A conserved amphipathic helix is required for membrane tubule formation by Yop1p. Proc. Natl. Acad. Sci. U. S. A. *112*, E639–E648.

Breeze, E., Dzimitrowicz, N., Kriechbaumer, V., Brooks, R., Botchway, S.W., Brady, J.P., Hawes, C., Dixon, A.M., Schnell, J.R., Fricker, M.D., et al. (2016). A C-terminal amphipathic helix is necessary for the in vivo tubule-shaping function of a plant reticulon. Proc. Natl. Acad. Sci. U. S. A. *113*, 10902–10907.

Byrnes, L.J., and Sondermann, H. (2011). Structural basis for the nucleotide-dependent dimerization of the large G protein atlastin-1/SPG3A. Proc. Natl. Acad. Sci. U. S. A. *108*, 2216–2221.

Byrnes, L.J., Singh, A., Szeto, K., Benvin, N.M., O'Donnell, J.P., Zipfel, W.R., and Sondermann, H. (2013). Structural basis for conformational switching and GTP loading of the large G protein atlastin. EMBO J. *32*, 369–384.

Chen, S., Novick, P., and Ferro-Novick, S. (2012). ER network formation requires a balance of the dynamin-like GTPase Sey1p and the Lunapark family member Lnp1p. Nat. Cell Biol. *14*, 707–716.

Chen, S., Novick, P., and Ferro-Novick, S. (2013). ER structure and function. Curr. Opin. Cell Biol. *25*, 428–433.

Chen, S., Desai, T., McNew, J. a., Gerard, P., Novick, P.J., and Ferro-Novick, S. (2015). Lunapark stabilizes nascent three-way junctions in the endoplasmic reticulum. Proc. Natl. Acad. Sci. *112*, 418–423.

Cherezov, V. (2011). Lipidic cubic phase technologies for membrane protein structural studies. Curr. Opin. Struct. Biol. *21*, 559–566.

Davies, K.M., Anselmi, C., Wittig, I., Faraldo-Gomez, J.D., and Kuhlbrandt, W. (2012). Structure of the yeast F1Fo-ATP synthase dimer and its role in shaping the mitochondrial cristae. Proc. Natl. Acad. Sci. U. S. A. *109*, 13602–13607.

Dreier, L., and Rapoport, T. a. (2000). In vitro formation of the endoplasmic reticulum occurs independently of microtubules by a controlled fusion reaction. J. Cell Biol. *148*, 883–898.

Drin, G., and Antonny, B. (2010). Amphipathic helices and membrane curvature. FEBS Lett. *584*, 1840–1847.

Dunham, J.H., and Hall, R.A. (2009). Enhancement of the surface expression of G protein-coupled receptors. Trends Biotechnol. *27*, 541–545.

English, A.R., and Voeltz, G.K. (2013). Endoplasmic reticulum structure and interconnections with other organelles. Cold Spring Harb. Perspect. Biol. *5*, 1–16.

Faust, J.E., Desai, T., Verma, A., Ulengin, I., Sun, T.-L., Moss, T.J., Betancourt-Solis, M.A., Huang, H.W., Lee, T., and McNew, J.A. (2015). The Atlastin C-terminal tail is an amphipathic helix that perturbs the bilayer structure during endoplasmic reticulum homotypic fusion. J. Biol. Chem. *290*, 4772–4783.

Fawcett, D.W. (1981). The cell (W. B. Saunders Co.).

Fehrenbacher, K.L., Davis, D., Wu, M., Boldogh, I., and Pon, L.A. (2002). Endoplasmic reticulum dynamics, inheritance, and cytoskeletal interactions in budding yeast. Mol. Biol. Cell *13*, 854–865.

Feiguin, F., Ferreira, A., Kosik, K.S., and Caceres, A. (1994). Kinesin-mediated organelle translocation revealed by specific cellular manipulations. J. Cell Biol. *127*, 1021–1039.

Friedman, J.R., and Voeltz, G.K. (2011). The ER in 3D: a multifunctional dynamic membrane network. Trends Cell Biol. *21*, 709–717.

Friedman, J.R., Webster, B.M., Mastronarde, D.N., Verhey, K.J., and Voeltz, G.K. (2010). ER sliding dynamics and ER-mitochondrial contacts occur on acetylated microtubules. J. Cell Biol. *190*, 363–375.

Geertsma, E.R., Chang, Y.-N., Shaik, F.R., Neldner, Y., Pardon, E., Steyaert, J., and Dutzler, R. (2015). Structure of a prokaryotic fumarate transporter reveals the architecture of the SLC26 family. Nat. Struct. Mol. Biol. *22*, 803–808.

Gonzalez, C., and Couve, A. (2014). The axonal endoplasmic reticulum and protein trafficking: Cellular bootlegging south of the soma. Semin. Cell Dev. Biol. *27*, 23–31.

Goyal, U., and Blackstone, C. (2013). Untangling the web: Mechanisms underlying ER network formation. Biochim. Biophys. Acta - Mol. Cell Res. *1833*, 2492–2498.

GrandPre, T., Nakamura, F., Vartanian, T., and Strittmatter, S.M. (2000). Identification of the Nogo inhibitor of axon regeneration as a Reticulon protein. Nature *403*, 439–444.

Grigoriev, I., Gouveia, S.M., van der Vaart, B., Demmers, J., Smyth, J.T., Honnappa, S., Splinter, D., Steinmetz, M.O., Putney, J.W.J., Hoogenraad, C.C., et al. (2008). STIM1 is a MT-plus-end-tracking protein involved in remodeling of the ER. Curr. Biol. *18*, 177–182.

Hamers-Casterman, C., Atarhouch, T., Muyldermans, S., Robinson, G., Hamers, C., Songa, E.B., Bendahman, N., and Hamers, R. (1993). Naturally occurring antibodies devoid of light chains. Nature *363*, 446–448.

Hassaine, G., Deluz, C., Grasso, L., Wyss, R., Tol, M.B., Hovius, R., Graff, A., Stahlberg, H., Tomizaki, T., Desmyter, A., et al. (2014). X-ray structure of the mouse serotonin 5-HT3 receptor. Nature *512*, 276–281.

Hsin, J., Gumbart, J., Trabuco, L.G., Villa, E., Qian, P., Hunter, C.N., and Schulten, K. (2009). Protein-Induced Membrane Curvature Investigated through Molecular Dynamics Flexible Fitting. Biophys. J. *97*, 321–329.

Hu, J., and Rapoport, T.A. (2016). Fusion of the endoplasmic reticulum by membrane-bound GTPases. Semin. Cell Dev. Biol. *60*, 105–111.

Hu, J., Shibata, Y., Voss, C., Shemesh, T., Li, Z., Coughlin, M., Kozlov, M.M., Rapoport, T. a, and Prinz, W. a (2008). Membrane proteins of the endoplasmic reticulum induce high-curvature tubules. Science *319*, 1247–1250.

Hu, J., Shibata, Y., Zhu, P.P., Voss, C., Rismanchi, N., Prinz, W. a., Rapoport, T. a., and Blackstone, C. (2009). A Class of Dynamin-like GTPases Involved in the Generation of the Tubular ER Network. Cell *138*, 549–561.

Hu, J., Prinz, W. a., and Rapoport, T. a. (2011). Weaving the web of ER tubules. Cell *147*, 1226–1231.

Hubner, C.A., and Kurth, I. (2014). Membrane-shaping disorders: a common pathway in axon degeneration. Brain *137*, 3109–3121.

Ishchenko, A., Abola, E.E., and Cherezov, V. (2017). Crystallization of Membrane Proteins: An Overview. Methods Mol. Biol. *1607*, 117–141.

Iwahashi, J., Kawasaki, I., Kohara, Y., Gengyo-Ando, K., Mitani, S., Ohshima, Y., Hamada, N., Hara, K., Kashiwagi, T., and Toyoda, T. (2002). Caenorhabditis elegans reticulon interacts with RME-1 during embryogenesis. Biochem. Biophys. Res. Commun. *293*, 698–704.

Klopfenstein, D.R., Klumperman, J., Lustig, A., Kammerer, R.A., Oorschot, V., and Hauri, H.P. (2001). Subdomain-specific localization of CLIMP-63 (p63) in the endoplasmic reticulum is mediated by its luminal alpha-helical segment. J. Cell Biol. *153*, 1287–1300.

Kulak, N.A., Pichler, G., Paron, I., Nagaraj, N., and Mann, M. (2014). Minimal, encapsulated proteomic-sample processing applied to copy-number estimation in eukaryotic cells. Nat.

Methods *11*, 319–324.

Lee, C., and Chen, L.B. (1988). Dynamic behavior of endoplasmic reticulum in living cells. Cell *54*, 37–46.

Lee, C., Ferguson, M., and Chen, L.B. (1989). Construction of the endoplasmic reticulum. J. Cell Biol. *109*, 2045–2055.

Li, D., Lee, J., and Caffrey, M. (2011). Crystallizing Membrane Proteins in Lipidic Mesophases. A Host Lipid Screen. Cryst. Growth Des. *11*, 530–537.

Li, L., Park, E., Ling, J., Ingram, J., Ploegh, H., and Rapoport, T.A. (2016). Crystal structure of a substrate-engaged SecY protein-translocation channel. Nature *531*, 395–399.

Liu, T.Y., Bian, X., Sun, S., Hu, X., Klemm, R.W., Prinz, W. a., Rapoport, T. a., and Hu, J. (2012). PNAS Plus: Lipid interaction of the C terminus and association of the transmembrane segments facilitate atlastin-mediated homotypic endoplasmic reticulum fusion. Proc. Natl. Acad. Sci. *109*, E2146–E2154.

Liu, T.Y., Bian, X., Romano, F.B., Shemesh, T., Rapoport, T.A., and Hu, J. (2015). Cis and trans interactions between atlastin molecules during membrane fusion. Proc. Natl. Acad. Sci. U. S. A.

McCorquodale, D.S. 3rd, Ozomaro, U., Huang, J., Montenegro, G., Kushman, A., Citrigno, L., Price, J., Speziani, F., Pericak-Vance, M.A., and Zuchner, S. (2011). Mutation screening of spastin, atlastin, and REEP1 in hereditary spastic paraplegia. Clin. Genet. *79*, 523–530.

McMahon, C., Baier, A.S., Zheng, S., Pascolutti, R., Ong, J.X., Erlandson, S.C., Hilger, D., Ring, A.M., Manglik, A., and Kruse, A.C. (2017). Platform for rapid nanobody discovery in vitro. bioRxiv.

McMahon, C., Baier, A.S., Pascolutti, R., Wegrecki, M., Zheng, S., Ong, J.X., Erlandson, S.C., Hilger, D., Rasmussen, S.G.F., Ring, A.M., et al. (2018). Yeast surface display platform for rapid discovery of conformationally selective nanobodies. Nat. Struct. Mol. Biol. *25*, 289–296.

Moreira, E.F., Jaworski, C.J., and Rodriguez, I.R. (1999). Cloning of a novel member of the reticulon gene family (RTN3): gene structure and chromosomal localization to 11q13. Genomics *58*, 73–81.

Muyldermans, S. (2013). Nanobodies: natural single-domain antibodies. Annu. Rev. Biochem. *82*, 775–797.

Oertle, T., Klinger, M., Stuermer, C.A.O., and Schwab, M.E. (2003a). A reticular rhapsody: phylogenic evolution and nomenclature of the RTN/Nogo gene family. FASEB J. Off. Publ. Fed. Am. Soc. Exp. Biol. *17*, 1238–1247.

Oertle, T., Huber, C., van der Putten, H., and Schwab, M.E. (2003b). Genomic structure and

functional characterisation of the promoters of human and mouse nogo/rtn4. J. Mol. Biol. *325*, 299–323.

Orso, G., Pendin, D., Liu, S., Tosetto, J., Moss, T.J., Faust, J.E., Micaroni, M., Egorova, A., Martinuzzi, A., McNew, J. a, et al. (2009). Homotypic fusion of ER membranes requires the dynamin-like GTPase atlastin. Nature *460*, 978–983.

Palade, G.E. (1956). The endoplasmic reticulum. J. Biophys. Biochem. Cytol. *2*, 85–98.

Palade, G.E., and Porter, K.R. (1954). Studies on the endoplasmic reticulum. I. Its identification in cells in situ. J. Exp. Med. *100*, 641–656.

Palade, G.E., and Siekevitz, P. (1956). Liver microsomes; an integrated morphological and biochemical study. J. Biophys. Biochem. Cytol. *2*, 171–200.

Park, S.H., and Blackstone, C. (2010). Further assembly required: construction and dynamics of the endoplasmic reticulum network. EMBO Rep. *11*, 515–521.

Park, S.H., Zhu, P.-P., Parker, R.L., and Blackstone, C. (2010). Hereditary spastic paraplegia proteins REEP1, spastin, and atlastin-1 coordinate microtubule interactions with the tubular ER network. J. Clin. Invest. *120*, 1097–1110.

Porter, K.R. (1953). Observations on a submicroscopic basophilic component of cytoplasm. J. Exp. Med. *97*, 727–750.

Puhka, M., Vihinen, H., Joensuu, M., and Jokitalo, E. (2007). Endoplasmic reticulum remains continuous and undergoes sheet-to-tubule transformation during cell division in mammalian cells. J. Cell Biol. *179*, 895–909.

Ramirez, O.A., Hartel, S., and Couve, A. (2011). Location matters: the endoplasmic reticulum and protein trafficking in dendrites. Biol. Res. *44*, 17–23.

Rasmussen, S.G.F., DeVree, B.T., Zou, Y., Kruse, A.C., Chung, K.Y., Kobilka, T.S., Thian, F.S., Chae, P.S., Pardon, E., Calinski, D., et al. (2011a). Crystal structure of the beta2 adrenergic receptor-Gs protein complex. Nature *477*, 549–555.

Rasmussen, S.G.F., Choi, H.-J., Fung, J.J., Pardon, E., Casarosa, P., Chae, P.S., Devree, B.T., Rosenbaum, D.M., Thian, F.S., Kobilka, T.S., et al. (2011b). Structure of a nanobody-stabilized active state of the beta(2) adrenoceptor. Nature *469*, 175–180.

Rigaud, J.-L., and Levy, D. (2003). Reconstitution of membrane proteins into liposomes. Methods Enzymol. *372*, 65–86.

Rismanchi, N., Soderblom, C., Stadler, J., Zhu, P.-P., and Blackstone, C. (2008). Atlastin GTPases are required for Golgi apparatus and ER morphogenesis. Hum. Mol. Genet. *17*, 1591–1604.

Roebroek, A.J., van de Velde, H.J., Van Bokhoven, A., Broers, J.L., Ramaekers, F.C., and Van

de Ven, W.J. (1993). Cloning and expression of alternative transcripts of a novel neuroendocrine-specific gene and identification of its 135-kDa translational product. J. Biol. Chem. *268*, 13439–13447.

Roebroek, A.J., Ayoubi, T.A., Van de Velde, H.J., Schoenmakers, E.F., Pauli, I.G., and Van de Ven, W.J. (1996). Genomic organization of the human NSP gene, prototype of a novel gene family encoding reticulons. Genomics *32*, 191–199.

Roebroek, A.J., Contreras, B., Pauli, I.G., and Van de Ven, W.J. (1998). cDNA cloning, genomic organization, and expression of the human RTN2 gene, a member of a gene family encoding reticulons. Genomics *51*, 98–106.

Sadaf, A., Cho, K.H., Byrne, B., and Chae, P.S. (2015). Amphipathic agents for membrane protein study. Methods Enzymol. *557*, 57–94.

Saini, S.G., Liu, C., Zhang, P., and Lee, T.H. (2014). Membrane tethering by the atlastin GTPase depends on GTP hydrolysis but not on forming the cross-over configuration. Mol. Biol. Cell *25*, 3942–3953.

Salinas, S., Proukakis, C., Crosby, A., and Warner, T.T. (2008). Hereditary spastic paraplegia: clinical features and pathogenetic mechanisms. Lancet. Neurol. *7*, 1127–1138.

Di Sano, F., Bernardoni, P., and Piacentini, M. (2012). The reticulons: guardians of the structure and function of the endoplasmic reticulum. Exp. Cell Res. *318*, 1201–1207.

Schlaitz, A.-L., Thompson, J., Wong, C.C.L., Yates, J.R. 3rd, and Heald, R. (2013). REEP3/4 ensure endoplasmic reticulum clearance from metaphase chromatin and proper nuclear envelope architecture. Dev. Cell *26*, 315–323.

Schuldiner, M., and Schwappach, B. (2013). From rags to riches - the history of the endoplasmic reticulum. Biochim. Biophys. Acta *1833*, 2389–2391.

Schwarz, D.S., and Blower, M.D. (2016). The endoplasmic reticulum: structure, function and response to cellular signaling. Cell. Mol. Life Sci. *73*, 79–94.

Shemesh, T., Klemm, R.W., Romano, F.B., Wang, S., Vaughan, J., Zhuang, X., Tukachinsky, H., Kozlov, M.M., and Rapoport, T. a. (2014). A model for the generation and interconversion of ER morphologies. Proc. Natl. Acad. Sci. *111*, E5243–E5251.

Shibata, Y., Voeltz, G.K., and Rapoport, T.A. (2006). Rough sheets and smooth tubules. Cell *126*, 435–439.

Shibata, Y., Voss, C., Rist, J.M., Hu, J., Rapoport, T.A., Prinz, W.A., and Voeltz, G.K. (2008). The reticulon and DP1/Yop1p proteins form immobile oligomers in the tubular endoplasmic reticulum. J. Biol. Chem. *283*, 18892–18904.

Shibata, Y., Hu, J., Kozlov, M.M., and Rapoport, T.A. (2009). Mechanisms shaping the membranes of cellular organelles. Annu. Rev. Cell Dev. Biol. *25*, 329–354.

Shibata, Y., Shemesh, T., Prinz, W.A., Palazzo, A.F., Kozlov, M.M., and Rapoport, T.A. (2010). Mechanisms determining the morphology of the peripheral ER. Cell *143*, 774–788.

Smirnova, I., Kasho, V., Jiang, X., Pardon, E., Steyaert, J., and Kaback, H.R. (2014). Outward-facing conformers of LacY stabilized by nanobodies. Proc. Natl. Acad. Sci. U. S. A. *111*, 18548–18553.

Terasaki, M. (2018). Axonal endoplasmic reticulum is very narrow. J. Cell Sci. *131*.

Terasaki, M., Song, J., Wong, J.R., Weiss, M.J., and Chen, L.B. (1984). Localization of endoplasmic reticulum in living and glutaraldehyde-fixed cells with fluorescent dyes. Cell *38*, 101–108.

Terasaki, M., Chen, L.B., and Fujiwara, K. (1986). Microtubules and the endoplasmic reticulum are highly interdependent structures. J. Cell Biol. *103*, 1557–1568.

Terasaki, M., Shemesh, T., Kasthuri, N., Klemm, R.W., Schalek, R., Hayworth, K.J., Hand, A.R., Yankova, M., Huber, G., Lichtman, J.W., et al. (2013). XStacked endoplasmic reticulum sheets are connected by helicoidal membrane motifs. Cell *154*, 285–296.

Tolley, N., Sparkes, I., Craddock, C.P., Eastmond, P.J., Runions, J., Hawes, C., and Frigerio, L. (2010). Transmembrane domain length is responsible for the ability of a plant reticulon to shape endoplasmic reticulum tubules in vivo. Plant J. *64*, 411–418.

Ueda, H., Yokota, E., Kutsuna, N., Shimada, T., Tamura, K., Shimmen, T., Hasezawa, S., Dolja, V. V, and Hara-Nishimura, I. (2010). Myosin-dependent endoplasmic reticulum motility and F-actin organization in plant cells. Proc. Natl. Acad. Sci. U. S. A. *107*, 6894–6899.

Veratti, E. (1961). Investigations on the fine structure of striated muscle fiber read before the Reale Istituto Lombardo, 13 March 1902. J. Biophys. Biochem. Cytol. *10(4)Suppl*, 1–59.

Voeltz, G.K., Rolls, M.M., and Rapoport, T.A. (2002). Structural organization of the endoplasmic reticulum. EMBO Rep. *3*, 944–950.

Voeltz, G.K., Prinz, W. a., Shibata, Y., Rist, J.M., and Rapoport, T. a. (2006). A class of membrane proteins shaping the tubular endoplasmic reticulum. Cell *124*, 573–586.

Walser, P.J., Ariotti, N., Howes, M., Ferguson, C., Webb, R., Schwudke, D., Leneva, N., Cho, K.-J., Cooper, L., Rae, J., et al. (2012). Constitutive formation of caveolae in a bacterium. Cell *150*, 752–763.

Wang, S., Romano, F.B., Field, C.M., Mitchison, T.J., and Rapoport, T. a. (2013). Multiple mechanisms determine ER network morphology during the cell cycle in Xenopus egg extracts. J. Cell Biol. *203*, 801–814.

Wang, S., Tukachinsky, H., Romano, F.B., and Rapoport, T.A. (2016). Cooperation of the ER-shaping proteins atlastin, lunapark, and reticulons to generate a tubular membrane network. Elife *5*.

Wang, S., Powers, R.E., Gold, V.A.M., and Rapoport, T.A. (2018). The ER morphology-regulating lunapark protein induces the formation of stacked bilayer discs. Life Sci. Alliance *1*.

Waterman-Storer, C.M., and Salmon, E.D. (1998). Endoplasmic reticulum membrane tubules are distributed by microtubules in living cells using three distinct mechanisms. Curr. Biol. *8*, 798–806.

Waterman-Storer, C.M., Gregory, J., Parsons, S.F., and Salmon, E.D. (1995). Membrane/microtubule tip attachment complexes (TACs) allow the assembly dynamics of plus ends to push and pull membranes into tubulovesicular networks in interphase Xenopus egg extracts. J. Cell Biol. *130*, 1161–1169.

Westrate, L.M., Lee, J.E., Prinz, W.A., and Voeltz, G.K. (2015). Form follows function: the importance of endoplasmic reticulum shape. Annu. Rev. Biochem. *84*, 791–811.

Wozniak, M.J., Bola, B., Brownhill, K., Yang, Y.-C., Levakova, V., and Allan, V.J. (2009). Role of kinesin-1 and cytoplasmic dynein in endoplasmic reticulum movement in VERO cells. J. Cell Sci. *122*, 1979–1989.

Wu, F., Hu, X., Bian, X., Liu, X., and Hu, J. (2015). Comparison of human and Drosophila atlastin GTPases. Protein Cell *6*, 139–146.

Xiang, J., Chun, E., Liu, C., Jing, L., Al-Sahouri, Z., Zhu, L., and Liu, W. (2016). Successful Strategies to Determine High-Resolution Structures of GPCRs. Trends Pharmacol. Sci. *37*, 1055–1069.

Yan, L., Sun, S., Wang, W., Shi, J., Hu, X., Wang, S., Su, D., Rao, Z., Hu, J., and Lou, Z. (2015). Structures of the yeast dynamin-like GTPase Sey1p provide insight into homotypic ER fusion. J. Cell Biol. *210*, 961–972.

Yang, Y.S., and Strittmatter, S.M. (2007). The reticulons: a family of proteins with diverse functions. Genome Biol. *8*, 234.

Yin, X., Xu, H., Hanson, M., and Liu, W. (2014). GPCR crystallization using lipidic cubic phase technique. Curr. Pharm. Biotechnol. *15*, 971–979.

Yu, H., and Schulten, K. (2013). Membrane Sculpting by F-BAR Domains Studied by Molecular Dynamics Simulations. PLOS Comput. Biol. *9*, e1002892.

Zhang, H., and Hu, J. (2016). Shaping the Endoplasmic Reticulum into a Social Network. Trends Cell Biol. *26*, 934–943.

Zhang, D., Vjestica, A., and Oliferenko, S. (2010). The cortical ER network limits the permissive zone for actomyosin ring assembly. Curr. Biol. *20*, 1029–1034.

Zhang, M., Wu, F., Shi, J., Zhu, Y., Zhu, Z., Gong, Q., and Hu, J. (2013). ROOT HAIR DEFECTIVE3 family of dynamin-like GTPases mediates homotypic endoplasmic

reticulum fusion and is essential for Arabidopsis development. Plant Physiol. *163*, 713–720.

Zhu, P.-P., Patterson, A., Lavoie, B., Stadler, J., Shoeb, M., Patel, R., and Blackstone, C. (2003). Cellular localization, oligomerization, and membrane association of the hereditary spastic paraplegia 3A (SPG3A) protein atlastin. J. Biol. Chem. *278*, 49063–49071.

Zhu, P.-P., Soderblom, C., Tao-Cheng, J.-H., Stadler, J., and Blackstone, C. (2006). SPG3A protein atlastin-1 is enriched in growth cones and promotes axon elongation during neuronal development. Hum. Mol. Genet. *15*, 1343–1353.

Zimmerman, B., Kelly, B., McMillan, B.J., Seegar, T.C.M., Dror, R.O., Kruse, A.C., and Blacklow, S.C. (2016). Crystal Structure of a Full-Length Human Tetraspanin Reveals a Cholesterol-Binding Pocket. Cell *167*, 1041–1051.e11.

Zurek, N., Sparks, L., and Voeltz, G. (2011). Reticulon short hairpin transmembrane domains are used to shape ER tubules. Traffic *12*, 28–41.

Appendix A
Appendix to Chapter 2

This chapter has been previously published as:

Powers, R.E.*, Wang, S.*, Liu, T.Y., and Rapoport, T.A. (2017). Reconstitution of the tubular endoplasmic reticulum network with purified components. *Nature* 543, 257–260.

* denotes equal contribution

A.1 Supplementary figures for chapter 2

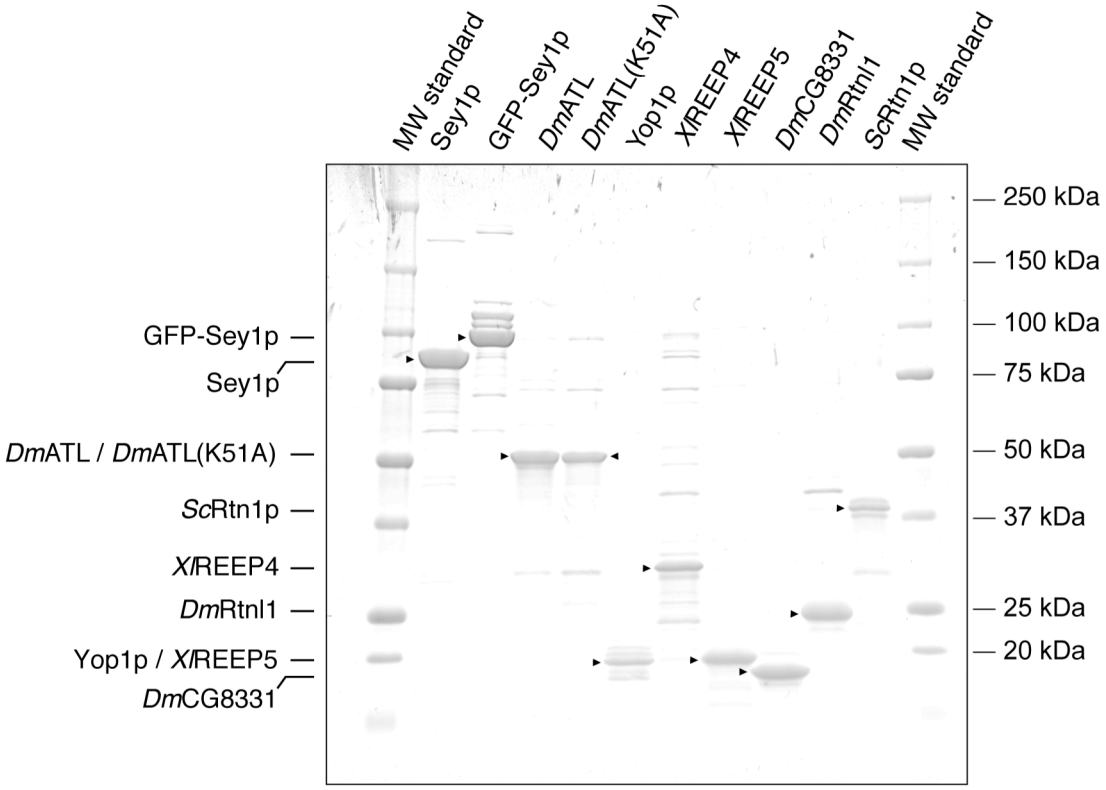

Figure A.1 Purity of ER-shaping proteins used in reconstitution experiments.
The indicated proteins were purified and subjected to SDS-PAGE and Coomassie blue staining.

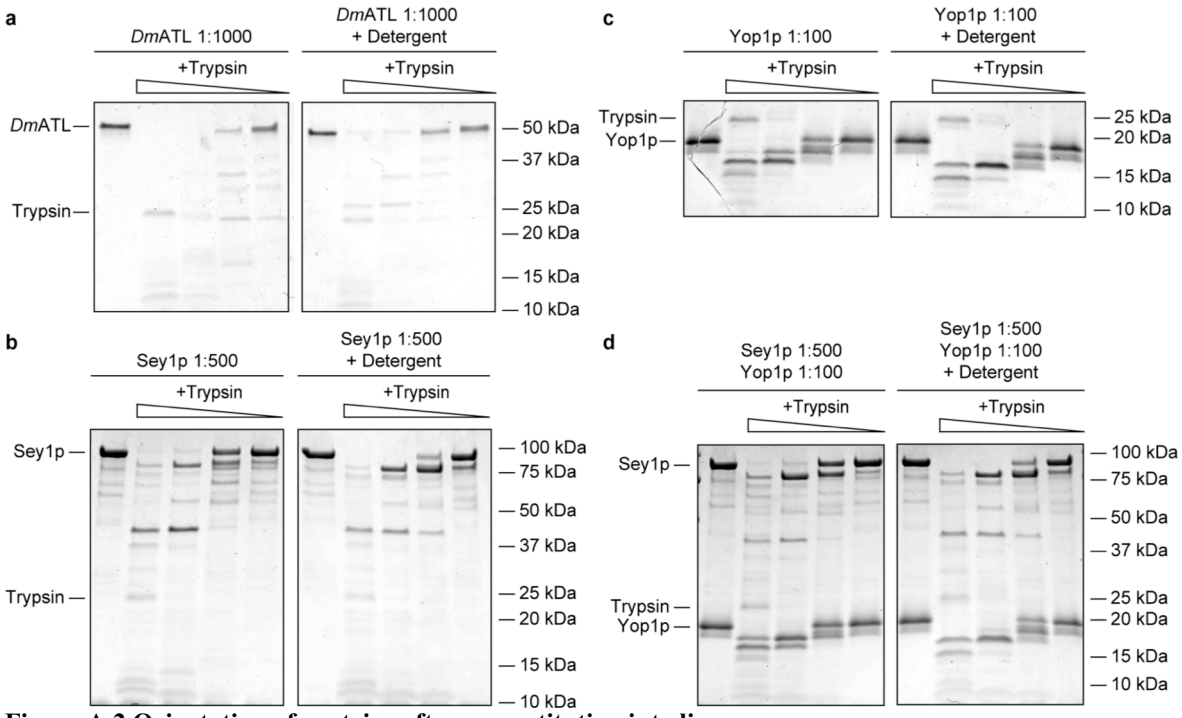

Figure A.2 Orientation of proteins after reconstitution into liposomes.

A) *D. melanogaster* ATL was reconstituted into rhodamine-PE labeled liposomes at a protein:lipid ratio of 1:1000. The vesicles were incubated with decreasing amounts of trypsin in the absence (left) or presence (right) of 0.2% Triton-X 100 for 30 min at room temperature. Samples were analyzed by SDS-PAGE and Coomassie blue staining. **B)** As in **A**, but with *S. cerevisiae* Sey1p at a protein:lipid ratio of 1:500. **C)** As in **A**, but with *S. cerevisiae* Yop1p at a protein:lipid ratio of 1:100. **D)** As in **A**, but with Sey1p and Yop1p at protein:lipid ratios of 1:500 and 1:100, respectively.

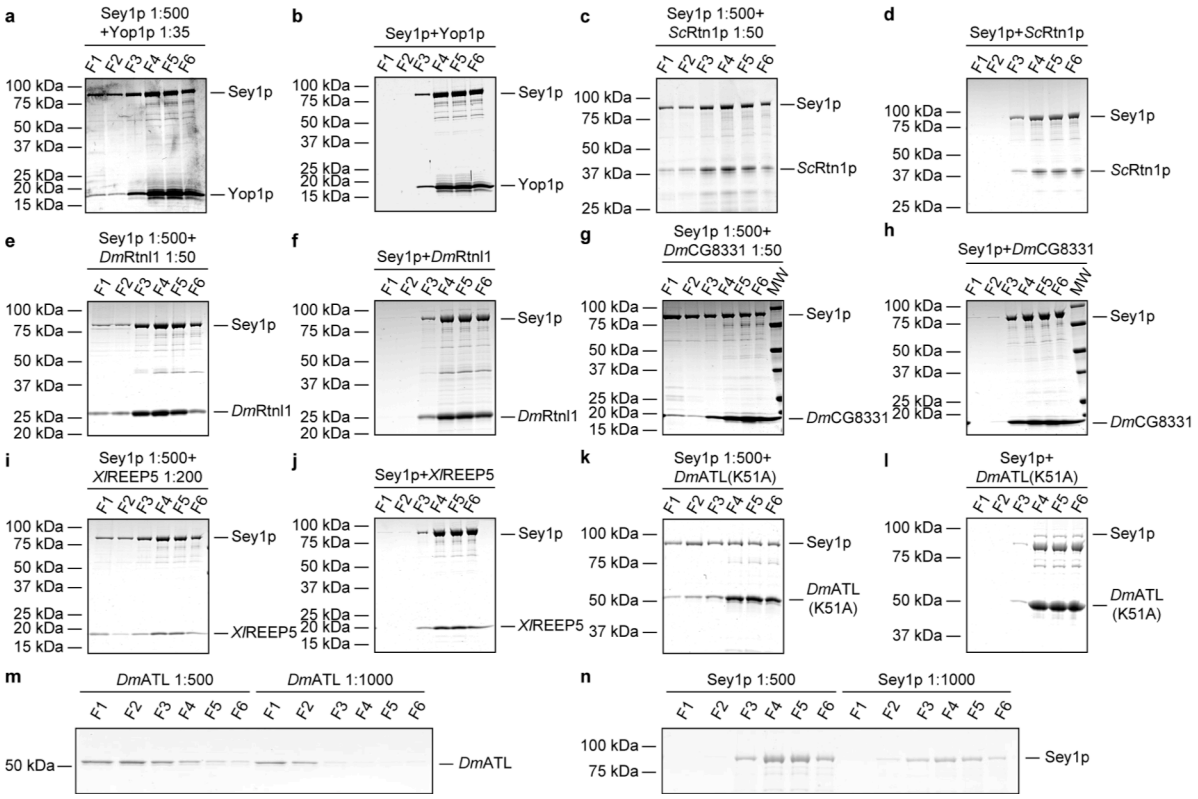

Figure A.3 Flotation of proteoliposomes generated with Sey1p and curvature-stabilizing proteins.
A) *S. cerevisiae* Sey1p and Yop1p were co-reconstituted into rhodamine-PE labeled liposomes at protein:lipid ratios of 1:500 and 1:35, respectively. The samples were centrifuged in a Nycodenz gradient, and fractions (F1-F6) were collected from the top and analyzed by SDS-PAGE and Coomassie blue staining. **B)** As in **A**, but with proteins only in the presence of 0.03% DDM. **C)** As in **A**, but with proteoliposomes containing *S. cerevisiae* Sey1p and Rtn1p at protein:lipid ratios of 1:500 and 1:50, respectively. **D)** As in **C**, but with proteins only in the presence of 0.03% DDM. **E)**, As in **A**, but with proteoliposomes containing Sey1p and *D. melanogaster* Rtn1p at protein:lipid ratios of 1:500 and 1:50, respectively. **F)** As in **E**, but with proteins only in the presence of 0.03% DDM. **G)** As in **A**, but with proteoliposomes containing Sey1p and *D. melanogaster* CG8331 at protein:lipid ratios of 1:500 and 1:50, respectively. **H**) As in **G**, but with proteins only in the presence of 0.03% DDM. **I)**, As in **A**, but with proteoliposomes containing Sey1p and *X. laevis* REEP5 at protein:lipid ratios of 1:500 and 1:200, respectively. **J)** As in **I**, but with proteins only in the presence of 0.03% DDM. **K**) As in **A**, but with proteoliposomes containing Sey1p and *D. melanogaster* ATL^{K51A} at protein:lipid ratios of 1:500 and 1:100, respectively. **L**) As in **K**, but with proteins only in the presence of 0.03% DDM. **M)** As in **A**, but with proteoliposomes containing *D. melanogaster* ATL at protein:lipid ratios of 1:500 or 1:1000. **N)** As in **A**, but with proteoliposomes containing *S. cerevisiae* Sey1p at protein:lipid ratios of 1:500 or 1:1000.

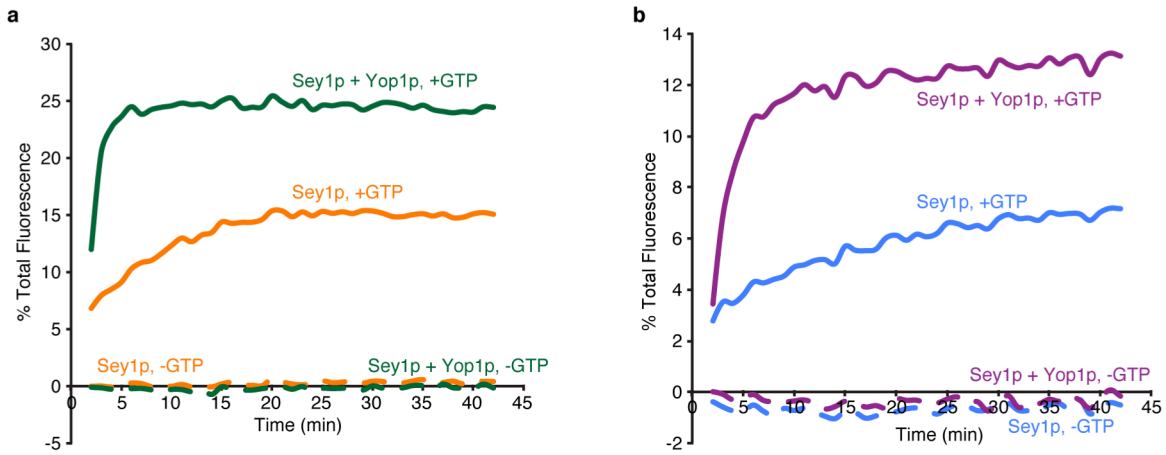

Figure A.4 Fusion activity of Sey1p-containing proteoliposomes.
A) Proteoliposomes were generated with either *S. cerevisiae* Sey1p alone (protein:lipid ratio of 1:500) or with Sey1p and *S. cerevisiae* Yop1p (protein:lipid ratios of 1:500 and 1:100, respectively). Donor vesicles contained NBD-PE and rhodamine-PE. Following addition of 1 mM GTP, fusion with unlabeled acceptor vesicles was measured by dequenching of the NBD fluorescence. Controls were performed in the absence of GTP. **B)** As in **A**, but with Sey1p and Yop1p at protein:lipid ratios of 1:1000 and 1:200, respectively. Each curve corresponds to the mean of three biological replicates.

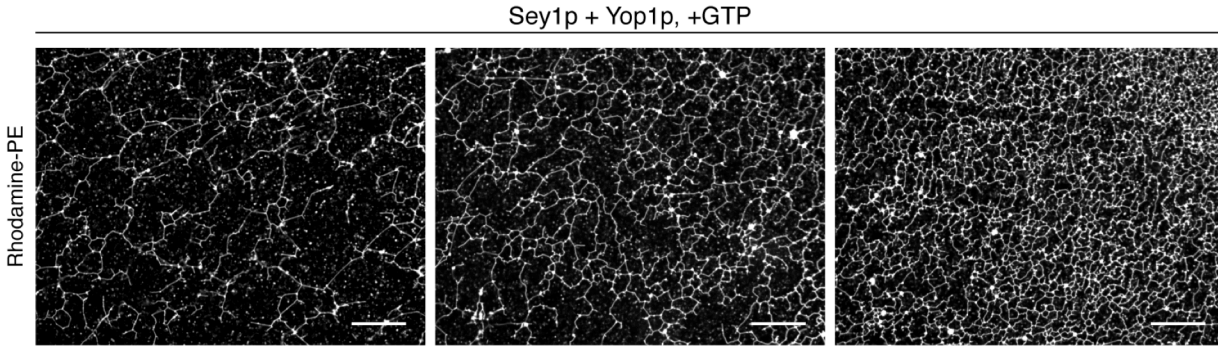

Figure A.5 Reconstituted networks display heterogeneity.
S. cerevisiae Sey1p and Yop1p were incorporated into rhodamine-PE labeled liposomes at protein:lipid ratios of 1:500 and 1:35, respectively. The proteoliposomes were incubated with 2 mM GTP, spotted on a cover slip, and imaged with a fluorescence microscope. Shown are different areas from the same coverslip. Note that the networks differ with respect to the density of three-way junctions and length of tubules. Scale bars = 20 μm.

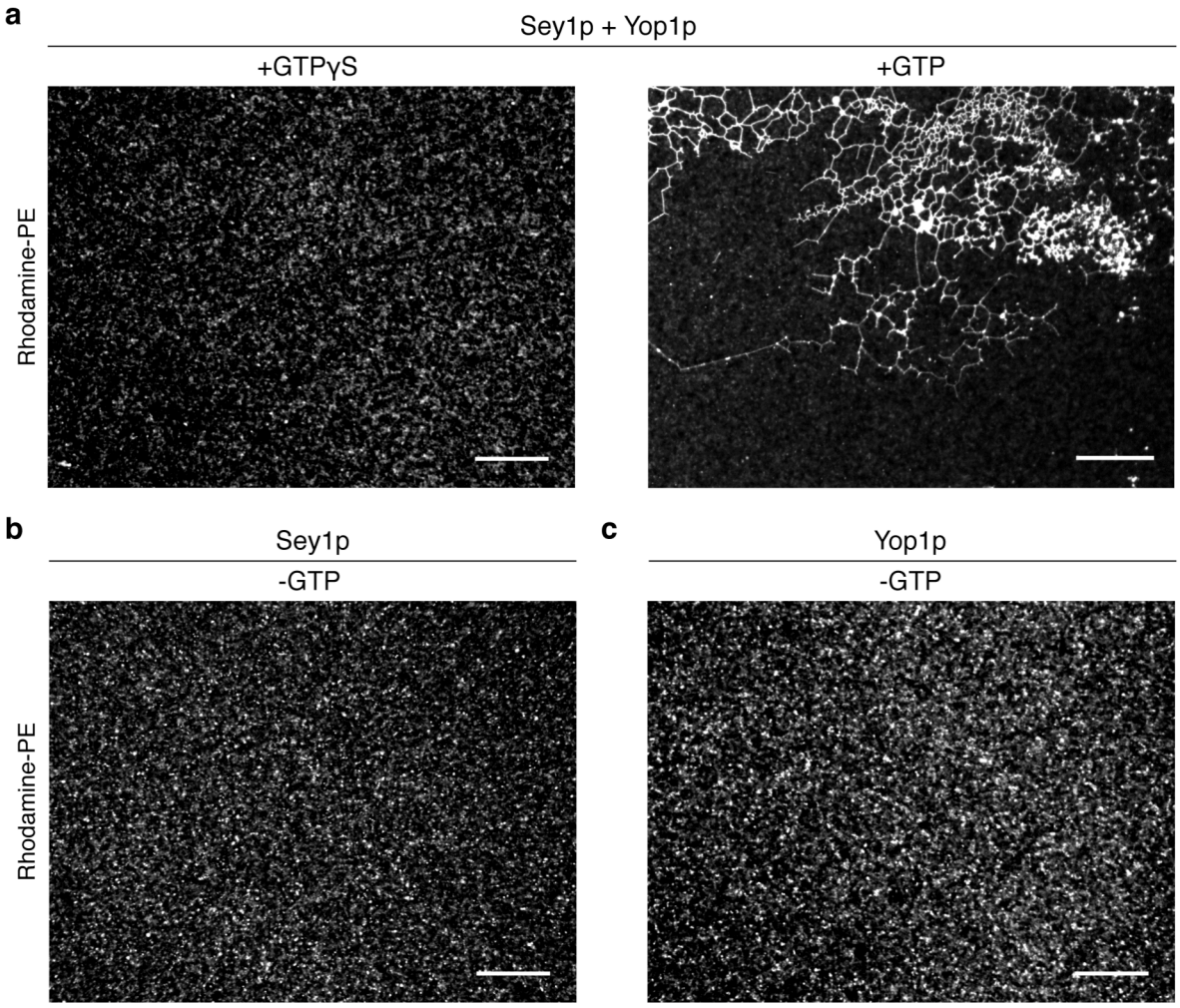

Figure A.6 Control experiments for network formation.
A) *S. cerevisiae* Sey1p and Yop1p were co-reconstituted into rhodamine-PE labeled liposomes at protein:lipid ratios of 1:500 and 1:35, respectively. The proteoliposomes were incubated with either 2 mM GTP or GTPγS and visualized by fluorescence microscopy. **B)** Proteoliposomes containing only *S. cerevisiae* Sey1p at a protein:lipid ratio of 1:500 were incubated in the absence of GTP. The same sample is shown incubated with GTP in Fig. 1d. **C)** As in **B**, but with proteoliposomes containing only *S. cerevisiae* Yop1p at a protein:lipid ratio of 1:35. The same sample is shown incubated with GTP in Fig. 1e. Scale bars = 20 μm.

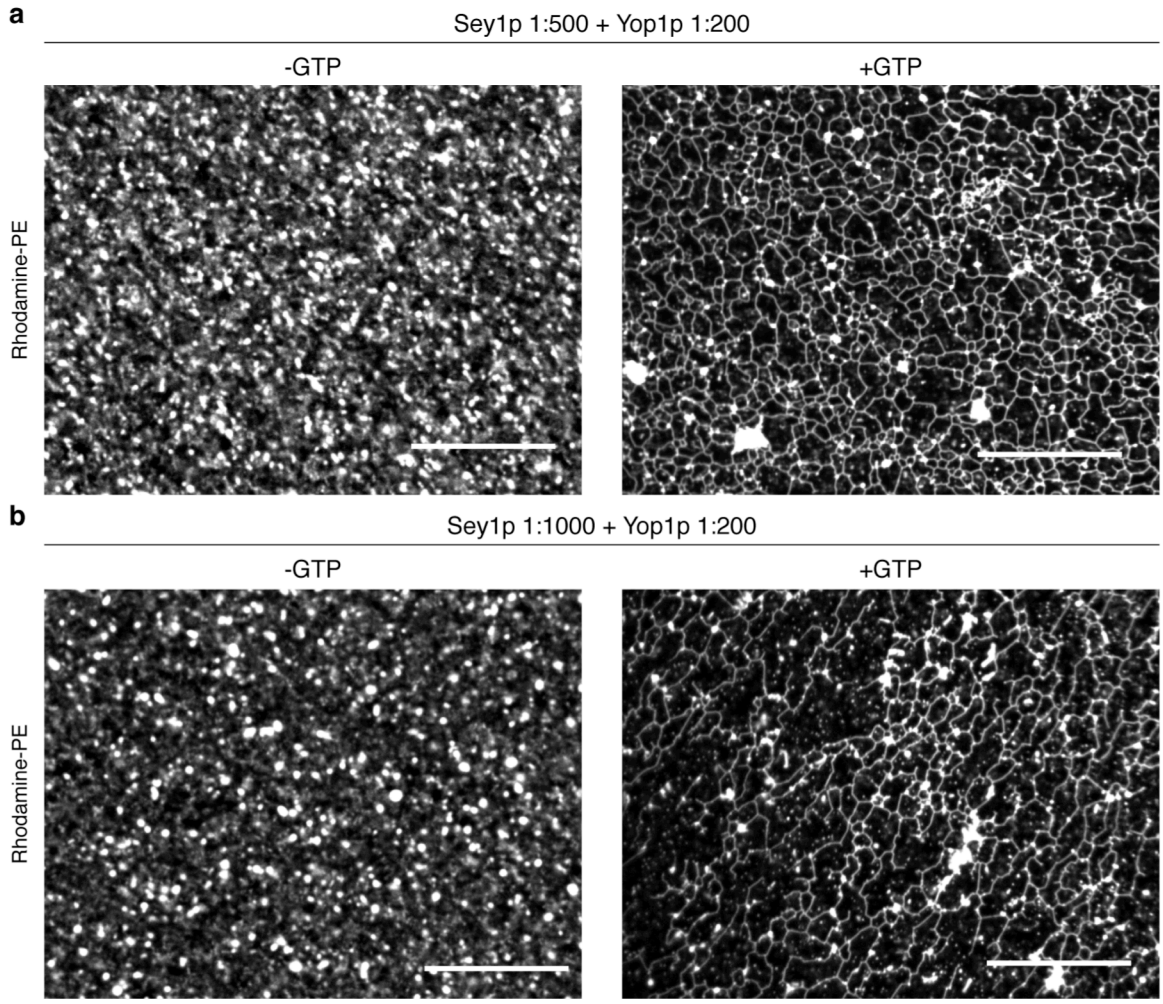

Figure A.7 Network formation with different concentrations of Yop1p and Sey1p.
A) *S. cerevisiae* Sey1p was co-reconstituted with *S. cerevisiae* Yop1p into rhodamine-PE labeled liposomes at protein:lipid ratios of 1:500 and 1:200, respectively (instead of the usual 1:500 and 1:35 ratios). The proteoliposomes were incubated with or without 2 mM GTP and visualized by fluorescence microscopy. **B)** As in **A**, but with protein:lipid ratios of 1:1000 and 1:200, respectively. Scale bars = 20 μm.

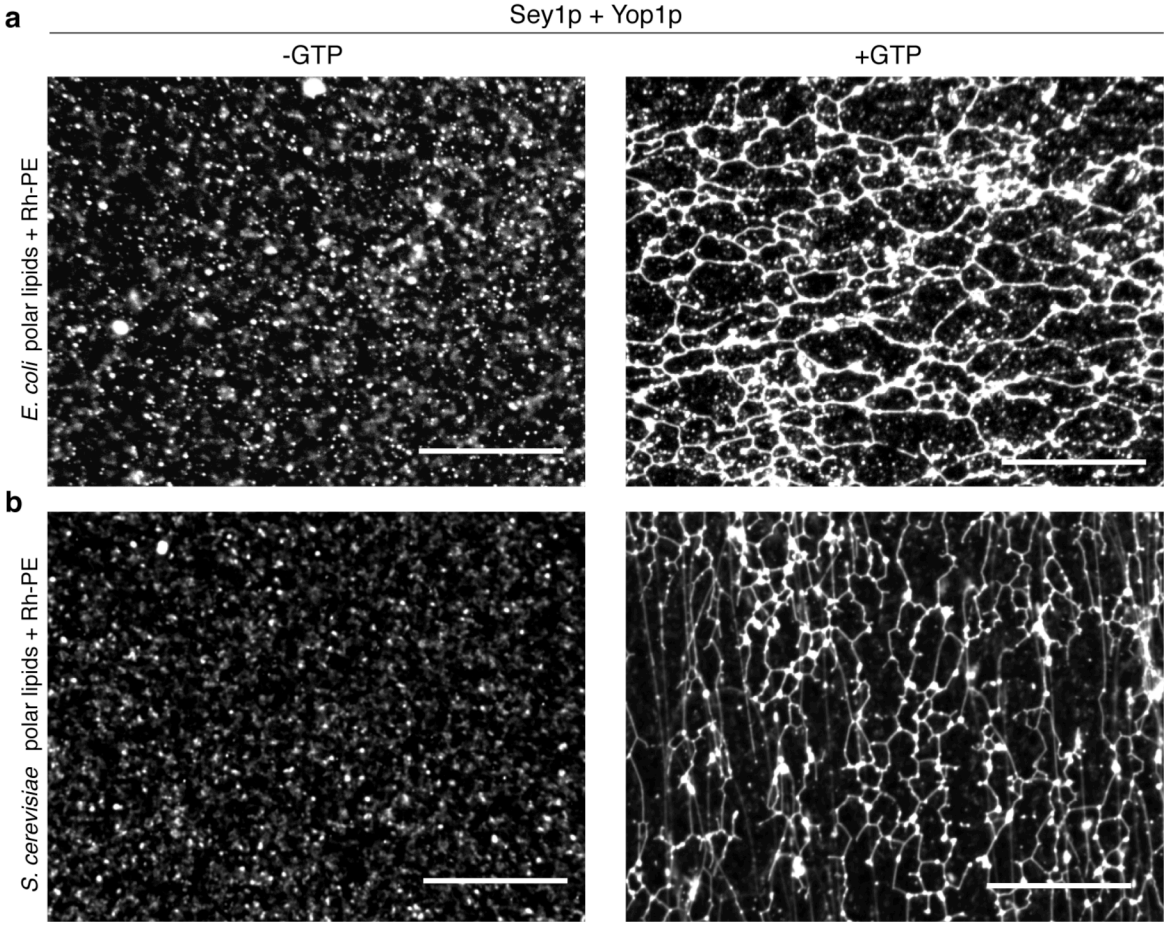

Extended Data Figure A.8 Tubular network formation with different lipid compositions.
A) *S. cerevisiae* Sey1p and Yop1p were co-reconstituted into rhodamine-PE labeled liposomes at protein:lipid ratios of 1:500 and 1:35, respectively. The liposomes were generated with a polar lipid extract from *E. coli*. The proteoliposomes were incubated with or without 2 mM GTP and visualized with a fluorescence microscope. **B)** As in **A,** but with liposomes generated with a polar lipid extract from *S. cerevisiae*. Scale bars = 20 μm.

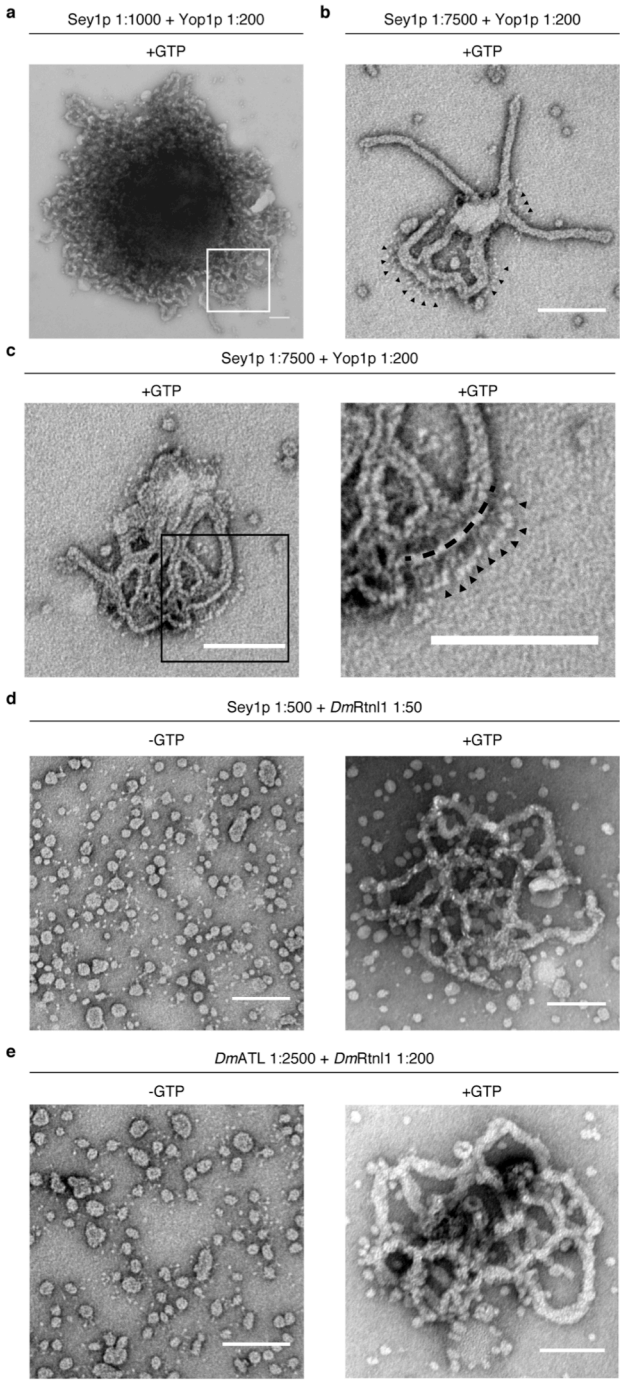

Extended Data Figure A.9 Sey1p-containing networks visualized with negative-stain EM.
A) *S. cerevisiae* Sey1p and Yop1p were co-reconstituted into liposomes at protein:lipid ratios of 1:1000 and 1:200, respectively. The samples were incubated with 1 mM GTP and visualized by EM after staining with uranyl acetate. The boxed area of this network is shown enlarged in Fig. 3a. **B)** As in **A**, but with Sey1p and Yop1p at protein:lipid ratios of 1:7500 and 1:200, respectively. Black arrowheads indicate Sey1p molecules. **C)** As in **B**, showing another area (left). Boxed area is shown enlarged (right) with black arrowheads indicating Sey1p molecules and the dotted black line traces approximate plane of the lipid bilayer. **D)** As in **A**, but with Sey1p and *D. melanogaster* Rtnl1 at protein:lipid ratios of 1:500 and 1:50, respectively, in the absence or presence of 1 mM GTP. **E)** As in **A**, but with *D. melanogaster* ATL *D. melanogaster* Rtnl1 at protein:lipid ratios of 1:2500 and 1:200, respectively, in the absence or presence of 1 mM GTP. Scare bars = 100 nm.

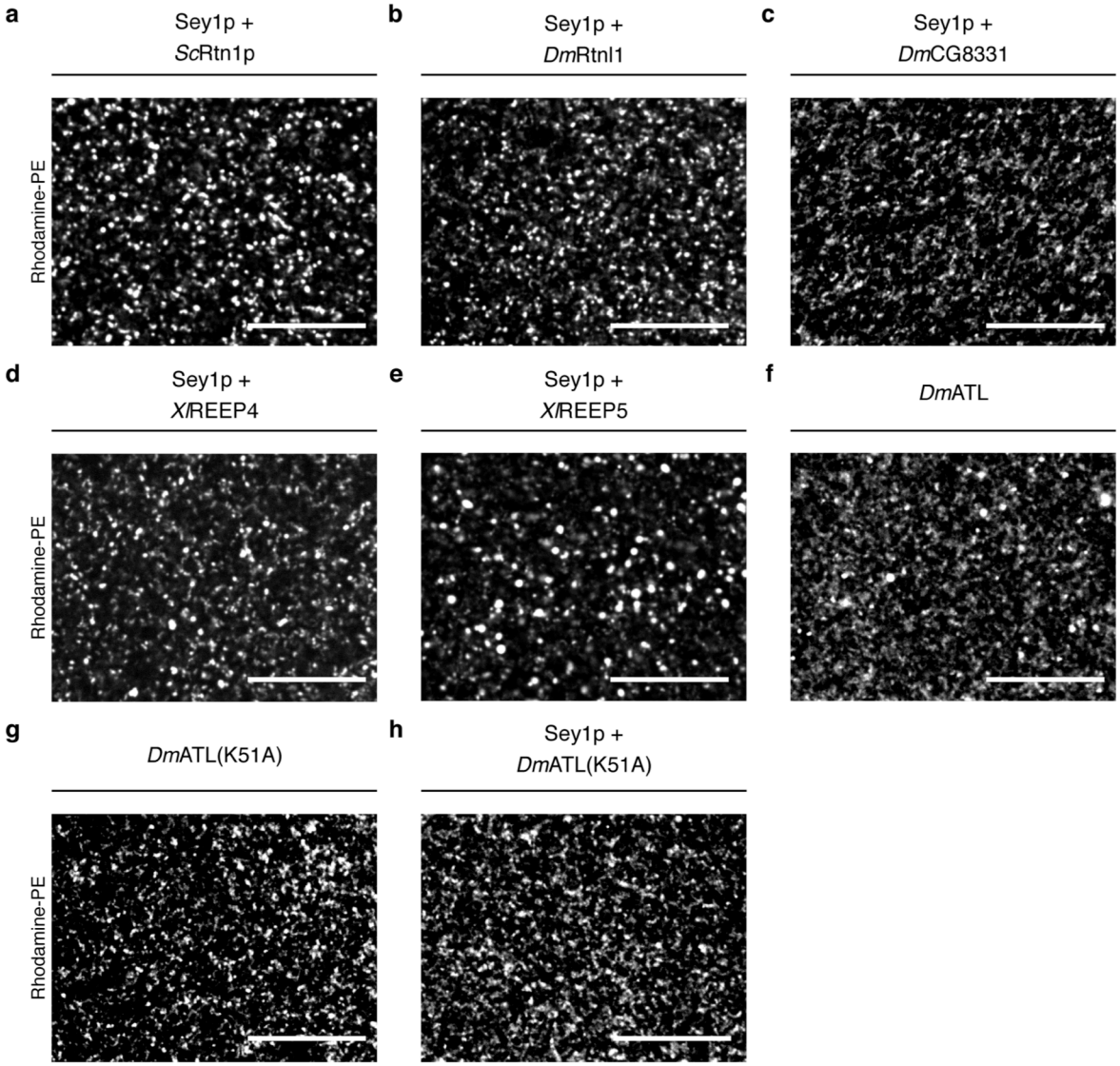

Figure A.10 Network formation with different membrane-fusing and curvature-stabilizing proteins requires GTP hydrolysis.
The samples shown in Figure 2.4 were incubated without GTP. Scale bars = 20 μm.

A.2 Legends for supplementary movies for Chapter 2

Supplementary video 1. Dynamics of a reconstituted network.

S. cerevisiae Sey1p and Yop1p were co-reconstituted into rhodamine-PE labeled liposomes at protein:lipid ratios of 1:500 and 1:35, respectively. The proteoliposomes were incubated in the presence of 2 mM GTP and visualized by fluorescence microscopy. The sample was imaged every 0.5 sec for 15 sec. The video is shown at 2 frames per sec. White arrows indicate sliding or fusing junctions that are shown in a magnified view in Fig. 1c. Cyan arrows indicate other sliding or fusing junctions. Frames from this video are shown in Fig 1c. Scale bars = 20 μm.

Supplementary video 2. Fragmentation of a reconstituted network after addition of GTPγS.

S. cerevisiae Sey1p and Alexa647-labeled Yop1p were co-reconstituted into rhodamine-PE containing liposomes at protein:lipid ratios of 1:500 and 1:35, respectively. Network was formed by incubating proteoliposomes with 2 mM GTP. After addition of 1 mM GTPγS, the samples were analyzed by fluorescence microscopy. The sample was imaged every sec for 30 sec. The video is shown at 2 frames per sec and displays the Alexa647-labeled Yop1p. Cyan arrows indicate points of fragmentation. Frames from this video are shown in Fig 2b. Scale bars = 20 μm.